STUDY OF SCALE-FREE CORRELATED CLUSTERS IN THE NON-EQUILIBRIUM AND EQUILIBRIUM CRITICAL PHENOMENA

THESIS SUBMITTED FOR THE DEGREE OF DOCTOR OF PHILOSOPHY (SCIENCE) OF THE UNIVERSITY OF JADAVPUR

RUMANI KARMAKAR

SATYENDRA NATH BOSE NATIONAL CENTRE FOR BASIC SCIENCES
BLOCK-JD, SECTOR-III, SALT LAKE
KOLKATA – 700098, INDIA

APRIL, 2005

STUDY OF SCALE-FREE CORRELATED CLUSTERS IN THE NON-EQUILIBRIUM AND EQUILIBRIUM CRITICAL PHENOMENA

THESIS SUBMITTED FOR THE DEGREE OF DOCTOR OF PHILOSOPHY (SCIENCE) OF THE UNIVERSITY OF JADAVPUR

RUMANI KARMAKAR

SATYENDRA NATH BOSE NATIONAL CENTRE FOR BASIC SCIENCES
BLOCK-JD, SECTOR-III, SALT LAKE
KOLKATA – 700098, INDIA

APRIL, 2005

CERTIFICATE FROM THE SUPERVISOR

This is to certify that the thesis entitled "**Study of scale-free correlated clusters in the non-equilibrium and equilibrium critical phenomena**" submitted by **Smt. Rumani Karmakar**, who got her name registered on **July 4,2002** for the award of **Ph.D.(Science) degree** of **Jadavpur University**, is absolutely based upon her own work under the supervision of **Dr. Subhrangshu Sekhar Manna** and that neither this thesis nor any part of it has been submitted for any degree / diploma or any other academic award anywhere before.

Date: 07 April, 2005.

Subhrangshu Sekhar Manna
Associate Professor
Satyendra Nath Bose National Centre for Basic Sciences
Block-JD, Sector-III, Salt Lake, Kolkata - 700098

Associate Professor
S N Bose National Centre
Salt Lake, Kolkata-700 098
Tel : 0091-33-335 5705-08
335 3057/61, 0312/13
Fax: 0091-33-3353477
E Mail: root@bose.res.in

Acknowledgements

This is my pleasure to introduce this thesis which I believe is the outcome of my research work during which period I have been accompanied and supported by a number of individuals. With pleasure I take this opportunity to acknowledge my gratitude to all of them.

First of all I am grateful to my supervisor Dr. Subhrangshu Sekhar Manna for all the constant encouragement, support and expert guidance he has provided me throughout my tenure here at the S. N. Bose National Centre for Basic Sciences, without which this work would not have materialized at all. I thank him for being patient with me. I feel priviledged to have learnt a lot from his expertise and dedication to physics.

There are so many others who needs my appreciation and I just hope to remember all of them!! It was my good fortune to have some terribly nice seniors and I learnt lots from them. I would like to thank specially Aninda Jiban Bhattacharya and Atisdipankar Chakrabarti for their assistance during my research period. Needless to say, I am amply benefitted by my colleagues particularly Sumana, Swarnali, Gautam da and Durga with whom I had discussions on several topics. It is my pleasure to thank all my friends at my host institution for their help in many direct and indirect ways. Special mention are due to Dipankar, Sudeshna, Aftab, Kunal, Venkat, whose company I really enjoyed.

I would also like to thank my SINP friends Anirban Chakraborti, Arnab Chatterjee, Sutarshi Pradhan and Sucheta Adhikari who have always been so helpful. I am greatly benefitted from discussions in our network group at Science College.

I would like to extent my warmest thanks to Dr. Tapati Dutta, lecturer in Physics, St. Xavier's College, Kolkata for her collaboration in significant portion of my research work. It was a great pleasure working with her. Her suggestions and constant encouragement were of the utmost value.

I thank Professor Sushanta Dattagupta, Director, S. N. Bose National Centre for Basic Sciences, Kolkata for the support provided by him during my research work at this centre. I am grateful to Professor Abhijit Mookerjee, Dean of Academic Affairs of the S. N. Bose Centre, for his active co-operation. I wish to acknowledge and express my heartfelt thanks to all the academic and non-academic staff members of this centre for their assistance.

A very special mention is deserved for Professor Monoranjan Saha, the Khaira Professor of physics, Calcutta University, who have been my mentor from my very childhood. His constant affection and encouragement has aroused interest in physics in me. I really feel priviledged to have such an eminent professor beside me.

My acknowledgement is incomplete without mentioning the constant support and encouragement from my parents, brothers and sisters. Last, but not the least, I am very much indebted to my husband, whose patience, understanding and encouragement helped me to fulfill my dreams.

Rumani Karmakar
Satyendra Nath Bose National Centre for Basic Sciences
Block-JD, Sector-III, Salt Lake, Kolkata - 700098

List of Publications

1. **Precise Toppling Balance, Quenched Disorder, and Universality for Sandpiles**
   R. Karmakar, S. S. Manna, and A. L. Stella
   Phys. Rev. Lett. **94**, 088002 (2005).

2. **Sandpile model on a quenched substrate generated by kinetic self-avoiding trails**
   R. Karmakar and S. S. Manna
   Phys. Rev. E **71**, 015101 (2005).

3. **Sandpile model on an optimized scale-free network on Euclidean space**
   R. Karmakar and S. S. Manna
   J. Phys. A: Math. Gen. **38**, L87-L93 (2005).

4. **Particle-hole symmetry in a sandpile model**
   R. Karmakar and S. S. Manna
   J. Stat. Mech., L01002 (2005).

5. **Directed fixed energy sandpile model**
   R. Karmakar and S. S. Manna
   Phys. Rev. E **69**, 067107 (2004).

6. **A Percolation Model of Diagenesis**
   S. S. Manna, T. Dutta, R. Karmakar and S. Tarafdar
   Int. J. Mod. Phys. C **13**, 319 (2002).

7. **A geometrical model of diagenesis using percolation theory**
   R. Karmakar, S. S. Manna and T. Dutta
   Physica A, **318**, 113 (2003).

Contents

Synopsis of the Thesis ..... *vii*

1. Introduction 1

1.1 Part I: Self-organized criticality 1

1.1.1 Sandpile experiments 3
1.1.2 The Bak, Tang and Wiesenfeld (BTW) sandpile model 3
1.1.3 Toppling matrix formulation 4
1.1.4 Abelian sandpile model (ASM) 4
1.1.5 The Manna sandpile model 6
1.1.6 Structure of avalanches 6
1.1.7 Avalanche size distributions 7
1.1.8 Finite size scaling of the avalanche size distributions 9
1.1.9 Moment analysis 10
1.1.10 Wave analysis 10
1.1.11 Some more sandpiles 11
1.1.12 Universality of sandpile models 12

1.2 Sandpile models on complex graphs 13

1.2.1 Scale-free networks (SFN) 15
1.2.2 Barabási-Albert model 16

1.3 Fixed energy sandpile (FES) 17

1.4 PART II: Conduction in sedimentary rocks 17

1.4.1 Diagenesis 18

2. Precise toppling balance, quenched disorder, and universality for sandpiles **21**

2.1 Introduction 21

2.2 The model 23

2.3 Precise toppling balance 24

2.4 Results and analysis 25

2.4.1 Avalanche structures 25
2.4.2 Avalanche size distributions and multi-fractal analysis 27
2.4.3 Wave analysis 29
2.4.4 Summary of [84] 30

2.5 Asymmetric TM that maintains precise $H_i = H_i'$ balance 31

2.5.1 Kinetic self-avoiding trail (KSAT) 32
2.5.2 Avalanche picture 34
2.5.3 Results and analysis 34

2.6 Conclusion 36

3. Sandpile model on an optimized scale-free graph on Euclidean space **37**

3.1 Introduction 37
3.2 Networks on Euclidean space 38
3.3 Sandpile model on a scale-free graph 38
3.3.1 Sandpile model on a SFG on the square lattice 39
3.3.2 Avalanche statistics for sandpile model on a SFG on the square lattice 41
3.4 Optimized SFG on Euclidean space 41
3.5 Sandpile model on an optimized SFG on Euclidean space 43
3.6 Conclusion 44

4. Particle-hole symmetry in a sandpile model **45**

4.1 Introduction 45
4.2 Particle-hole addition model 46
4.3 Results 47
4.3.1 Mean number of particles per site 47
4.3.2 Autocorrelation of the fluctuating mass 49
4.3.3 Particle-hole avalanche statistics 50
4.4 Conclusion 51

5. Directed fixed energy sandpile model **53**

5.1 Introduction 53
5.2 Directed fixed energy sandpile (DFES) 55
5.2.1 Deterministic directed FES (DDFES) 55
5.2.2 Stochastic directed FES (SDFES) 58
5.3 Comparison: DDFES and SDFES 60
5.4 Conclusion 60

6. A Percolation model of Diagenesis **61**

6.1 Introduction 61
6.1.1 Bootstrap percolation 63
6.2 Our model of Diagenesis 65
6.2.1 Stable configuration (SC) 66
6.2.2 Clusters in the stable configurations 67
6.3 Results 67

6.3.1 The Diagenetic percolation threshold 68
6.3.2 Cluster statistics 71
6.3.3 Order parameter 73
6.3.4 Percolation threshold for different m-values 73
6.4 Conclusion 74

Bibliography **75**

Synopsis of the Thesis

Title: Study of scale-free correlated clusters in the non-equilibrium and equilibrium critical phenomena

Quite often the properties of a thermodynamic system are studied on a regular lattice having the discrete / continuous values of some physical entity associated with each site of the lattice. A cluster on a lattice is a set of lattice sites connected by nearest neighbor bonds such that each cluster site has at least one neighbor in the cluster. In general the physical entity at a site in the cluster interacts with its neighboring sites and therefore two sites of the same cluster even when they are far apart may also feel the mutual influence of each other propagated through the intermediate sites. This reflects the correlations among the different cluster sites. A sample of clusters is called scale-free when their sizes vary over all length scales, i.e., the probability distribution of the cluster sizes has long tails, typically power law variations which ensures the presence of very large macroscopic clusters of the order of system sizes. These scale-free clusters are very important since they signify the presence of long-range correlations in the system, the signature of criticality in Critical Phenomena.

Clusters appear in many different branches of Physics in many different forms. For example the cluster sites in percolation theory of conductivity in impure materials represent the metal atoms embedded in insulating materials, in polymer physics they represent monomers, in magnetism they represent spins, where as in astrophysics they may represent stars or galaxies etc.

In this thesis we studied statistical properties of scale-free clusters occurring in both non-equilibrium as well as equilibrium systems. Namely, in Part I we studied the avalanche clusters occurring in the sandpile models of Self-Organized Criticality where as the Part II is devoted to the study of clusters in equilibrium system i.e., the percolation model of Diagenesis in sedimentary rocks.

Part I: Avalanche clusters in sandpile models of Self-Organized Criticality

Spontaneous emergence of long-range correlations in non-equilibrium stationary critical states of non-linear dissipative externally driven systems without any fine tuning parameter is the basic idea of Self-Organized Criticality (SOC). Sandpile models are prototypical models of SOC. The deterministic Bak, Tang and Wiesenfeld (BTW) sandpile and the stochastic Manna sandpile are two very important and well studied models. The question if the critical behaviors of these two models are the same or different has attracted a lot of attention in this field but these researches were not fully successful to yield much insight into the understanding and differentiating the two models.

In our two recent papers [1,2] we have studied a single sandpile model with quenched random toppling matrices that captures the crucial features of different sandpile models of self-organized criticality. With symmetric toppling matrices avalanche statistics falls in the multi-scaling BTW universality class. In the asymmetric case the simple scaling of the Manna model is observed. The presence or absence of a precise toppling balance between the amount of sand released by a toppling site and the total quantity of sand the same site receives when all its neighbors topple once, determines the appropriate universality class. In [2] we extended our

conjecture in [1] and showed that even with asymmetric toppling matrices one can ensure the precise balance at all sites except on the boundary and this model also behaves like the BTW model.

In the paper [3] we studied the deterministic as well as stochastic sandpile models on the scale-free graphs embedded in the Euclidean space. We observed that for the cost optimized graph, the sandpile model has the same critical behavior as the BTW sandpile which is consistent with our conjecture in [1], whereas for the un-optimized scale-free graph the critical behavior is mean-field like.

Holes are introduced in [4] as the absence of particles (sand grains). Toppling rules for hole columns are defined in a similar but reverse way as the sand column topplings. Particle-hole symmetry in a sandpile model is studied by adding particles with a probability p and holes with $1-p$. It has been found that the system is critical for particle avalanches for $p > 1/2$ and for hole avalanches for $p < 1/2$ where as at $p = 1/2$ the power spectrum for the time series of fluctuating system masses has $1/f$ noise.

A simple fixed energy sandpile model is studied in [5] on an oriented square lattice using both deterministic as well as the stochastic dynamical rules. The critical behavior of this model is observed to be different from the directed percolation critical behavior.

Part II: A percolation model for Diagenesis in sedimentary rocks

Diagenesis is a complex restructuring process by which granular systems evolve in geological time scales from unconsolidated, high-porosity packings toward more consolidated, less porous structures. We studied a percolation model to investigate the phenomenon of Diagenesis [6]. The cementation and the dissolution processes are modeled by the culling of occupied sites in rarefied and growth of vacant sites in dense environments. Starting from sub-critical states of ordinary percolation the system evolves under the diagenetic rules to critical percolation configurations. The same model in a three dimensional cubic system has been studied in [7].

This thesis is based on the following publications:

1. *Precise Toppling Balance, Quenched Disorder, and Universality for Sandpiles*
   R. Karmakar, S. S. Manna, and A. L. Stella, Phys. Rev. Lett. **94**, 088002 (2005).
2. *Sandpile model on a quenched substrate generated by kinetic self-avoiding trails*
   R. Karmakar and S. S. Manna, Phys. Rev. E **71**, 015101 (2005).
3. *Sandpile model on an optimized scale-free network on Euclidean space*
   R. Karmakar and S. S. Manna, J. Phys. A: Math. Gen. **38**, L87-L93 (2005).
4. *Particle-hole symmetry in a sandpile model*
   R. Karmakar and S. S. Manna, J. Stat. Mech., L01002 (2005).
5. *Directed fixed energy sandpile model*
   R. Karmakar and S. S. Manna, Phys. Rev. E **69**, 067107 (2004).
6. *A Percolation Model of Diagenesis*
   S. S. Manna, T. Dutta, R. Karmakar and S. Tarafdar, Int. J. Mod. Phys. C **13**, 319 (2002).
7. *A geometrical model of diagenesis using percolation theory*
   R. Karmakar, S. S. Manna and T. Dutta, Physica A, **318**, 113 (2003).

Chapter 1

Introduction

1.1 PART I: Self-organized criticality

A self-similar pattern is made of parts which look similar to the whole pattern. Around late seventies, Mandelbrot observed that there exists large number of such patterns in nature. For example coast lines of a country is well known to be self-similar. The same type of tortuosity of the coast line is observed over many length scales ranging from few kilometers to several thousand kilometers. Similarly mountain landscapes, electrical breakdown patterns, viscous fingering patterns or vortices in turbulence etc. are known to have self-similar structures. This is an important observation since it means that these patterns are correlated over large distances [1, 2].

Much effort had been devoted for characterization of these patterns. Mandelbrot also observed that many such patterns have non-trivial non-integral Hausdorff-Besicovitch dimensions. Mandelbrot coined the word 'fractal' for these self-similar objects. The mass $M(R)$ of an object of physical size R varies as $M(R) \propto R^{d_f}$ where d_f is known as the fractal dimension of the object [1, 2, 3].

There is another ubiquitous phenomenon which has not been understood fully for decades. When a direct current flows through an electrical device, a low frequency flicker noise voltage arises between the contacts. It has been observed that the low frequency noise power spectra of such systems show a power law dependence on the frequency f of the voltage source [4, 5]. In a similar way the fluctuating time signals in random resistor networks, intensity of light waves from distance stars or even price indices in economic stock markets etc. have power spectra decaying as power laws with exponents nearly equal to unity at low frequencies: $S(f) \propto f^{-\beta}$. This phenomenon also represent long-ranged correlations in temporal behavior of these systems.

Bak, Tang and Wiesenfeld (BTW) first argued that different ways to characterize the self-similar fractals or studying the $1/f$ type power spectra of different fluctuating signals may not be sufficient in understanding these phenomena. They tried to put forward their argument that both these phenomena may not be independent and often are actually the "two sides of the same coin" i.e., they are the spatial and temporal manifestations of the same phenomenon [6].

Their argument is as follows. It is well known that self-similar structures are observed in systems undergoing second order phase transitions. In laboratories

control parameters like temperature is tuned to arrive at the critical points to observe these self-similar patterns where the spatial and temporal correlation functions are invariant under scale transformations, implying that these systems at critical points have no intrinsic length and time scales [7].

Bak and his collaborators argued that in nature there is no one to do this fine tuning, yet extended dynamical systems do show self-similarities or long range correlations. How this can then happen in nature? They suggested that there are self-organization processes in built in these systems which by themselves may evolve to critical states and therefore do not need the hands of experimentalists to tune the control parameters. In 1987 BTW introduced and defined the phenomenon of self-organized criticality to explain the occurrence of spatial self-similar fractal structures as well as $1/f$ type power spectra in slowly driven spatially extended dissipative systems in the following way:

In the phenomenon of Self-Organized Criticality (SOC) an externally driven system dynamically evolves to a non-equilibrium stationary critical state showing spontaneous emergence of the long-range spatio-temporal correlations in the absence of any fine tuning parameter [8, 9, 10].

BTW suggested that such a system under the evolution of its own dynamical rules self-organizes itself to spontaneously reach the critical states where small perturbations can lead to bursts of activities called avalanches whose sizes and durations vary up to limits determined by the finite size of the system. There are two widely different time scales involved in such systems, the larger one corresponds to the rate of external driving and the smaller one due to the microscopic evolution rate of the avalanches. The critical states of these systems are robust with respect to the arbitrary initial conditions the systems start with. This critical state is different from those in the classical critical phenomena in equilibrium statistical mechanics in the sense that no fine tuning like temperature, pressure etc. is necessary to arrive at this state - the system is attracted to the basin of attraction which is the critical state of the self-organizing dynamics. The signature of the long-range correlation in the critical state is the power law distribution of the avalanche sizes and their durations.

BTW proposed that a sandpile should be one of the simplest possible system exhibiting the self-organized criticality. Consider the formation of a sandpile on a fixed horizontal base. The pile is being grown by adding one or few sand grains at a time at arbitrary locations on the platform. At the early stage the growing shape of the pile is quite random and varies from one experiment to the other. At this stage, addition of sand grains create sand avalanches on the surface of the growing sandpile whose sizes are tiny i.e., they disturb only small local regions on the pile. However after a long time the sandpile takes a steady fixed shape in the form of a cone, characterized by certain angle of repose (the angle between the surface of the pile and the horizontal plane). Further addition of sand grains at this stage create sand avalanches whose sizes may occasionally be very large and more and more avalanches drop out sand mass through the boundary so that the steady shape of the pile is maintained. BTW argued that appearance of large avalanches which are as big as the system itself reflects the appearance of long-range correlations in space as the signature of criticality. They suggested that the strengths (size and durations) of these avalanches should have power-law distributions.

It has also been proposed that the concept of SOC may be applicable to describe physical phenomena in many other complex systems like spread of forest fires [11, 12], river networks [13, 14, 15], energy release during earthquakes [16, 17], biological evolution [18] etc. All models describing these systems have all features of self-organized critical systems.

1.1.1 Sandpile experiments

Motivated by the idea of Self-Organized Criticality, several experiments have been done on sandpiles.

In one experiment [19] a semicircular drum filled with a granular material was slowly rotated about its horizontal axis creating a sandpile. Grains fell vertically downward across its edge and were allowed to pass through the plates of a capacitor. Power spectrum analysis of the time series for the fluctuating capacitance showed that small avalanches obeyed power law distributions of limited size while big avalanches followed a different distribution.

In a second experiment [20] a sandpile was formed by dropping sand on a horizontal circular disc. On further addition of sand, avalanches were created on the surface of the pile whose size is measured by the mass of the avalanches of sand leaving the plate. It was found that for smaller piles the avalanche size distribution obey a scaling behavior while for larger piles the scaling did not work very well.

In another experiment [21] a pile of rice is formed by dropping grains of rice in the narrow gap between two vertical glass plates. Due to the anisotropy of the grains, various packing configurations were observed. The energy dissipated between two consecutive profiles determined the size of an avalanche. SOC behavior was observed for grains with a large aspect ratio but not for less elongated grains. Thus laboratory experiments on sandpiles do not always show criticality.

1.1.2 The Bak, Tang and Wiesenfeld (BTW) sandpile model

If a sandpile is built up on a flat surface by randomly adding sand, the slope of the pile increases and will reach a critical value beyond which sand slides off. BTW mimicked this dynamics by their sandpile model, commonly known as BTW model [8]. In BTW sandpile automata, the prototype model for SOC, due to slow external driving the system evolves to a critical state with activity distributed on all length scales. Generally the sand grains can also be identified as energy, stress or pressure quanta.

In the simplest possible version, the BTW model is defined on a d-dimensional hyper-cubic lattice of linear extent L. Every site i of the lattice is associated with a non-negative integer variable h_i representing the height of the sand column at that site measured by the number of sand grains. Starting from an arbitrary initial sand distribution profile corresponding to a specific set of values of the heights of sand columns at every lattice site the system is externally driven by adding sand grains one at a time at randomly selected sites i and thus increasing the heights at those sites by unity:

$$h_i \rightarrow h_i + 1. \tag{1.1}$$

However, the sand column at every site is stable up to a certain height $H-1$, beyond that the column becomes unstable. An unstable sand column is called *active* and therefore it topples with probability one. Without the loss of generality in BTW model the value of the threshold height H is chosen to be equal to $2d$ at all lattice sites. Therefore when $h_i \geq H$ the active sand column at the site i topples and relaxes by reducing its height by H as:

$$h_i \rightarrow h_i - 2d \tag{1.2}$$

and these many grains are distributed equally among the $2d$ neighboring sites j as:

$$h_j \rightarrow h_j + 1. \tag{1.3}$$

In some situations some of the neighboring sites may have their column heights $H-1$ before the toppling. On receiving grains due to toppling at the site i, these sites also become active and therefore topple. Consequently the topplings at these sites may create additional topplings at their further neighborhood in a similar way. This creates a cascade of sand column topplings in the system. The dynamical process thus created in the system which is extended over a certain region of space and continues for a certain interval of time is called an *avalanche.* This avalanche terminates when sand columns at all sites become stable again. Lattice sites on the boundary have less than $2d$ neighbors within the system. Therefore when a site on the boundary topples, some grains are dropped outside the boundary. This implies that corresponding to the inflow of grains in the system due to the external driving, there is an outflow of grains from the system through the boundary as well. As a result a stationary state is ensured when the fluxes of inflow and outflow currents of sand grains balance. It is to be noted that the presence of a boundary through which grains can flow out is absolutely essential without which there can not be any stationary state.

1.1.3 Toppling matrix formulation

Toppling rules in the BTW model can be generalized by defining an integer 'toppling matrix' (TM) Δ [22, 23]. Here the sandpile model is defined for an arbitrary connected graph $\mathcal{G}$ of N vertices. As before non-negative integer height variable h_i is associated with all vertices of the graph. During a toppling at the vertex i, all heights are updated as $h_j \rightarrow h_j - \Delta_{ij}$, with $\{j = 1, N\}$ where the toppling matrix satisfies the conditions: $\Delta_{ii} > 0$ for all i, and $\Delta_{ij} \leq 0$ for all $i \neq j$. This means that due to a toppling at the vertex i, $-\Delta_{ij}$ grains are transferred to the vertex j. Without the loss of generality the threshold heights may be chosen as $H_i = \Delta_{ii}$. Clearly the BTW model is a special case of this formulation where $\Delta_{ii} = 4, \Delta_{ij} = -1$ for $|i-j| = 1$ and $\Delta_{ij} = 0$ for $|i-j| > 1$.

1.1.4 Abelian sandpile model (ASM)

It was first observed by Dhar that the same final stable configuration $\mathcal{C}$ of sand column heights ($h_i < H, i = 1, N$) is obtained independent of the sequence in which grains are added at different sites of the system to reach this stable configuration [22].

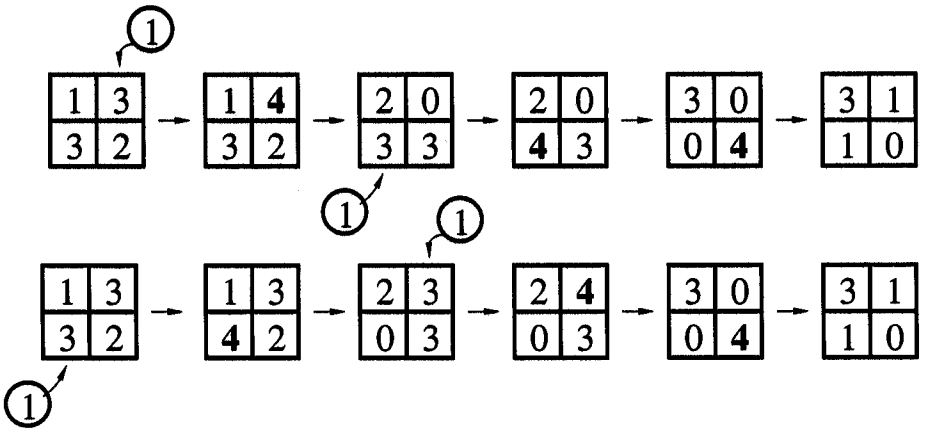

Figure 1.1: Abelian dynamics

This is the result of the fact that the stable configuration is actually independent of even the sequence of microscopic toppling events that led to this stable configuration. For example, if at an intermediate stage during the progress of an avalanche if two sites i and j are both active, the same height configuration is obtained if i is toppled first and then j or the vice versa. Successive application of this argument shows that $\mathcal{C}$ is independent of the sequence of sand grain additions at different sites of the graph as shown in Fig.1.1.

Dhar proposed that adding a sand grain at the site i may be represented by an operator a_i [22]. Therefore if a stable configuration $\mathcal{C}'$ is obtained by adding a sand grain to a site i of a stable configuration $\mathcal{C}$ and then relaxing, it is represented by:

$$\mathcal{C}' = a_i \mathcal{C}. \tag{1.4}$$

Therefore in terms of sand addition operators the independence of an arbitrary configuration $\mathcal{C}''$ obtained by adding two sand grains at sites i and j on $\mathcal{C}$ is represented by:

$$a_i a_j \mathcal{C} = a_j a_i \mathcal{C} = \mathcal{C}'' \quad \text{which implies} \quad a_i a_j = a_j a_i \quad \text{or} \quad [a_i, a_j] = 0 \tag{1.5}$$

This implies that the grain addition operators commute for all i, j. These operators a_i have unique inverse and they form an Abelian group satisfying the algebraic relation, $\prod_j a_i^{\Delta_{ij}} = I$ for all i, which means that adding Δ_{ii} particles at site i is same as adding one particle at each of the neighbors of i. This is called the Abelian Sandpile model (ASM).

Due to the Abelian property it has been possible to obtain many exact results for the ASM [22, 23]. Dhar showed that the ASM dynamics partitions the whole state space of the sandpile into two regions, namely: *Recurrent* and *Transient*. Sandpile height configurations occurring in the stationary state are the recurrent states and they occur with uniform probability. All other states are transient states which never occur in the stationary state. It is estimated that compared to the transient states the recurrent states are of measure zero. Therefore an arbitrarily selected random configuration is almost always a transient configuration. Under the sandpile dynamics the system moves through a sequence of several transient states till it

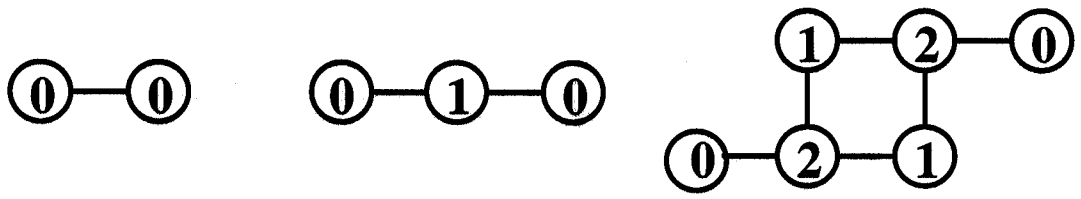

Figure 1.2: Three examples of FSC on a square lattice BTW sandpile.

reaches a recurrent state. Once it reaches a recurrent state the system remains in the recurrent state and cannot come out of it. An important result of the ASM is that the total number of distinct recurrent configurations is given by the determinant of the toppling matrix i.e., $\det\Delta$ [22, 23].

Dhar had formulated a very precise prescription to identify if a stable configuration is recurrent or transient. This is done by defining a forbidden sub-configuration (FSC). A FSC is a set of connected vertices on the graph $\mathcal{G}$ such that the height of the sand column h_i at each vertex i is less than the number of neighbors of i in the set. Dhar showed that a recurrent state can never have a FSC. Simple examples of FSCs on the square lattice graph are shown in Fig.1.2. To check that if an arbitrary stable height configuration has any FSC or not, a burning algorithm [24] is proposed. If the fire completely burns the graph the stable state has no FSC and it is a recurrent configuration. On the other hand if it is not completely burnt the state must have at least one FSC and therefore the state is transient.

1.1.5 The Manna sandpile model

Manna introduced a simple stochastic version of the BTW sandpile model [25]. In this model not only the sand grains are added to the system in randomly selected positions but also the grains are distributed randomly during the topplings. The heights of the sand columns at every site have only two possible values: either $h_i = 0$ i.e., empty site or $h_i = 1$ i.e., site occupied by a single grain only. The threshold height H value for each lattice site is assigned to be 2. When the height h_i of the sand column at a site i exceeds the height $H - 1$, a toppling event takes place:

$$\text{If,} \qquad h_i \geq H \qquad h_i \rightarrow 0 \tag{1.6}$$

and each grain at the site i is transferred to a randomly selected neighboring site j.

There is also a simpler version of Manna model when the toppling site i loses only two grains i.e., $h_i \rightarrow h_i - 2$ and each of these two grains is transferred to a randomly selected neighboring site. It may be noticed that even after transferring the pair of grains the site i may remain unstable.

1.1.6 Structure of avalanches

In a sandpile model a site can topple more than once in a single avalanche. In general different sites visited by the avalanche topple different number of times. The structural details of an avalanche become very distinct if the sites which toppled the same number of times are marked by one color. Therefore different colors are used

for marking different subsets of sites. In Fig.1.3 we show such color pictures of a BTW and a Manna avalanches. It is observed that the BTW avalanche has a very nice structure. The outermost sites form the set_1 which have toppled only once. Adjacent to these sites and inside the avalanche are the set of sites which have toppled twice (set_2). These sites are completely surrounded by the set_1 sites. The general rule is the set_n of sites which have toppled n times are completely surrounded by the set_{n-1} sites. Different sets form different toppling zones and the maximally toppled zone form the innermost core of the avalanche. The origin of the avalanche where the sand grain was added must be within the maximally toppled zone and it must be situated at the boundary of this zone.

The structure of the BTW avalanches can be explained in the following way. An arbitrary site i (other than the origin) topples for the first time by receiving grains from the topplings of its $\{j_2\}$ neighbors. It then donates grains to its $\{j_1\}$ untoppled neighbors and gives back grains to the $\{j_2\}$. Therefore $\{j_2\}$ neighbors get back one grain each as they transferred to the site i. This implies that the site i topples for the second time only if its all $\{j_2\}$ neighbors have toppled at least twice or more. This is true in general and a site which topples for the n-th time must have few neighbors which have toppled n-th times or more. This indicates that the $(n+1)$-th toppling zone is completely surrounded by the n-th toppling zone and the avalanche is divided into multiple toppling zones. The origin where a sand grain was dropped does not need to follow this but necessarily it has to be situated on the perimeter of the maximally toppled zone.

Another point to note is BTW avalanches are fully compact and cannot have holes or cluster of sites which have not toppled but are completely surrounded by the toppled sites. For example, a single site hole is not possible since even if it was empty it will get four grains from the neighbors and therefore will topple. Similarly a hole with a pair of adjacent sites is also not possible since each of them should have received three grains each. In spite of that they have not toppled implies that both the sites were vacant and therefore the pair of sites is an FSC which cannot be present in the stationary state.

In Manna model the avalanches do not have such a systematic structure. This is because in a toppling each grain is transferred to a randomly selected neighboring site. Let during a toppling at the site i, the neighbor sites j_1 and j_2 get one grain each. In case both j_1 and j_2 had already one grain each, these sites will topple. It may happen that none of the four grains distributed by j_1 and j_2 comes back to the original site i and therefore there is no guarantee that the site i will topple for the second time. Therefore unlike BTW avalanche, in a Manna avalanche the multiply toppled sites are randomly scattered over the region covered by the avalanche. Moreover, unlike BTW avalanche, there may be holes in the Manna avalanche.

1.1.7 Avalanche size distributions

It is necessary to measure the strength of an avalanche quantitatively, generally called the *size* of the avalanche which is usually defined in a number of ways. For example, the total number s of topplings in an avalanche is the most popular measure of its size. The spatial area of the avalanche measured by the number a of distinct sites which toppled at least once. The length r of one side of the smallest square

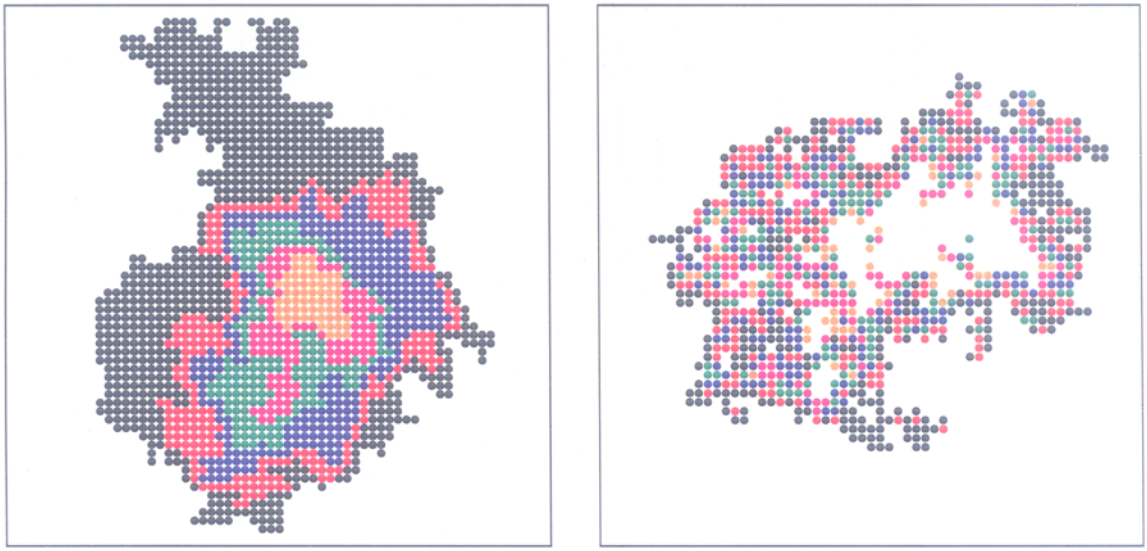

Figure 1.3: Multiply toppled sites within the avalanches are shown by circles of different colors: 1(black), 2(red), 3(blue), 4(green), 5(magenta) and 6(orange) for (a) BTW model and (b) Manna model.

which covers the avalanche is the spatial extent of the avalanche. Lastly the life time T of the avalanche is the duration over which the activity persists.

During the progress of the avalanche one unit time is defined through the following four steps in a parallel updating process:

- At an intermediate time t, a list is made of all vertices that are unstable.
- The heights at these vertices i are reduced by Δ_{ii} each.
- Corresponding to every vertex i of this list $-\Delta_{ij}$ grains added to all vertices j.
- All vertices in the list and their neighbors are searched to make a renewed list of unstable sites in time $t+1$.

The signature of the criticality in the non-equilibrium stationary state of the system is the development of the long-range spatio temporal correlations. This is reflected in the power law variations of the probability distributions of the avalanche sizes. If four measures i.e., $\{s, a, r, t\}$ of the avalanche size are denoted by a general notation x then in the critical state their probability distributions vary as:

$$\text{Prob}(x) \sim x^{-\tau_x}. \tag{1.7}$$

Since these four measures are different measurements of the same random avalanche, all of them are not independent variables and therefore are related to one another by scaling relations. Between any two measures $x, y \in \{s, a, t, r\}$ one can define mutual dependence as

$$\langle y \rangle \sim x^{\gamma_{xy}}. \tag{1.8}$$

These exponents are related to one another, e.g.

$$\gamma_{ts} = \gamma_{tr}\gamma_{rs}. \tag{1.9}$$

Also since the number of avalanches between x and $x + dx$ is the same as that between x' and $x' + dx'$ we have the relation $\text{Prob}(x)dx \sim \text{Prob}(x')dx'$ which implies

another scaling relation:

$$\gamma_{xy} = (\tau_x - 1)/(\tau_y - 1). \tag{1.10}$$

The variation of the average avalanche size $\langle s(L)\rangle$ with the system size can be estimated using the following argument. Since in the stationary state the inflow rate of grains is equal to the outflow rate of grains, corresponding to each grain added, one grain must have to drop out of the system thorough the boundary. Since grains are dropped at randomly selected locations the dropping point is on the average at a distance proportional to L from the boundary in system of linear extension L. Since in a toppling the grains are distributed among the neighbors isotropically in all directions, the individual motion of a typical grain must be diffusive. Therefore on the average a grain, while executing a diffusive motion, takes $\mathcal{O}(L^2)$ steps to travel a distance L to reach the boundary which is done by executing L^2 topplings. This implies that average avalanche size must grow with L as L^2:

$$\langle s(L)\rangle \sim L^2 \tag{1.11}$$

It may be noted that this result is very general and independent of precise shape of the boundary and dimension as long as the grain distribution in every toppling event is isotropic, short range and each grain has to travel a distance $\mathcal{O}(L)$ to reach the boundary.

1.1.8 Finite size scaling of the avalanche size distributions

There is an upper bound for each measure of the avalanche sizes which strongly depends on the system size. For example in the case of BTW model on a square lattice of size L the upper bound of the avalanche area a is obviously L^2. Similarly the upper bound of the avalanche size s varies with the system size as L^3. This is easily understood in a sandpile on an odd size square lattice $L = 2n+1$ having $h_i = 3$ at all sites. Now if a grain is dropped at the center then the resulting avalanche has the largest size with $n+1$ different concentric square shaped toppling zones and the avalanche size is proportional to L^3.

However when we collect a large sample of data for the avalanche sizes in the stationary state we hardly get an avalanche whose size equals the upper bound. Actually the avalanche size distribution decays much faster than the corresponding power law in Eqn. (1.7) at a cut-off size $x_c(L)$ and it depends on the system size as:

$$x_c(L) \sim L^{D_x}. \tag{1.12}$$

It is generally assumed that the avalanche size distributions in a finite size system obeys standard finite size scaling (FSS) [26, 27, 28] forms for any measure $x \in \{s, a, t, r\}$ as:

$$\text{Prob}(x, L) \sim x^{-\tau_x} \mathcal{F}_x(x/L^{D_x}), \tag{1.13}$$

where the scaling function $\mathcal{F}_x(y) \sim$ *constant* in the limit of $y \to 0$ and $\mathcal{F}_x(y)$ approaches zero very fast for $y \gg 1$. The critical exponents τ_x and D_x characterize the scaling of the distribution. D_x determines the cutoff value of the quantity x with system size L.

1.1.9 Moment analysis

To check the validity or violation of FSS exponents various moments of $\mathrm{Prob}(x, L)$ were evaluated [26, 27, 29]. The q-th moment is defined as

$$\langle x^q \rangle_L = \int x^q \mathrm{Prob}(x, L) dx \tag{1.14}$$

Assuming a power law behavior of the probability distribution for the whole accessible range of avalanche sizes, the q-th moment has the size dependence

$$\langle x^q \rangle_L \sim L^{D_x(q-\tau_x+1)} \tag{1.15}$$

In general one can write $\langle x^q \rangle_L \sim L^{\sigma_x(q)}$, where the exponent $\sigma_x(q)$ can be estimated from the slope of the $\log - \log$ plot of $\langle x^q \rangle_L$ as a function of L. Thus $\sigma_x(q) \sim D_x(q - \tau_x + 1)$ for $q > \tau_x - 1$ and $\sigma_x(q) = 0$ for $0 < q < \tau_x - 1$. If FSS hypothesis is correct one can compute D_x by calculating $d\sigma_x(q)/dq$ which takes the constant value D_x for large q. For very small values of q the behavior of $\sigma_x(q)$ is nonlinear with respect to q as the determination of $\sigma_x(q)$ is easily affected by finite size effects. Once the exponent D_x is computed the corresponding τ_x is obtained by an extrapolation to the horizontal axis. In case of Manna model this derivative of the exponent $\sigma_x(q)$ saturates quickly with increasing q indicating a constant D value [27] whereas for the BTW model the derivative is marked by a finite curvature which indicates that the exponent D is not well defined for this model.

1.1.10 Wave analysis

An important property of the sandpile avalanches is that they can be decomposed into waves of topplings [30, 31]. In other words an arbitrary avalanche can be considered as a superposition of a number of waves of topplings. These waves yields more informations about the structural details of the avalanche.

Waves of topplings are generated by adding one grain of sand at a given lattice site O, and allowing the site to relax. The first wave is the set of all toppled sites due to the toppling at the origin at O, while the origin is prevented from a second toppling. After the completion of the first wave if O is still unstable it is toppled for the second time and the second wave is allowed to propagate but a possible third toppling of O is prevented until the second wave is finished. The set of sites which toppled for the second time give the second wave of toppling. This process continues until the origin O becomes stable and the avalanche terminates. An interesting property of waves in the BTW model is that the set of lattice sites which topple has no holes. On the contrary for the Manna model this is no longer true. In this case the waves can have holes and can include sites which topple more than once.

Now if a set of a large number of avalanches is considered, each avalanche is decomposed its constituent waves and if all these waves are treated on the same footing then the wave sizes s, the number of sites visited by a wave, have a probability distribution which satisfies the following finite size scaling form:

$$\mathrm{P}_w(s, L) \sim s^{-\tau_w} f_w(s/L^{D_w}), \tag{1.16}$$

where f_w is a suitable scaling function. For BTW waves $\tau_w = 1$ and $D_w = 2$ in $d = 2$ [31] whereas the waves in Manna model obeys FSS with $\tau_w \approx 1.31$ and $D_w \approx 2.75$ [32].

A special set of avalanches in the BTW model consists of avalanches which start from the boundary having only one wave each whose size distribution obeys FSS with $D_w = 2$ and $\tau_w = 1.5$ [31].

It is also observed that the successive waves of topplings in an avalanche, and the whole set of waves in a series of successive avalanches are non-trivially correlated. If $\{s_1, s_2, s_3, ..\}$ constitute the time series of successive wave sizes the autocorrelation function of this series is defined by:

$$C(t, L) = \frac{\langle s_{k+t} s_k \rangle_L - \langle s_k \rangle_L^2}{\langle s_k^2 \rangle_L - \langle s_k \rangle_L^2} \tag{1.17}$$

where the expectation values refer to samples with different L. Recently it has been shown [32] that for the BTW model in $d = 2$ the autocorrelation function has long range correlations which approximately scales as

$$C(t, L) \sim t^{-\tau_c} g(t/L^{D_c}) \tag{1.18}$$

with $\tau_c \approx 0.40$ and $D_c \approx 1.02$, whereas for the Manna model the size of a wave is just uncorrelated as the autocorrelation function approaches 0 as soon as $t > 0$.

1.1.11 Some more sandpiles

• Directed sandpile model (DSM)

A simple but non-trivial and exactly solvable version of the sandpile model is the directed sandpile model [33, 34]. Here the sand grains are transported along a preferred direction. The directed ASM [33] was introduced to account for the fact that under gravity particle would only fall down. This model is simply defined on a 45^o oriented square lattice. Sand grains are added on the top edge with equal probability. On toppling one grain of sand is distributed to each of the two downward neighbors. Periodic boundary conditions is imposed in the horizontal direction. Particles can leave the system from the bottom. For DSM the distribution of avalanche size s varies as $s^{-\tau_s}$ for large s with $\tau_s = 4/3$ and the distribution of avalanche duration t varies as $t^{-\tau_t}$ with $\tau_t = 3/2$. Further the directed version of the two-state Manna sandpile model was studied and it was found that the set of critical exponents defines a different universality class [35, 36]. In a recent paper [37] several sandpile models with stochastic toppling rules is studied. Any grain arriving at a site during the avalanche process get stuck there with a certain nonzero probability. It is found in this paper that for models with a preferred direction, the avalanche exponents corresponds to those of critical directed percolation clusters, whereas for models without a preferred direction, avalanche exponents are those of directed percolation clusters in one higher dimension.

• Continuous energy model (CEM)

Zhang [38] had introduced a model where the energy E is stored at the lattice sites. An amount of energy δ which varies uniformly within $(0 < \delta < 1)$ is added at

randomly selected sites: $E_i \rightarrow E_i + 1$. When the energy at a site exceeds a threshold E_{max} an activation event occurs at i and the full amount of energy at this site is divided into $2d$ equal parts and transferred to the neighboring sites. The transferred energy in turn can excite further activations in their neighborhood resulting to an avalanche of successive activations. This model has power law distributions of the avalanche sizes like: $D(s) \sim s^{-\tau}$ and using some assumptions about compactness of avalanche clusters Zhang predicted $\tau = 2 - 2/d$ as well as the dynamical exponent $z = (d+2)/3$ in d-dimensions for $1 \leq d < \infty$. For $d = 2$ this value disagrees with the numerical estimate $\tau = 1.22$ obtained in [39, 40].

- **Critical slope model (CSM)**

In the critical slope model, the stability of a sand column depends on the local slope of the surface of the sandpile i.e. the first derivative of the height function [41]. When the local slope at a site along any of the neighboring directions exceeds a preassigned value z_c , the site topples. For example in [41] the toppling rule used is the following:

$$\text{If, } h_{i,j} - h_{i+1,j} \geq z_c, \text{ or } h_{i,j} - h_{i,j+1} \geq z_c, \text{ or } h_{i,j} - h_{i-1,j} \geq z_c, \text{ or } h_{i,j} - h_{i,j-1} \geq z_c \tag{1.19}$$

then the sand column at site (i, j) becomes unstable and topples. During the toppling the grain distribution rule is same as in BTW model. Outside the system the height is always maintained at zero. It is to be noted that CSM is a non-Abelian sandpile model [41].

- **Critical Laplacian model (CLM)**

In a similar way, in the critical Laplacian model the stability of a sand column depends on the local Laplacian i.e. the second derivative of the height function [41]. When the local Laplacian exceeds a preassigned value l_c the sand column topples. For example in [41] the toppling rule used is the following:

$$\text{If, } 4h_{i,j} - h_{i+1,j} - h_{i,j+1} - h_{i-1,j} - h_{i,j-1} \geq l_c \tag{1.20}$$

then the sand column at site (i, j) becomes unstable and topples. After toppling the dynamics is same as in the BTW model. CLM is also non-Abelian.

1.1.12 Universality of sandpile models

Though some efforts have been given towards the analytical calculation of different quantities of the Abelian sandpile model [22, 23] the exact values of the critical exponents of ASM are still not known. The numerical and mean-field values of the critical exponents of different sandpile models are listed in Table 1.1. In spite of extensive efforts over last several years it has been found that BTW model shows scaling anomalies. Numerical estimate of the exponents have yielded scattered values, for example, estimate of the exponent τ_s for ASM model in two dimensions ranges from 1.2007 [41] to 1.27 [42] and 1.293 [43] etc. It has been shown recently that the ASM obey a multi-scaling behavior [26, 29]. On the other hand the stochastic Manna

Model	Ref.	d	τ_s	τ_a	τ_r	τ_t	D_s	D_a
BTW	[41]	2	1.2007			1.313		
BTW	[42]	2	1.27				2.73	2.01
BTW	[43]	2	1.293	1.330	1.665	1.480		
BTW	[44]	3	4/3	4/3	2	8/5	3	3
BTW	[44]	4,5,6	3/2	3/2		2	4	4
Manna	[25]	2	1.28			1.47	2.75	
Manna	[42]	2	1.27				2.74	2.02
Manna	[43]	2	1.275	1.373	1.743	1.493		
DSM	[33]	d	4/3			3/2		
Zhang	[38]	d	$2(1-1/d)$					
Zhang	[43]	2	1.282	1.338	1.682			
CLM	[41]	2	1.288			1.508		

Table 1.1: Critical exponents of different sandpile models.

sandpile model is observed to be better behaved and there is good agreement of numerical values of its exponents determined in different investigations. Thus the issue whether the deterministic BTW model and the Manna model belong to the same universality class or not is not fully settled yet and has attracted much attention. A number of works [25, 42, 45, 46] claimed that they belong to the same universality class, whereas a number of other papers [27, 28, 43, 44, 47, 48] argued in favor of their universality classes being different. Real space renormalization group calculation [45, 46] suggested that different sandpile models like the BTW and the Manna model belong to the same universality class. Then universality was found between the discrete BTW model and the continuous Zhang model in the dynamical renormalization group calculations [49, 50]. Early stage numerical simulations of the Manna and BTW models show that the avalanche distributions are described by the same power law exponents and obey the same scaling [25]. Later Ben-Hur and Biham [47] analyzed the scaling of conditional expectation values [51] of various quantities and found significant differences in the exponents for the two models and predicted that Manna model belong to a different universality class from that of BTW model. This method was later applied to the Zhang model which was declared non-universal [48]. The moment analysis of the size distribution of the BTW and Manna sandpile model led Chessa et. al. [42] to the conclusion that both models are characterized by the same scaling exponents and thus belong to the same universality class but Lübeck showed that the moment behavior of both the BTW and the Manna model differ significantly [27]. Thus the precise identification of a key factor which may control the two behavior was absent before our works described in chapter 2.

1.2 Sandpile models on complex graphs

It was Dhar [23, 52] who first observed that the sandpile model can be defined on an arbitrary connected graph $\mathcal{G}$. Such a graph is defined in terms of two sets: $\mathcal{V}$ a set

	Networks	Nodes	Links
1.	Population	Individuals	Acquaintances
2.	Internet	Routers / Auto. Systems	Ethernet Cables
3.	World-Wide Web	Web pages	Hyperlinks
4.	Telephone Networks	Telephones	Calls
5.	Railway Networks	Stations	Trains
6.	Power Grids	Relay Stations	Transmission Lines
7.	Actor Networks	Actors	Movies
8.	Sports Persons	Players	Clubs
9.	Collaboration Networks	Authors	Joint Papers
10.	Citation Networks	Papers	Citations

Table 1.2: Examples of different real-world networks.

of N vertices $\{v_1, v_2, v_3, ..., v_N\}$ and another set $\mathcal{E}$ of L edges $\{e_1, e_2, e_3, ..., e_L\}$ such that each member of the set $\mathcal{E}$ corresponds to a pair of vertices in the set $\mathcal{V}$. On a connected graph one can go from one vertex to any other vertex by hopping through the edges. In a sandpile model defined on an arbitrary connected graph, unit grains of sand added at the vertices of the graph one by one. The threshold height H_i^c at each vertex i depends on the vertex i. Without the loss of generality H_i^c is made equal to the degree k_i of the vertex which is the number of edges meeting at this vertex. Some vertices of the graph are defined as the *sinks* which absorb grains and play the role of the boundary to ensure that the non-equilibrium steady state is reached.

Studying the properties of different types of complex graphs has attracted a lot of attention over the last couple of years. This is because the different types of complex networks are suitably represented by the complex graphs. Studying the properties of the associated graphs gives insight into the structural details, properties etc. of the related networks. There is a long list of real-world networks from diverse fields which are being looked into and studied by the network researchers which range from social to electronic to biological networks. A number of them are listed in Table 1.2.

The nodes (vertices) and the links (edges) can be identified for every network. For example, living systems form a huge genetic network whose nodes are proteins and genes and the chemical interactions between them represents links. A biological network showing protein-protein interactions in Baker's Yeast [53] is shown in Fig.1.4. Complex networks occur in social science where nodes are individuals or organizations and the links are the social interactions or mutual friendships between them [54, 55]. Communication systems like the Internet [56] is a complex network of routers or autonomous systems linked by various physical or wireless links. Study of the Internet's topological structure is important for designing efficient routing protocols and modeling Internet traffic. Other much studied network is movie actor collaboration network [57] in which the nodes are the actors and two nodes have a common edge if the corresponding actor has acted in a movie together. Similarly a collaboration network [58] was studied where the nodes are scientists and two nodes are connected if the two scientists have written an article together. Another com-

plex network studied is the citation network [59] where nodes are published articles and a directed link represents a reference to a previously published article. Citation networks are acyclic because papers can only cite other papers that have already been written, not those that have yet to be written. Besides this there are power grid network [57] where nodes are generators, transformers and substations and the links are high voltage transmission lines.

The topological size of a graph is measured by the 'diameter' of the graph. The distance between two vertices on the graph is the number of edges on the shortest path connecting the two vertices. The diameter $\mathcal{D}(N)$ of a graph $\mathcal{G}$ is the maximum of all shortest paths. Therefore though a graph has no spatial size, the diameter acts as a measure of its topological size.

The local correlations among the neighboring links are measured by the clustering co-efficient $\mathcal{C}(N)$. In real-world networks such correlations are observed to be more than the corresponding random graphs of same number of vertices and edges. For example, it is likely that A and C are friends if both of them are friends of B. If n_i is the number of edges within the k_i neighbors of i then the clustering co-efficient $\mathcal{C}_i$ of the i-th vertex is $n_i/\{k_i(k_i-1)/2\}$. Clustering co-efficient of the whole graph is average of $\mathcal{C}_i$ over all vertices.

The simplest of all types of complex graphs are the Random graphs introduced by Erdös and Rényi [60]. A random graph has N vertices and between every pair of vertices there exists an edge with probability p and the vertices remain unconnected with probability $1-p$. The degree distribution of such graphs for large N is Poissonian as:

$$P(k) = e^{-\langle k\rangle}\langle k\rangle^k/k! \tag{1.21}$$

A *Small-World Network* (SWN) has a very small diameter but large clustering coefficient:

$$\langle \mathcal{D}(N)\rangle \sim \log N \qquad \text{and} \qquad \mathcal{C}(N) \sim 1. \tag{1.22}$$

It has been observed that most of the real-world networks have small diameters reflecting the efficiency of the networks as well as the high value of the clustering coefficient reflecting local correlations among the links. Watts and Strogatz showed that a regular network which has large diameter and large clustering coefficient crosses over to a small-world network on rewiring the edges with a 0+ probability [57, 61].

1.2.1 Scale-free networks (SFN)

The inhomogeneity and complex nature of the real-world networks is also measured by the degree distribution $P(k)$. It has been observed that unlike random graphs many real-world networks are highly inhomogeneous and their nodal degrees follow power law distributions:

$$P(k) \sim k^{-\gamma}. \tag{1.23}$$

World Wide Web [62] which is a network of webpages(nodes) and the hyperlinks(links) among various pages and the internet network [56] of routers or autonomous systems are examples of SFNs. Due to the absence of a characteristic value for the degrees, these networks are called scale-free networks (SFN) and the exponent γ varies between 2 and 3 for these real-world networks.

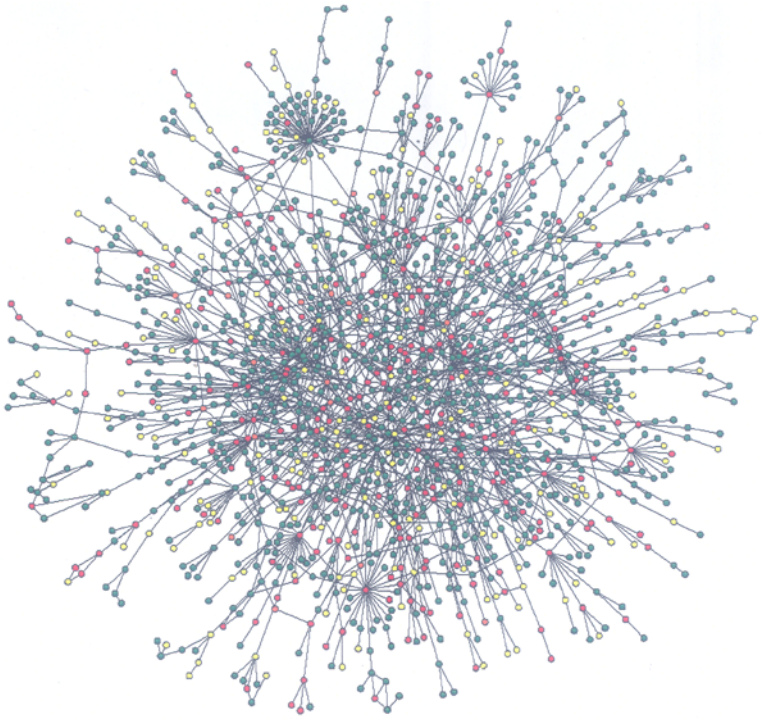

Figure 1.4: Baker's Yeast by Hawoong Jeong, Ref: http://www.nd.edu/ networks/gallery.htm, see [53].

1.2.2 Barabási-Albert model

Barabási-Albert (BA) proposed a simple model for an evolving SFN that has the following two essential criterion-

i. A network grows from an initial set of m_0 nodes with $m < m_0$ links among them. Further, at every time step a new node is introduced and is randomly connected to m previous nodes.

ii. Any of these m links of the new node introduced at time t connects a previous node i with an attachment probability $\pi_i(t)$ which is linearly proportional to the degree $k_i(t)$ of the ith node at time t,

$$\pi_i^{BA}(t) \sim k_i(t) \tag{1.24}$$

For the BA model $\gamma = 3$ [63].

The diameter $\mathcal{D}(N)$ of the BA graphs grow logarithmically as $\log N$ like small-world networks, whereas the clustering coefficient of the BA model decreases with the network size, following approximately a power law $\mathcal{C}(N) \sim N^{-0.75}$, which decays slower than the $\mathcal{C}(N) \sim N^{-1}$, observed for random graphs, is still different from the behavior of the small-world models, where $\mathcal{C}(N)$ is independent of N.

1.3 Fixed energy sandpile (FES)

Many non-equilibrium systems show transitions between 'active' and 'absorbing' states: examples are directed percolation [64], the depinning of interfaces in quenched disorder [65] etc. Sandpile models in the Self-organized Criticality in infinitely large system sizes possess an infinite number of absorbing configurations. Under an external drive of repeated particle inputs the system jumps from one absorbing configuration to another via avalanche like rearrangements.

In Fixed Energy Sandpile [66, 67, 68] the sandpile model is defined on a closed system of size L with periodic boundary conditions along all independent directions.

Here the rules for sandpile dynamics remain same but there is neither any external driving nor any boundary dissipation. As the system is closed, its total mass of N grains is conserved which is fixed by the initial condition and the mass density i.e., the number of grains per site $\zeta = N/L^d$ is used as a tuning parameter, where d is the dimension of the lattice. If ζ is large enough, the system reaches a stationary state with sustained activity i.e. it is in the active phase. On the other hand for small values of ζ, the system relaxes with probability one into a frozen configuration, i.e. it is in the absorbing phase. In between these two regimes there exists a critical point at $(\zeta = \zeta_c)$ separating an absorbing phase from an active phase.

In the FES model the system initially starts with ζL^d particles distributed among the L^d sites yielding a distribution that is spatially homogeneous and uncorrelated. The order parameter is the stationary average density of active sites ρ_a, which equals zero for $\zeta < \zeta_c$, and follows a power law $\rho_a \sim (\zeta - \zeta_c)^\beta$ for $\zeta > \zeta_c$. The correlation length ξ and relaxation time τ both diverges as $\zeta \to \zeta_c$, their critical behavior is characterized by the exponents $\nu_\perp$ and $\nu_\parallel$, defined via $\xi \sim |\zeta - \zeta_c|^{-\nu_\perp}$ and $\tau \sim |\zeta - \zeta_c|^{-\nu_\parallel}$ respectively. The dynamical critical exponent is defined via $\tau \sim \zeta^z$ which implies $z = \nu_\parallel/\nu_\perp$. In BTW FES model the activity was found to show a step like behavior for increasing energies [69]. It has been found that systems showing continuous absorbing state transitions in absence of a conservation law fall generically into the universality class of directed percolation [70, 71]. It has been claimed that FES with stochastic dynamics belongs to a new universality class of absorbing phase transition in which the activity is coupled to a static conserved field [66]. Further it was found in [67] that the Manna and BTW FES models shows critical exponents different from those of DP. The Manna FES in $2 - d$ was claimed to belong to the universality class of linear interface depinning [67] while $1 - d$ Manna FES belong to a new universality class different from linear interface depinning and from that of directed percolation [68]. BTW FES showed a violation of simple scaling and showed several anomalies associated to non ergodic effect in its dynamics [67]. FES was claimed to belong to a new universality class.

1.4 PART II: Conduction in sedimentary rocks

Rocks, in general, particularly sedimentary rocks e.g. sandstones, limestones etc., have a pore structure which is a highly branched and interconnected network. This connected pore space plays a very important role in transport properties like conductivity and permeability in rocks, where the brine solution filling up the pore-space

is responsible for transport. Thus the study of the pore structure of sedimentary rocks is important in problems such as oil-exploration, ground water flow, spread of pollutants etc. An interesting property of these rocks is that they appear not to have a finite percolation threshold [72]. When the pore space of these rock materials is saturated with salt water, they become conducting even when the porosity is less than one percent.

Several empirical laws reflect this property. Archie's law [73] connects the electrical conductivity of brine filled rocks $\sigma(\phi)$ and the porosity ϕ i.e., the volume fraction of the void space in the following way:

$$\sigma(\phi)/\sigma_w = a\phi^z \tag{1.25}$$

Here, σ_w is the conductivity of water, $a \sim 1$ is an empirical parameter and $z \sim 2$ is a non-universal exponent that depends on characteristics of the rock structure. This law suggests that a finite conductivity persists even in the limit of $\phi \to 0$ and therefore the percolation threshold is zero.

Another empirical law known as the Kozeny equation [74] relates the permeability $K(\phi)$ of the rock structure to the porosity ϕ through a similar power law,

$$K(\phi) = c\phi^{z'}/S_o^2 \tag{1.26}$$

where, $z' \approx 3$, S_o is the specific surface area and c is an empirical constant. This equation also suggests that the pore space is connected in the $\phi \to 0$ limit. The permeability of rock structure is defined as the velocity of the fluid per unit pressure gradient times the viscosity of the fluid. This is known as Darcy's law [75, 76].

1.4.1 Diagenesis

Granular materials undergo a restructuring process in nature over a geological time scale from an unconsolidated, high porosity packing to a more consolidated less porous structures. This is known as diagenesis. Formation of sedimentary rocks start with sedimentation of sand grains under water or in air [77, 78, 79] giving an highly porous $\sim 40-50\%$ sediment. Sedimentation is followed by compaction under pressure and diagenesis [80, 77] and finally a consolidated sandstone is formed.

The final characteristic of the pore network depends strongly on the diagenetic process. Depending on the nature of the pore-filling fluids, deposition of salts may take place as crystallites in the crevices or along the pore walls by a process called "cementation". Otherwise, portions of the existing solid structure may get eroded or dissolved out in a "dissolution" process. The former decreases the porosity of the rock while the latter increases porosity. The two processes may take place simultaneously. The details of the chemical nature of the solid and pore filling fluid determines whether diagenesis leads finally to a stable structure, or to a continuously developing structure eventually giving rise to caverns of macroscopic size.

Sahimi had classified the theoretical studies of modeling diagenesis in two ways [79]. The approach of "chemical modeling" deals with reaction kinetics and mass transfer ignoring the morphology of pore space. The second approach is "geometrical modeling" which deals with the geometrical descriptions of initial unconsolidated pore space which evolves under simple rules leading to reduction of porosity but maintaining the connectivity [77].

Wong et al. [81] in 1984 proposed the bond shrinkage model where they consider a random resistor network on a simple cubic lattice. Each bond of the lattice represents a fluid filled cylindrical tube of uniform radius. By random bond shrinkage mechanism, a bond of the network is randomly selected and its radius is reduced by a constant factor. This mechanism will simultaneously reduce the porosity and the conductivity of the network. The model maintains the network connectivity even in the limit of $\phi \rightarrow 0$ and reproduces Archie's law and the Kozeny equation.

Roberts and Schwartz [82] in 1985 proposed a geometrical model for diagenesis in sedimentary rocks. They used Bernal distribution i.e. the coordinates of dense random identical spheres of equal radii for the location of the particle centers. The spheres are allowed to expand simultaneously which reduces the porosity. The porosity and the resistivity of the material are determined as a function of the radius. This model give rise to a percolating threshold of $\phi_c \approx 3.5\%$.

Tarafdar and Roy in 1998 [83] simulated a porous rock structure by ballistic deposition of grains of two different shapes ($1 \times 1 \times 1$ and $2 \times 1 \times 1$). These grains are dropped on a cubic lattice with certain probability. On such modeled porous structure they calculated the electrical conductivity using a parallel resistor network and permeability using the Kozeny relation. They reported a transition in the linearity of Kozeny relation at a porosity value of about 25%. But this paper does not address the problem of diagenesis.

Chapter 2

Precise toppling balance, quenched disorder, and universality for sandpiles

2.1 Introduction

Accurate determination of the critical exponents and thereby precise distinction of critical behaviors among the different universality classes are always regarded as very important tasks in the field of critical phenomena since this analysis helps in understanding as well as identification of the crucial factors that determine the critical behaviors. This problem however is still open in the phenomenon of Self-organized criticality in spite of extensive research over last several years. More precisely, in the sandpile model of SOC the question if the two very important models namely the deterministic model by Bak, Tang and Wiesenfeld [8, 22] and the stochastic Manna sandpile [25] belong to the same universality class or not has not been fully settled yet.

In spite of extensive efforts over last several years it has been found that BTW model shows scaling anomalies. Numerical estimate of the exponents have yielded scattered values, for example, estimate of the exponent τ_s for ASM model ranges from 1.2 [41] to 1.27 [42] and 1.29 [43]. It has been shown recently that the ASM obey a multi-scaling behavior [26, 29]. On the other hand the stochastic Manna sandpile model is believed to be better behaved and there is good agreement of numerical values of its exponents determined by different investigations.

A number of works [25, 42, 45, 46] claimed that they belong to the same universality class, whereas a number of other papers [27, 28, 43, 44, 47, 48] argued in favor of different universality class.

- Real space renormalization group calculation [45, 46] suggested that different sandpile models like the BTW and the Manna model belong to the same universality class. Then universality was found between the discrete BTW model and the continuous Zhang model in the dynamical renormalization group calculations [49, 50].
- Early stage large scale numerical simulation of the Manna and BTW models show that the avalanche distributions are described by the same power law exponents and obey the same scaling [25].
- Later Ben-Hur and Biham [47] analyzed the scaling of conditional expectation val-

(a)

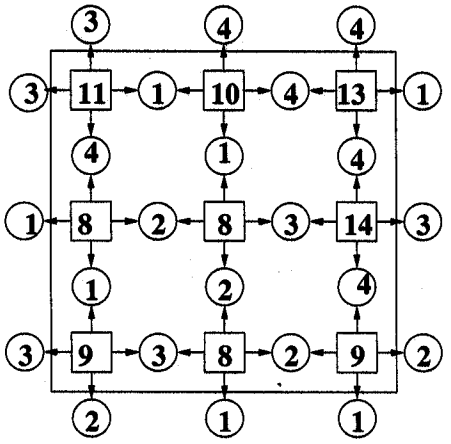

(b)

11	-1	0	-4	0	0	0	0	0
-1	10	-4	0	-1	0	0	0	0
0	-4	13	0	0	-4	0	0	0
-4	0	0	8	-2	0	-1	0	0
0	-1	0	-2	8	-3	0	-2	0
0	0	-4	0	-3	14	0	0	-4
0	0	0	-1	0	0	9	-3	0
0	0	0	0	-2	0	-3	8	-2
0	0	0	0	0	-4	0	-2	9

Figure 2.1: (a) Random grain flow distribution along the bonds of a 3×3 square lattice for the undirected model, and (b) the corresponding toppling matrix is shown.

ues [51] of various quantities and found significant differences in the exponents for the two models and predicted that Manna model belongs to a different universality class from that of BTW model. This method was later applied to the Zhang model which was declared non-universal [48].

• The moment analysis of the size distribution of the BTW and Manna sandpile model led Chessa et. al. [42] to the conclusion that both models are characterized by the same scaling exponents and thus belong to the same universality class.

• Lübeck showed that the moment behavior of both the BTW and the Manna model differ significantly [27].

To summarize, the status of the debating issue if BTW and Manna sandpile models belong to the same universality class or not is the following. Though it was possible to calculate several quantities analytically in both the models, exact determination of the critical exponents characterizing the avalanche size distributions have not been possible yet. On the other hand it has been realised that BTW model is very difficult to tackle numerically. It refuses to obey the finite size scaling hypothesis mainly in two ways: (i) the slope of the $\log \text{Prob}(s, L)$ vs. $\log s$ plot shows a systematic variation with the system size L in the range of small to intermediate avalanche size regime and also (ii) the tail of the distribution corresponding to the large avalanches which see the finiteness of the system falls increasingly slowly with increasing the system size. As a result of these two factors, the avalanche size distribution data for the BTW sandpile refuses to scale for the different system sizes. For the stochastic Manna sandpile the situation is much more well behaved. Finite size scaling works very well in this case and the critical exponents have been estimated with reasonably good accuracies.

It may be observed that all these efforts devoted to the issue if BTW and Manna sandpile models belong to the same universality or not are numerical. No theoretical argument have been put forward to understand the difference or similarity if any. It may also be observed that not even a single key factor has been possible to identify which may control the two possibly different behaviors.

In two recent papers [84, 85], we have been able to identify a simple crucial factor

(a)

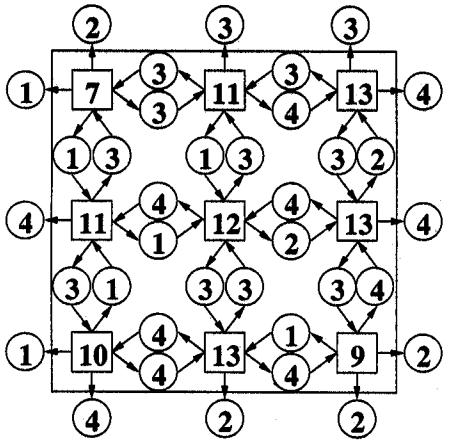

(b)

7	-3	0	-1	0	0	0	0	0
-3	11	-4	0	-1	0	0	0	0
0	-3	13	0	0	-3	0	0	0
-3	0	0	11	-1	0	-3	0	0
0	-3	0	-4	12	-2	0	-3	0
0	0	-2	0	-4	13	0	0	-3
0	0	0	-1	0	0	10	-4	0
0	0	0	0	-3	0	-4	13	-4
0	0	0	0	0	-4	0	-1	9

Figure 2.2: (a) Random grain flow distribution along the bonds of a 3×3 square lattice for the directed model, and (b) the corresponding toppling matrix is shown.

that controls the two different behavior.

In this chapter we describe our works in [84, 85] where a single sandpile model with quenched random toppling matrices captures the crucial features of the different sandpile models. With the associated symmetric toppling matrices avalanche statistics falls in the multiscaling BTW universality class. In the asymmetric case the simple scaling of the Manna model is observed. The presence or absence of a precise toppling balance between the amount of sand released by a toppling site and the total quantity of sand the same site receives when all its neighbors topple once, determines the appropriate universality class. In §2.2 we describe our model, in §2.3 we discuss the precise toppling balance condition, in §2.4 we discuss the numerical results for our model, in §2.5 we discuss how the kinetic self avoiding trail is used to maintain the precise toppling balance and finally we conclude in §2.6.

2.2 The model

The grain flow field in the BTW model is a constant and has no variation along the lattice bonds. This means that across an arbitrary bond if the sand column at either of its end site topples, only one grain flows through this bond to the other end.

In our present model we assumed a random field for the grain flow distribution along the bonds. More specifically the number of grains that flows through a bond when there is a toppling at one end is a quenched random variable. Non-zero values of these flow rates are assigned initially and they remain invariant throughout the sandpile dynamics. In terms of the toppling matrices $-\Delta_{ij}$ grains flow to the site j when there is a toppling at the site i. Before the sandpile is constructed the elements of the Δ matrix are randomly assigned negative integers $-1, -2, .., -m$, m being a positive integer parameter and $\Delta_{ij} = 0$ for $|i - j| > 1$. The diagonal elements Δ_{ii} are chosen to be equal to $-\sum_{j \neq i} \Delta_{ij}$. Thus the different elements of Δ matrix values remain fixed for the full samples of avalanches for one realization. As usual the avalanche statistics is collected and averaged for many such independent

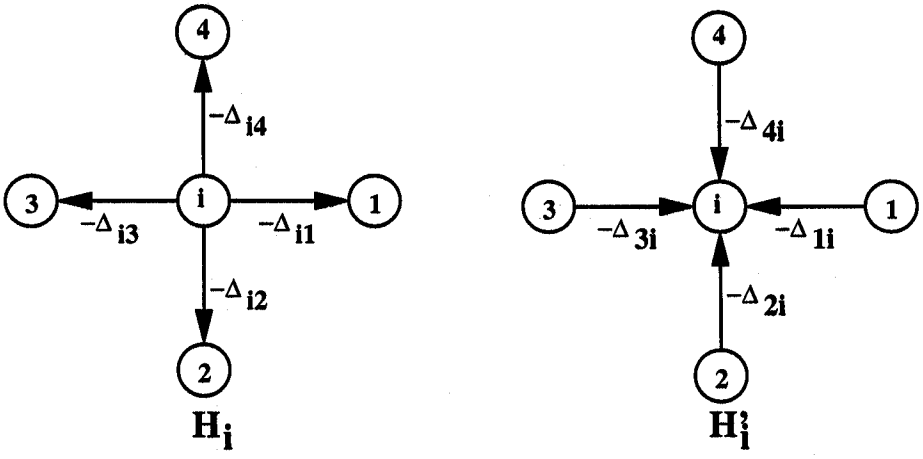

Figure 2.3: The out degree $H_i = -\sum_{j\neq i}\Delta_{ij}$ is pictorially represented by the four outgoing arrows and associated elements of the toppling matrix Δ whereas the in degree $H_i' = -\Sigma_{j\neq i}\Delta_{ji}$ is represented by the four incoming arrows with associated matrix elements.

realizations.

Two different sandpile models have been studied depending on the detailed type of the quenched randomness on a square lattice. In the first type which we call the 'undirected quenched sandpile model' each bond of a square lattice is assigned only one random integer which denotes the number of grain flow in either direction during toppling. The corresponding TM in this case is symmetric i.e. $\Delta_{ij} = \Delta_{ji}$. In Fig.2.1(a) we show the random but symmetric grain flow along the bonds of a 3×3 square lattice for the undirected model and the corresponding toppling matrix is shown in Fig.2.1(b). On the other hand for the directed model both Δ_{ij} and Δ_{ji} are assigned independently drawn random integers [84]. The corresponding TM in this case is asymmetric. In Fig.2.2(a) we show the asymmetric grain flow along the bonds of a 3×3 square lattice for the directed model and the corresponding toppling matrix is shown in Fig.2.2(b). Irrespective of whether Δ is symmetric or not, both the directed and undirected model are Abelian and therefore possess properties similar to the stationary state, recurrent configurations, etc. of the ASM [23].

2.3 Precise toppling balance

At any site of the lattice we defined the threshold height for stability of the sand column at that site as $H_i = \Delta_{ii} = -\sum_{j\neq i}\Delta_{ij}$. Thus H_i denotes the total number of grain flowing out of the site i during its toppling and we also called this as the out degree of the site i (Fig.2.3) . Further we also defined a quantity called $H_i' = -\Sigma_{j\neq i}\Delta_{ji}$ which denotes the total number of grains received by the site i when its every neighbor j topple for once. In a similar way we call H_i' as the in degree of the site i (Fig.2.3). We argue that at all sites except for those on the boundary if the condition of precise balance:

$$H_i = H_i' \tag{2.1}$$

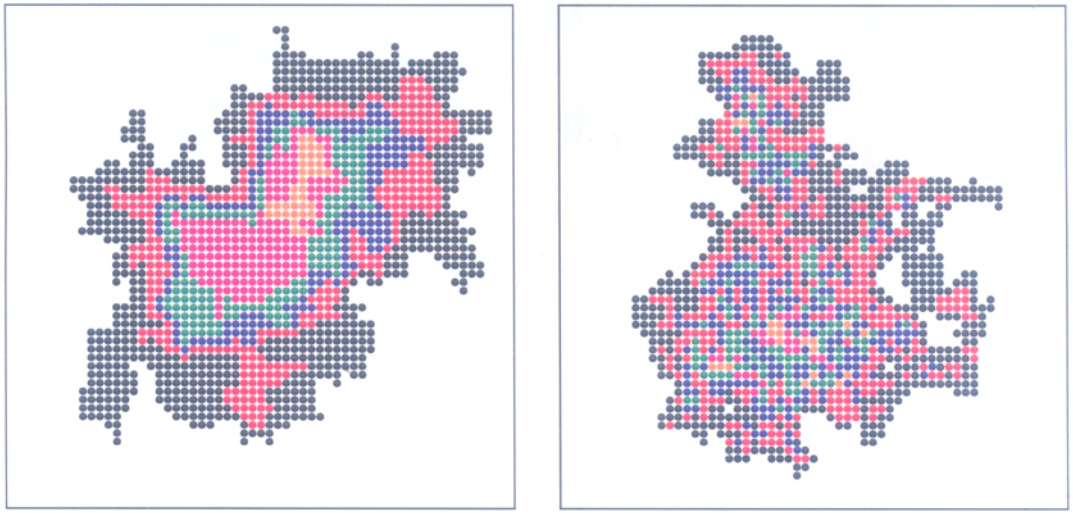

Figure 2.4: Multiply toppled sites within the avalanches are shown by circles of different colors: 1(black), 2(red), 3(blue), 4(green), 5(magenta) and 6(orange) for the (a) undirected model and (b) directed model.

is satisfied then the model belongs to the BTW universality otherwise it belongs to the Manna universality class.

It is to be noticed that in case of undirected model the precise toppling balance is maintained at all sites except at the boundary sites, on the other hand for the directed model this precise balance is absent in general.

2.4 Results and analysis

Different properties of the two models are studied and compared with BTW and Manna models in the three following ways:

2.4.1 Avalanche structures

The structure of avalanches in the undirected model are found to be very similar to those in the BTW model. The validity of the precise balance equation (2.1) ensures that there cannot be any hole (a set of sites which have not toppled at all) within the avalanches of this model similar to the BTW sandpile avalanches. For example, a single untoppled site can not be fully surrounded by toppled sites. Indeed, in the undirected model the equality $H_i = H_i'$ is strictly maintained at all sites except at the boundary, which implies that a site must topple irrespective of its height, if all its neighbors topple once. Moreover, similar to the BTW sandpile avalanches again, the n-th toppling zone (the set of sites which have toppled n times) is a set of sites connected by nearest neighbors and is completely surrounded by the $(n-1)$-th toppling zone. As n increases the corresponding toppling zone comes closer to the origin. The origin contains the maximally toppled zone and is situated at the boundary of this zone. All these properties are very similar to the BTW sandpile avalanches.

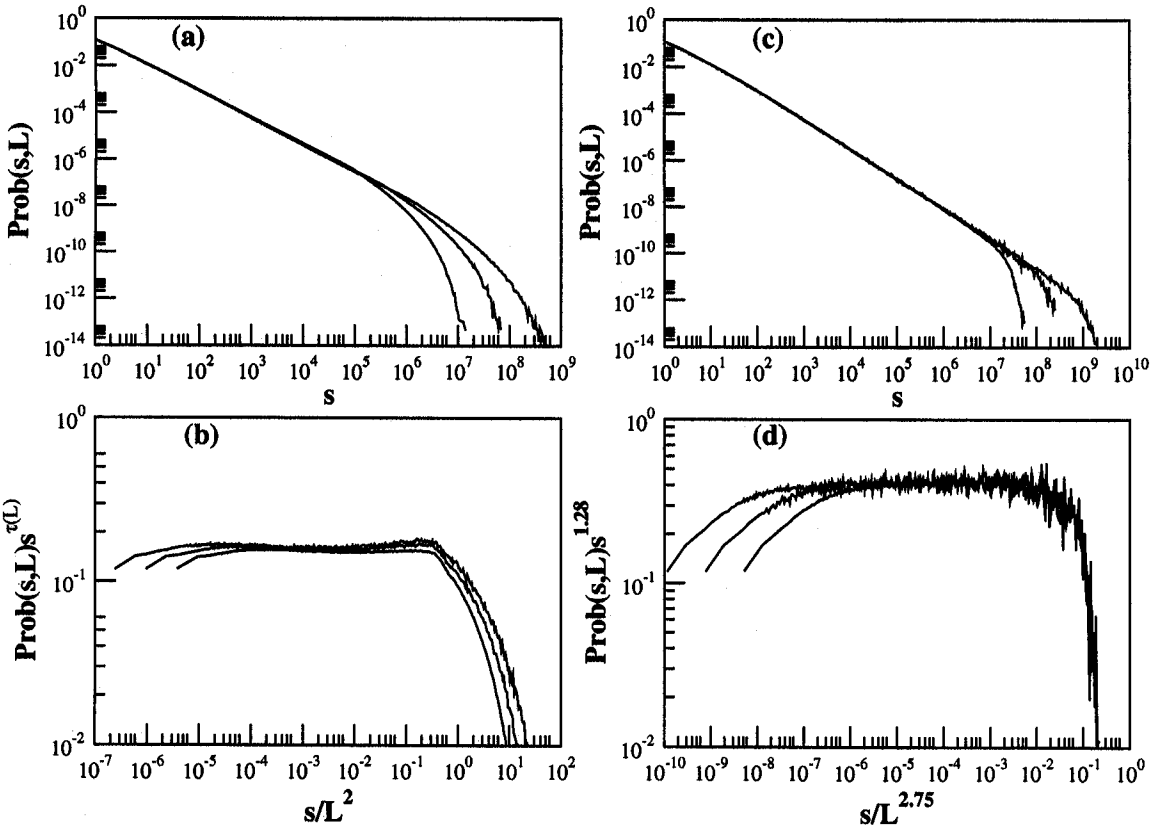

Figure 2.5: For the undirected model (a) the avalanche size distribution Prob(s, L) vs. s for system sizes $L = 512$, 1024 and 2048, (b) shows an attempt of scaling with $\tau(L) = 1.13$, 1.145 and 1.15 for $L = 512$, 1024 and 2048 respectively. Similarly for the directed model (c) shows the avalanche size distribution data for $L = 1024$, 2048 and 4096 and (d) shows a scaling of Prob$(s, L)s^{1.28}$ vs. $s/L^{2.75}$.

All these are not true anymore for directed model. In this case the avalanches can have holes without any restriction of size. Sites which have toppled same number of n times do not necessarily form a connected set of sites, actually these sites are scattered throughout the avalanche and form disconnected small clusters. Indeed, in the directed model, $H_i \neq H_i'$ in general and a site with $H_i > H_i'$ does not topple even if all its neighbors topple once. This creates a single site hole in the avalanche. On the other hand, if a site i has out degree sufficiently smaller than its in degree, it may topple for the second time even if none of its neighbors have toppled for the second time. Thus, all these properties of the avalanche structures of the directed quenched sandpile are very similar to avalanche structures in the Manna model.

The compactness and uniformity of waves in the undirected model leads us to expect for them and for the resulting avalanches a structure similar to that of the BTW model (Fig.2.4(a)). The non-uniformity introduced by disorder should not be relevant at large scales when one counts toppling events. The situation is quite different for the directed model: the structures of waves and of avalanches in this case (Fig.2.4(b)) look in fact similar to those of the Manna model [32] where the numbers of grains transmitted upon in the two directions of a given bond are differ-

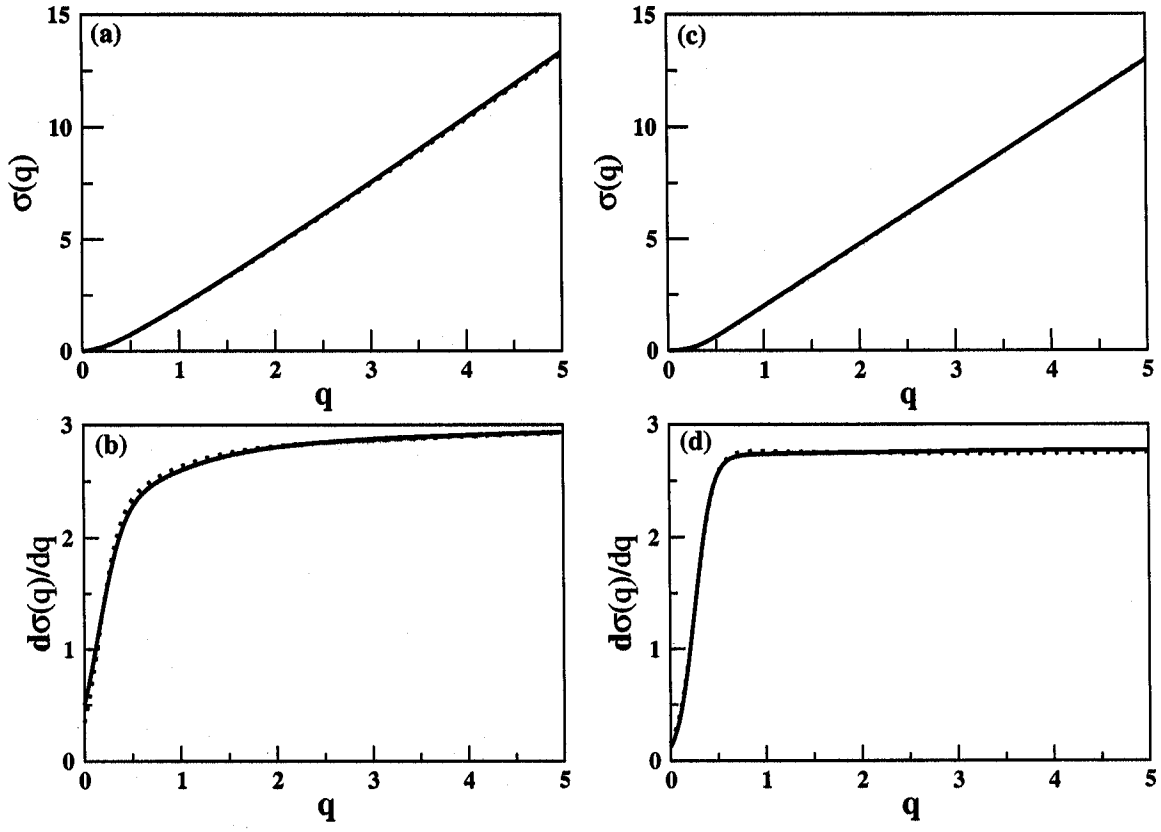

Figure 2.6: (a) Plot of $\sigma(q)$ vs. q for the BTW (solid line), undirected (dotted line) models. (b) Comparison of $d\sigma(q)/dq$ vs. q plots between BTW (solid line) and undirected (dotted line) models. (c) Plot of $\sigma(q)$ vs. q for the Manna (solid line), directed (dotted line) models and (d) comparison of $d\sigma(q)/dq$ vs. q plots between Manna (solid line) and directed (dotted line) models.

ent in general, and this imbalance is maintained dynamically due to the stochastic distribution of sand grains.

2.4.2 Avalanche size distributions and multi-fractal analysis

In the BTW model, the probability distribution Prob(s, L) of the total number of topplings, s, in an avalanche has been found recently to obey a multi-scaling ansatz [26, 29]. On the other hand, it is pretty well established [27] by now that in the Manna stochastic sandpile this distribution obeys simple FSS as:

$$\text{Prob}(s, L) \sim s^{-\tau} f(\frac{s}{L^D}), \tag{2.2}$$

where the scaling function $f(x) \sim$ *constant* in the limit of $x \to 0$ and $f(x)$ approaches zero very fast for $x >> 1$. The exponent τ and the dimension D fully characterize the scaling of Prob in this case. One immediate way to check validity of Eqn. (2.2) is to attempt a data collapse by plotting s^{τ}Prob vs. s/L^D with trial values of the exponents. We collected extensive data for both our models ($m = 4$) for $L = 128$, 256, 512, 1024, 2048 and 4096, namely 50 million avalanches in 500

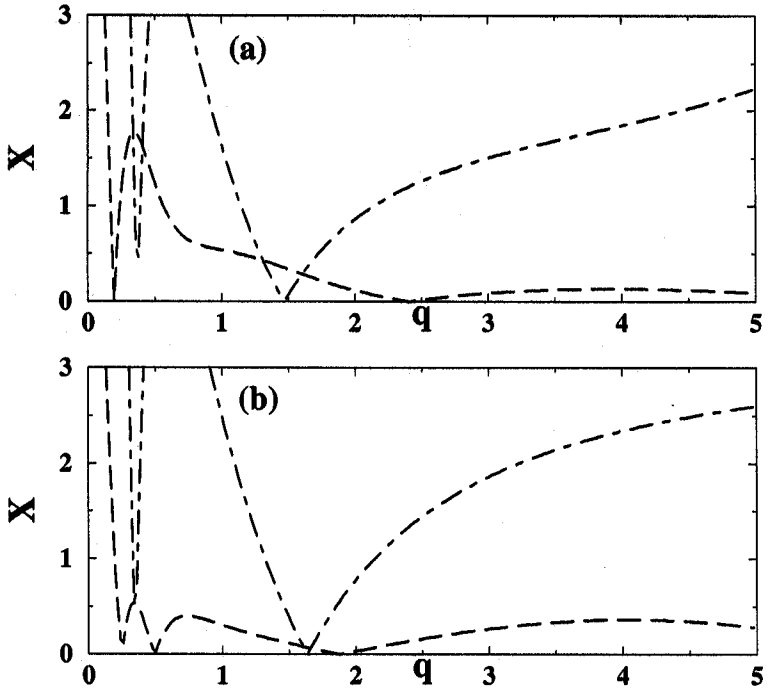

Figure 2.7: (a) The deviations $X_{BTW,undir}$ (dashed) and $X_{BTW,direc}$ (dot-dashed) are plotted with 40 times magnification. (b) Similar $X_{Manna,direc}$ and $X_{Manna,undir}$ are plotted with same magnifications.

independent configurations for $L = 128$ down to ≈ 1.1 million avalanches for 9 configurations for $L = 4096$ skipping first $\approx 4L^2$ avalanches to reach the steady state. For the undirected model, similar to the BTW model, the collapse does not work for a single set of τ and D and for all values of s and L (Fig.2.5 (a) & (b)). For the directed case collapse works very nicely giving $\tau \approx 1.28$ and $D \approx 2.75$ (Fig.2.5 (c) & (d)), close to the most reliable estimates of the Manna sandpile exponents [27].

A more reliable and quantitative check of the validity, or violation, of FSS, is based on the evaluation of the various moments of Prob [26, 27, 29]. The q-th moment is defined as $\langle s^q \rangle = \int s^q \text{Prob}(s, L) ds$. Assuming that FSS holds, it is easy to show that $\langle s^q \rangle \sim L^{\sigma(q)}$ with the moment exponent given by $\sigma(q) = D(q - \tau + 1)$ for $q > \tau - 1$ and $\sigma(q) = 0$ for $0 < q < \tau - 1$. In the case of multi-scaling σ should have a nonlinear dependence on q. A comparison of $\sigma(q)$ is also a key to establish if different sandpile models belong to the same universality class, or not. The value of $\sigma(q)$ is determined from the slope of the plot of $\log\langle s^q(L)\rangle$ vs. $\log L$ for $L = 1024$, 2048 and 4096 with an error ≈ 0.01 and for 251 values of q between 0 and 5 (Fig.2.6). The derivative of σ is determined by the finite difference method. Slow but monotonic increase of $d\sigma(q)/dq$ with q clearly indicates the multi-scaling in BTW as well as in undirected models (Fig.2.6(a) & (b)) where as a saturation of $d\sigma(q)/dq$ indicates a FSS in Manna and in directed models (Fig.2.6(c) & (d)).

To measure the deviation quantitatively we define a quantity

$$X_{a,b} = 2\frac{|(d\sigma(q)/dq)_a - (d\sigma(q)/dq)_b|}{(d\sigma(q)/dq)_a + (d\sigma(q)/dq)_b}. \tag{2.3}$$

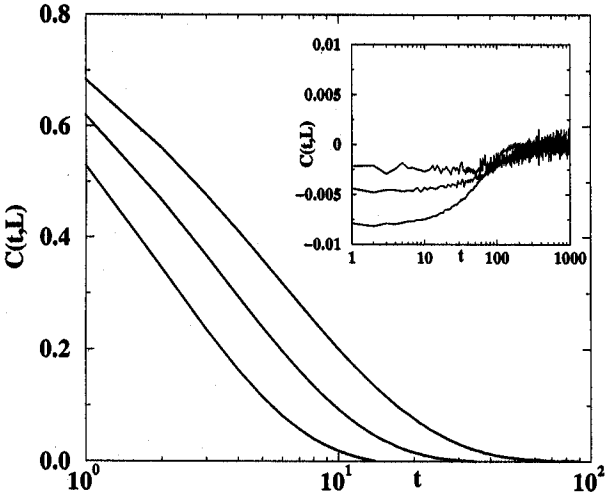

Figure 2.8: Autocorrelation function of the wave time series of the undirected and the directed (inset) sandpile in the inset for L=128, 256 and 512.

It is observed that after some initial fluctuations $X_{BTW,undir}$ has a maximum value 0.33% within q=2 and 5 whereas $X_{BTW,direc}$ gradually increases to 5.5 % at q =5 (Fig.2.7(a)). This analysis implies that undirected model is almost negligibly different from the BTW model in the $d\sigma(q)/dq$ vs. q plot where as the deviation of directed model from BTW model is much larger and gradually increases with q. Similarly $X_{Manna,direc}$ is limited within 0.91 % whereas $X_{Manna,undir}$ gradually increases to 6.5 % at q =5 (Fig.2.7(b)), which also implies that directed model is very similar to the Manna model but much different from the BTW model. The above described results concerning X for the various couples of models are altogether strongly supporting the conclusion that while the directed model belongs most likely to the Manna universality class, the undirected one has the multi-scaling features known to be peculiar of the standard BTW sandpile.

2.4.3 Wave analysis

By decomposing a large sequence of successive avalanches into waves in the undirected and directed cases, we obtained global wave size distributions which obey FSS with the exponents expected for the BTW model [31] and the Manna model [32], respectively. For the BTW sandpile globally sampled waves have a size distribution with a form as in Eq. (1.16), with $\tau_w = 1$ and $D_w = 2$. In the case of the Manna stochastic sandpile, waves can not be defined as in the deterministic Abelian sandpiles, but a wave-like decomposition was proposed in Ref. [32]. The global size distribution of the corresponding waves obeys FSS with the same exponents obtained for the avalanche distribution [32]. As already remarked above, waves can be consistently defined [22] in the same way for each quenched disorder realization of our directed and undirected models. The global wave scalings obtained here further support the expectation that they fall in the Manna and BTW universality classes, respectively.

Further insight into the different behaviors of the directed and undirected mod-

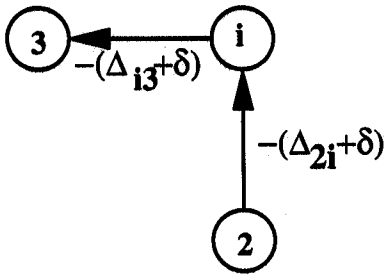

Figure 2.9: If Δ values of an incoming bond as well as an outgoing bond of an arbitrary site i are increased by the same amount δ, the precise balance $H_i = H_i'$ remains unaltered at the site i.

els can be obtained by analyzing the wave time series $\{s_1, s_2, s_3, ..\}$ of the sizes of successive waves as in ref. [32]. In Fig.2.8 we plot the autocorrelation function:

$$C(t,L) = \frac{\langle s_{k+t}s_k\rangle_L - \langle s_k\rangle_L^2}{\langle s_k^2\rangle_L - \langle s_k\rangle_L^2} \tag{2.4}$$

where the expectation values refer to samples with different L and include quenched disorder averaging. The plots in Fig.2.8 are fully consistent with similar ones for the BTW and Manna sandpiles [32]. While in the directed case the autocorrelation function is essentially zero as soon as $t > 0$, in the undirected model it grows steadily with L, and approximately scales as $C(t,L) \sim t^{-\tau_c}\mathcal{G}(t/L^{D_c})$ with $\tau_c \approx 0.35$ and $D_c \approx 1$. These exponents should be compared to 0.40 and 1.02, respectively, as determined for the BTW model [32]. This long range autocorrelation must be a consequence of the coherent and uniform spatial structure of each wave in the undirected case. In the directed model correlations are destroyed by the much more irregular pattern of topplings, with inhomogeneities and holes, in each wave. The correlation patterns show marked self-averaging, being reproducible on the basis of very few disorder realizations.

2.4.4 Summary of [84]

The local out/in degree balance $H_i = H_i'$ at all sites in the undirected model is essential for the BTW multi-scaling behavior to prevail. Numerically, with quenched disorder realization as described above, we find that the density of unbalanced sites with $H_i \neq H_i'$ in the directed model is around 0.88 and those of the sites with $H_i' > H_i$ and $H_i' < H_i$ are equal to 0.44. Now we ask if there is any critical density of unbalanced sites which demarcates the behaviors of the undirected and directed models. To study this we first generated an asymmetric TM in which the fraction of the bonds with unequal Δ values is found to be ≈ 0.75. We tuned this fraction, and thus the density of unbalanced sites, by randomly selecting these bonds and making their Δ values equal by assigning a random integer number between -1 and $-m$. We find that even the presence of as low as 5 percent bonds with unequal Δ values is sufficient to destroy the multi-scaling and to ensure FSS as in the directed model. Thus, as soon as precise toppling balance is broken, FSS holds, and the

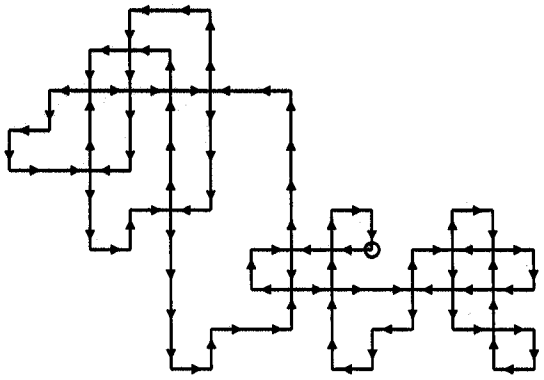

Figure 2.10: A KSAT loop on the square lattice starting from the encircled site and coming back to the same site after 90 steps.

universality class turns into that of the Manna sandpile. The transition to Manna behavior does not require a nonzero threshold density of unbalanced sites. Thus, for the undirected model the symmetry of precise toppling balance is a crucial requisite for the multi-scaling to hold. This requisite is of course satisfied also by the ordinary BTW sandpile.

To conclude, we studied sandpile models with quenched disorder where the elements of the TM are randomly assigned. With asymmetric TM the precise toppling balance between in- and out-degrees at each site is not maintained. This imbalance suppresses the wave correlations leading to the BTW-like multi-scaling behavior of the avalanche size distribution and results a FSS regime in the universality class of the Manna stochastic sandpile. Thus, a symmetry mechanism underlies the puzzling difference between BTW and Manna scalings.

2.5 Asymmetric TM that maintains precise $H_i = H'_i$ balance

Can there be an asymmetric toppling matrix Δ whose elements are selected in such a way that the precise balance $H_i = H'_i$ is maintained at all sites except on the boundary? We investigated this question in [84] and found that indeed it is possible. This is done in the following way.

We start with an empty periodic $L \times L$ lattice with the corresponding TM Δ whose all elements are initially zero. Therefore $H_i = H'_i = 0$ is true at all sites initially. The asymmetric Δ matrix will be generated gradually step by step. We start from an arbitrarily selected site i. Let the neighbors of the site i be denoted by 1, 2, 3 and 4. We first observe that if one increases the Δ value of any one of the four outgoing bonds, say $(i3)$ by an amount δ, the bond $(i3)$ becomes asymmetric and it increases H_i by the same amount. Similarly if we increase the Δ value of an arbitrary incoming bond to the site i, say $(2i)$ by δ again, the bond $(2i)$ also becomes asymmetric and H'_i increases by an amount δ. Therefore as a result of both the operations the precise balance of $H_i = H'_i$ is strictly maintained at the site i, as shown in Fig.2.9. Next, following the outgoing bond $(i3)$ we go to the site 3 and

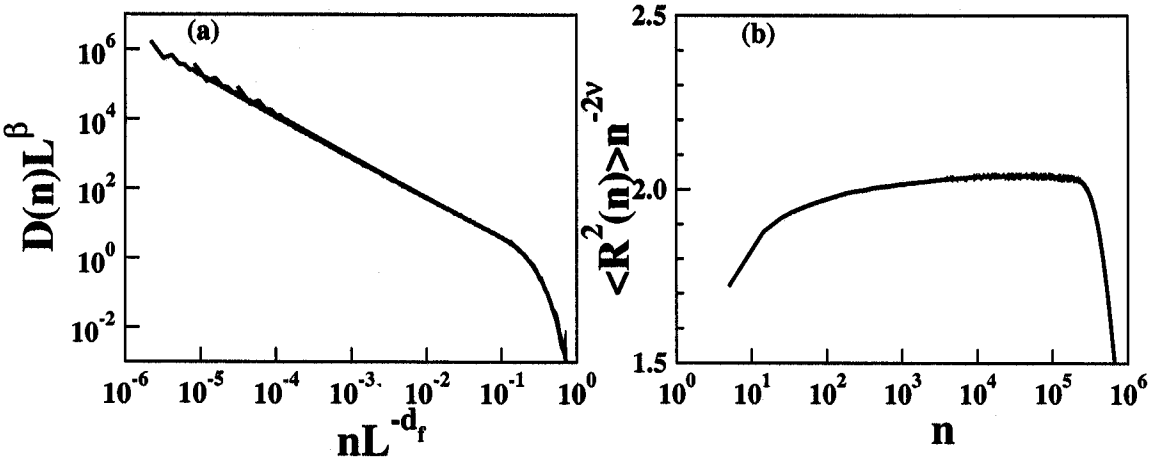

Figure 2.11: (a) Scaling of KSAT loop length distribution for system sizes $L = 513, 1025$, and 2049. The estimated exponents are $d_f \approx 1.905$ and $\beta \approx 2.237$. (b) The mean-square end-to-end distance of KSATs after n steps grows as $n^{2\nu}$ with $\nu \approx 0.530$.

increase the Δ value of any of the outgoing bond of the site 3 by the same amount δ. This ensures that $H_i = H_i'$ is maintained at the site 3. In this way a series of such bond asymmetrizations can be done randomly by starting from any arbitrary site i, selecting randomly an arbitrary outgoing bond (ij), increasing Δ_{ij} by δ, going to the site j, selecting an arbitrary outgoing bond (jk) $(\neq (ji))$ and increasing Δ_{jk} also by the same amount δ, then going to the site k and so on. The path obviously cannot visit a bond of the lattice more than once and the final point to stop must be the starting point. Such a path can intersect itself but always one of the outgoing bonds which has not been asymmetrized yet is selected randomly. Since at each site on the path the Δ values of either a single or a double pair of incoming and outgoing bonds have been increased by the same amount δ the balance of $H_i = H_i'$ is maintained at all sites on the path. Such a random closed path is the path of a special type of walker and we call them as 'Kinetic self-avoiding trails' as described below.

2.5.1 Kinetic self-avoiding trail (KSAT)

A self-avoiding trail is a random walk which does not visit one bond of the lattice more than once [86, 87]. A random configuration of self-avoiding trail is generated by growing a random walk which terminates when a bond is visited more than once. We studied kinetic self-avoiding trail (KSAT) which is executed with a little more intelligence [85]. At each site, to make a step, the walker first finds out the subset of bonds which has not been visited yet and then steps randomly along any one of these bonds with equal probability. Such a walk can also terminate only when it visits the origin for the third time as shown in Fig.2.10.

A similar definition of kinetic growth walk or growing self-avoiding walks have been studied in the literature and it is argued that very long such walks behave in the same way as ordinary self-avoiding walks [88, 89, 90].

(a)

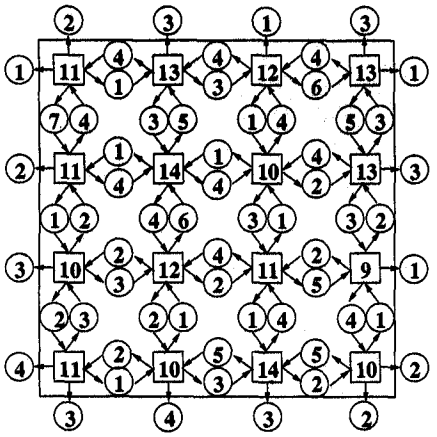

(b)

11	-1	0	0	-7	0	0	0	0	0	0	0	0	0	0
-4	13	-3	0	0	-3	0	0	0	0	0	0	0	0	0
0	-4	12	6	0	0	-1	0	0	0	0	0	0	0	0
0	0	-4	13	0	0	0	-5	0	0	0	0	0	0	0
-4	0	0	0	11	-4	0	0	-1	0	0	0	0	0	0
0	-5	0	0	-1	14	-4	0	0	-4	0	0	0	0	0
0	0	-4	0	0	-1	10	-2	0	0	-3	0	0	0	0
0	0	0	-3	0	0	-4	13	0	0	0	-3	0	0	0
0	0	0	0	-2	0	0	0	10	-3	0	0	-2	0	0
0	0	0	0	0	-6	0	0	-2	12	-2	0	0	-2	0
0	0	0	0	0	0	-1	0	0	-4	11	-5	0	0	-1
0	0	0	0	0	0	0	-2	0	0	-2	9	0	0	0	-4
0	0	0	0	0	0	0	0	-3	0	0	0	11	-1	0	0
0	0	0	0	0	0	0	0	0	-1	0	0	-2	10	-3	0
0	0	0	0	0	0	0	0	0	0	-4	0	0	-5	14	-2
0	0	0	0	0	0	0	0	0	0	0	-1	0	0	-5	10

Figure 2.12: (a) Random grain flow distribution along the bonds of a 4×4 square lattice for the quenched model generated by KSATs, and (b) the corresponding toppling matrix is shown.

KSATs are found to have very interesting and non-trivial statistics. For example the probability distribution that a KSAT returns to the origin for the first time after n steps has a scaling form like:

$$D(n) \sim L^{-\beta}\mathcal{G}(n/L^{d_f}) \tag{2.5}$$

where the scaling function $\mathcal{G}(x) \sim x^{-\gamma}$ as $x \to 0$ such that $\gamma = \beta/d_f$ and $\mathcal{G}(x) \to$ decreases to zero very fast when $x \to 1$. We estimated $d_f \approx 1.905$, $\beta \approx 2.237$ which give $\gamma \approx 1.174$ (Fig.2.11(a)). The cut-off exponent d_f is also recognized as the fractal dimension of the KSATs since the number of steps on the walks whose sizes are of the order of L varies as L^{d_f}. One can also measure the value of d_f directly. The mean square end-to-end distance $\langle R^2(n)\rangle$ of the walker from the origin after n steps varies as $n^{2\nu}$, where $\nu = 1/d_f$. Simulation of walks of lengths up to a million steps on a lattice of size $L = 4097$ gives $\nu \approx 0.530$ so that $d_f \approx 1.886$ (Fig.2.11(b)). Therefore we conclude a mean value of $d_f \approx 1.895$.

KSATs are therefore used to asymmetrize the TM. We start with a TM whose all elements are initially zero corresponding to a periodic $L \times L$ lattice. The walker starts from an arbitrarily selected site, executes a KSAT which finally stops when it comes back to the origin for the first time. The Δ values of every outgoing bond visited from each site are then increased by δ which is selected as a random integer number between 1 and 2. A number of such KSAT loops are then generated one by one starting from arbitrarily selected sites and with randomly selected δ values. The process stops only when all bonds are asymmetrized at least once. The periodic boundary condition is then lifted. In Fig.2.12(a) we show the asymmetric grain flow along the bonds of a 4×4 square lattice for the quenched model generated by KSATs and the corresponding TM is shown in Fig.2.12(b). The TM so generated is asymmetric in ≈ 92.5 % bonds but maintains the precise balance of $H_i = H_i'$ strictly at all sites except on the boundary. The lattice is now ready to study the sandpile model where the threshold height at each site is denoted by H_i. Such a system has a large fluctuation of threshold heights and their average increases by increasing the

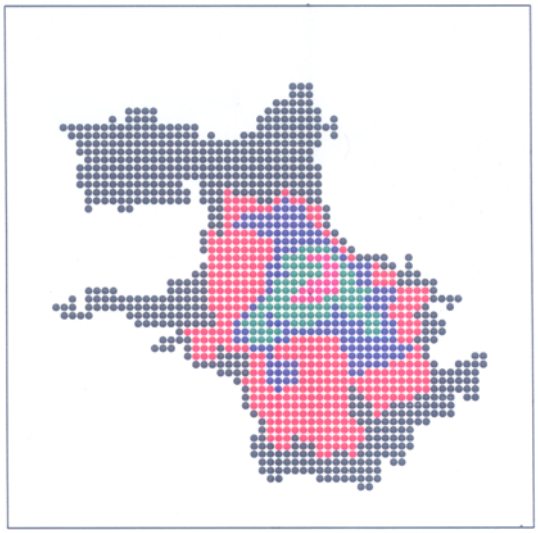

Figure 2.13: Multiply toppled sites within the avalanches for the quenched model generated by KSATs are shown by circles of different colors: 1(black), 2(red), 3(blue), 4(green), 5(magenta) and 6(orange).

system sizes.

We studied three aspects of the sandpile model on the quenched substrate generated by KSATs which are: (i) the inner structure of the avalanches (ii) the avalanche statistics and the (iii) wave size distributions. We observe very close similarities of our model with BTW model in all three aspects as reported below.

2.5.2 Avalanche picture

We find that the waves in case of the quenched model generated by KSATs like in the BTW model are compact having no holes. The set of sites toppling the same number of times form a connected toppling zone. The avalanche is characterized by the formation of multiply toppled zones with an inner hierarchy in the number of topplings. The n-th toppling zone is completely surrounded by the $(n-1)$-th toppling zone with the origin situated within the maximally toppled zone. A typical picture of the multiply toppled zone within an avalanche for the quenched model generated by KSATs is shown in Fig.2.13.

2.5.3 Results and analysis

Like any ordinary sandpile model, the dynamics starts from an arbitrary stable distribution of sand heights and then grains are added to the system one by one. The system eventually reaches the stationary state when the average height per site fluctuates around a mean value but does not grow any further. The size of an avalanche is measured by the total number of topplings s.
The finite size scaling behavior of the probability distribution $\text{Prob}(s, L)$ of avalanche sizes has the following general form:

$$\text{Prob}(s, L) \sim L^{-\mu} \mathcal{F}(\frac{s}{L^D}), \tag{2.6}$$

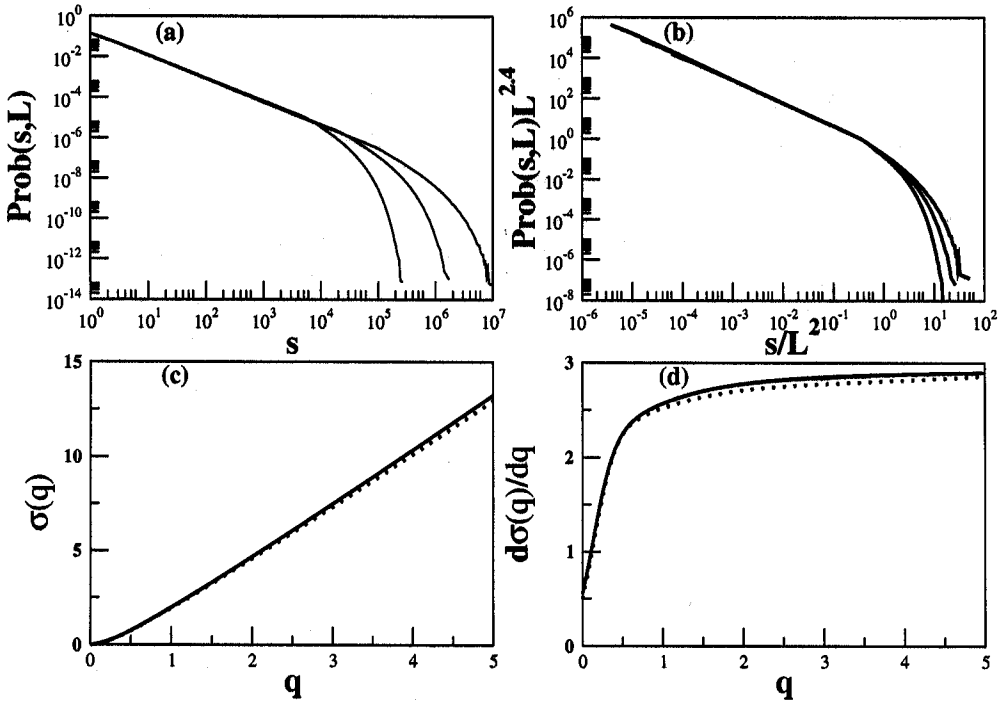

Figure 2.14: Data for the avalanche size distribution for the quenched model generated by KSATs. (a) Plot of Prob(s, L) vs. s for L =128, 256 and 512 (b) a scaling attempt of Prob$(s, L)L^{2.4}$ vs. s/L^2 with the same system sizes. (c) Comparison of the moment exponents $\sigma(q)$ vs. q and (d) $d\sigma(q)/dq$ vs. q for the quenched model generated by KSATs (dotted line) and for the BTW model (solid line).

where the scaling function $\mathcal{F}(x) \sim x^{-\tau}$ in the limit of $x \to 0$ and $\mathcal{F}(x)$ approaches zero very fast when $x \to 1$. It is now known that BTW model does not follow this FSS form but has a multi-scaling behavior [26, 29] where as the Manna model follows this FSS behavior quite accurately [27].

For the quenched model generated by KSATs it is observed that the collapse does not work for a single set of μ and D and for all values of s and L. This is a similar situation as found in the BTW sandpile model and also in the case of undirected quenched model [84]. For example in Fig.2.14(a & b) we have tried an unsuccessful attempt for a data collapse as: Prob$(s, L)L^{2.4}$ vs. sL^{-2} for L = 128, 256 and 512. Evidently the three curves separate out from one another beyond $s/L^2 \sim 1$. Even for smaller s values within $1 < s < L^2$ their slopes differ slightly but systematically as 1.132, 1.135 and 1.144 for L = 128, 256 and 512 respectively, very similar to the BTW model behavior.

Further to check that the quenched model generated by KSATs indeed behaves like the multi-scaling BTW model the various moments of Prob are evaluated [26, 27, 29]. The q-th moment of the avalanche size distribution is defined as $\langle s^q \rangle = \Sigma s^q \text{Prob}(s, L)$. Assuming that FSS holds for the whole accessible range of avalanche sizes, it is known that $\langle s^q \rangle \sim L^{\sigma(q)}$ where $\sigma(q) = D(q - \tau + 1)$ for $q > \tau - 1$ and $\sigma(q) = 0$ for $0 < q < \tau - 1$. Estimates of $\sigma(q)$ are obtained from the slopes of the plot of $\log\langle s^q(L)\rangle$ with $\log L$ for L = 128, 256 and 512 and for 251 equally spaced q values ranging from 0 to 5. We compared the plot of $\sigma(q)$ vs. q for the quenched model

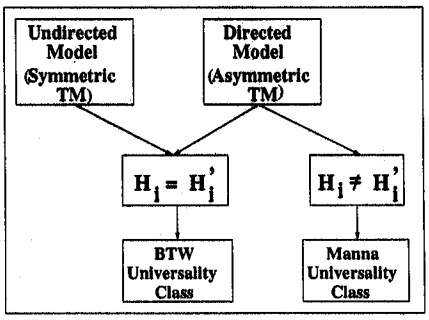

Figure 2.15: This flow chart shows that the precise balance $H_i = H_i'$ or absence of it determines the universality classes of different sandpile models.

generated by KSATs with a similar plot for the BTW model calculated for the same system sizes, and the agreement is found to be very good, within 2% (Fig.2.14(c)). For both the models $\sigma(q)$ shows marked deviation from linearity. To analyze this non-linearity in more detail it is an usual practice to calculate $d\sigma(q)/dq$ which takes the constant value D for large q had the FSS been valid. In contrast, in our present case we find in Fig.2.14(d) that $d\sigma(q)/dq$ increases steadily with q for $q > 1$ and this plot coincides within the same accuracy with a similar plot for the BTW model.

The autocorrelation function of the wave time series $\{s_1, s_2, s_3, \ldots\}$ of successive waves [32] is defined as $C(t, L) = [\langle s_{k+t} s_k \rangle_L - \langle s_k \rangle_L^2]/[\langle s_k^2 \rangle_L - \langle s_k \rangle_L^2]$ where the $\langle .. \rangle$ refers quenched disorder averaging. This long range autocorrelation is the consequence of the coherent and uniform spatial structure of each wave. For the quenched model generated by KSATs, $C(t, L)$ is found to grow steadily with L. It scales as $C(t, L) \sim t^{-\tau_c} G(t/L^{D_c})$ with same exponents as undirected model with $\tau_c \approx 0.35$ and $D_c \approx 1$. These exponents should be compared to 0.40 and 1.02, respectively, as determined for the BTW model [32].

2.6 Conclusion

We studied sandpile models with quenched disorder where the elements of the TM are randomly assigned. With symmetric TM the equality between the outflow (H_i) of grains during toppling of site i and the total number of grains flowing to the site i when all its neighbors topple once is always maintained at all sites except the boundary sites. With asymmetric TM the toppling balance $H_i = H_i'$ may or may not be maintained. Using random kinetic self-avoiding trail loops on the square lattice we have generated an asymmetric toppling matrix maintaining the precise toppling balance condition between the outflow of grains during a single toppling at a site and the total number of grains flowing into the same site when all its neighbors topple for once. We conclude, as displayed in a flow chart in Fig.2.15 that it is only the local flow balance or absence of it, irrespective of it being generated from a symmetric or asymmetric TM, that determines the universality class of the sandpile model. Thus if the local outflow or inflow balance of grain is maintained at all sites the model shows BTW scaling behavior otherwise it will show Manna scaling behavior.

Chapter 3

Sandpile model on an optimized scale-free graph on Euclidean space

3.1 Introduction

In the last chapter we made a conjecture that given a sandpile model if the precise balance between the number of grains H_i distributed during a toppling at a lattice site i to its neighboring sites is equal to the number of grains H_i' received by this site when all its neighbors topple for once is maintained, in other words if Eqn. 2.1 $H_i = H_i'$ is valid at all sites of the lattice except at those on the boundary, then the sandpile follows the multi-scaling critical behavior of the BTW sandpile model.

In this chapter we discuss our recent work [91] where we studied the sandpile model on highly inhomogeneous scale-free graphs (SFG) which have attracted a lot of interests recently and which have been discussed briefly in sections 1.2 of the introductory chapter 1. The motivation of this study is to acquire further support for the validity of our recent conjecture [84] mentioned above. In our study the SFG is embedded in the Euclidean space, namely a square lattice of size $L \times L$. The degree distribution of such a SFG varies over a wide range of values and follows a power law distribution. We study the BTW as well as the Manna sandpile models on such graphs and suitably define the toppling rules in such a way that equation (2.1) is valid. We observe that the critical behavior of this model when the graph is cost-optimized is very similar to that of the BTW model. In the following we define and describe the sandpile model on the SFG where H_i is equal to the degree k_i of the vertex i and therefore is a strongly fluctuating quantity. In spite of that the equality $H_i = H_i'$ is attained by construction. The result is that the sandpile model on the optimized SFG indeed behaves like the BTW model. We consider this result as a support to our conjecture mentioned above and expect that it enhances the possibility that this conjecture may indeed be true.

In §3.2 we discuss networks on Euclidean space, in §3.3 we study sandpile model on a scale-free graph, in §3.4 we discuss the construction of optimized scale-free graph on Euclidean space, in §3.5 we study sandpile model on an optimized scale-free graph on Euclidean space and finally we conclude in §3.6.

3.2 Networks on Euclidean space

There are networks in which the nodes are geographically located in different positions on a two-dimensional Euclidean space, for e.g., electrical networks, Internet, postal and even transport networks etc. The edges of the graphs representing these networks carry non-uniform weights which in most cases are either equal or proportional to the Euclidean lengths of the links. In these networks a relevant question is how to optimize the total cost of the connections, e.g. electrical wires, Ethernet cables, or say travel distances of postal carriers [92].

On the other hand a detailed knowledge of link length distribution is also important in the study of Internet's topological structure for designing efficient routing protocols and modeling Internet traffic. For example, Waxman model describes the Internet with exponentially decaying link length distribution: $D(\ell) \sim \exp(-\ell/\ell_0)$ [93]. Yook *et al.* observed that nodes of the router level network maps of North America are distributed on a fractal set and the link length distribution is inversely proportional to the link lengths [94].

It is suggested that in the growing Internet, when a new node becomes a member of the network, two competing factors control the decision to which node of the already grown Internet the new node will be connected - the degree k_i of the existing node i and in general the αth power of the length ℓ of the link connecting the new node and the node i. The preferential attachment probability for the ith node is therefore: $\pi_i \propto k_i \ell^{\alpha}$. Recently in [95] it has been argued that such a network is scale-free for all values of $\alpha > \alpha_c$ and the degree distribution decays stretched exponentially for the other values of α but $D(\ell)$ still maintains a power law.

3.3 Sandpile model on a scale-free graph

Recently, BTW sandpile model has been studied on a static model of SFG [96]. In contrast to the usual sandpile models there are no specific sinks at fixed positions in this study. Instead, during a toppling any grain can evaporate from the system from any arbitrary vertex with a small probability f. The distribution of avalanche sizes (s) which do not dissipate (i.e., grains do not evaporate in these avalanches) is:

$$\text{Prob}(s) \sim s^{-\tau} \exp(-s/s_c) \tag{3.1}$$

where the cut-off of the avalanche size $s_c \sim 1/f$. It is to be noted that the cut-off size does not depend on the graph size N but only on the dissipation rate.

To claim that a dynamical process active in a system is self-organized critical, it is important to ensure that both long ranged spatial and temporal correlations dynamically evolve in this system. For the ordinary sandpiles grown on systems of spatial extension L this is verified in the following ways: (i) Though the avalanche size distribution has a power law distribution $\text{Prob}(s) \sim s^{-\tau}$ for infinitely large systems, for the finite size systems the power law is valid for some intermediate range obeying the finite size scaling form in Eqn. 1.13 and this range increases with the system size as the cut-off of the avalanche size distribution increases as $s_c(L) \sim L^D$. (ii) The average size of the avalanches increases with the system size L as $\langle s(L) \rangle \sim L^{\nu}$ with $\nu = 2$ due to the diffusive motion of the sand grains as

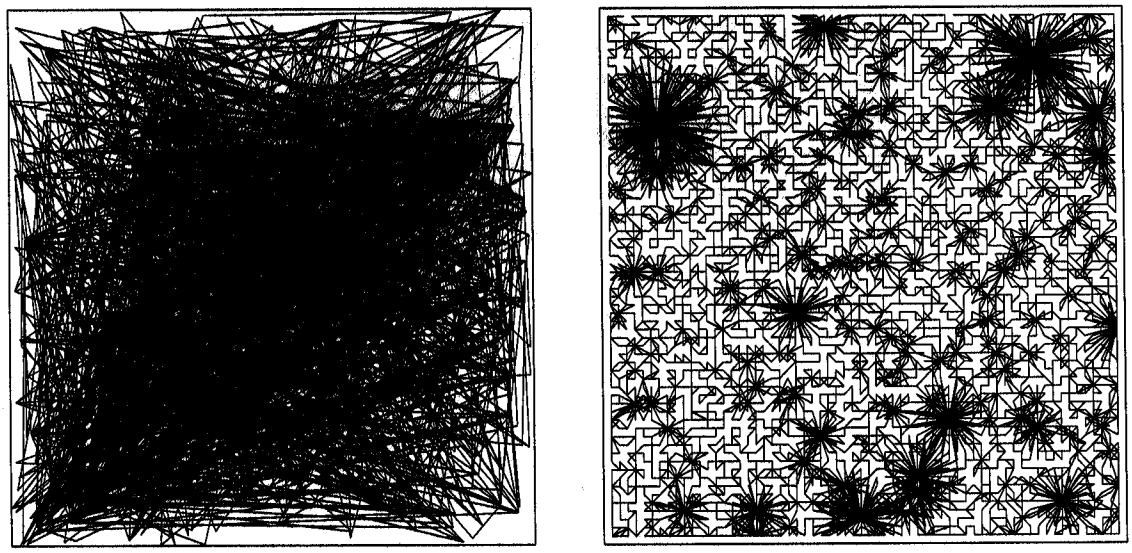

Figure 3.1: Barabási-Albert scale-free graphs of $N = L^2$ vertices are generated on the square lattice of size $L = 26$ (left) and 64 (right) respectively and vertices are assigned random positions on the lattice. The graph on the left is un-optimized where as for the graph on the right the cost function $\mathcal{C}$ (the total wiring length) is minimized by a large number of trials as described in the text keeping the degree distribution intact. Large degree vertices are visible.

explained in section 1.1.7. Non-zero values of τ, ν and D indicate that system has avalanches of all length scales and the process is indeed critical.

If a sandpile is grown in a closed system (i.e., a system which has no sinks to absorb sand grains and also grains do not evaporate from this system) the sandpile eventually reaches a situation when an "infinite avalanche" emerges which continues for ever and the system refuses to become stable again in a finite time. In this situation if a slow dissipation rate is introduced like every $1/f$ topplings one grain is dissipated from any arbitrary site of the system, then the infinite avalanche disappears and the system indeed reaches a stationary state, but the avalanche sizes are no more of all length scales. This is because the large avalanches loose their strengths by dissipation of grains.

For a network or a graph in general, there is no concept of physical space, only the connections by edges between the vertices. A small world graph has the diameter varying logarithmically with the number of vertices: $\mathcal{D}(N) \propto \log N$. Since scale-free graphs are also small world graphs, it is difficult to observe long ranged spatial correlations in sandpile model on SFGs. Therefore it is necessary to place the scale-free graphs on the Euclidean space and study the sandpile model on this graph so that long range spatial and temporal correlations become evident.

3.3.1 Sandpile model on a SFG on the square lattice

We first construct a Barabási-Albert SFG of $N = L^2$ vertices [63, 97, 98]. The graph starts growing from an initial set of $m_o = (m + 1)$ vertices. Each of these vertices is

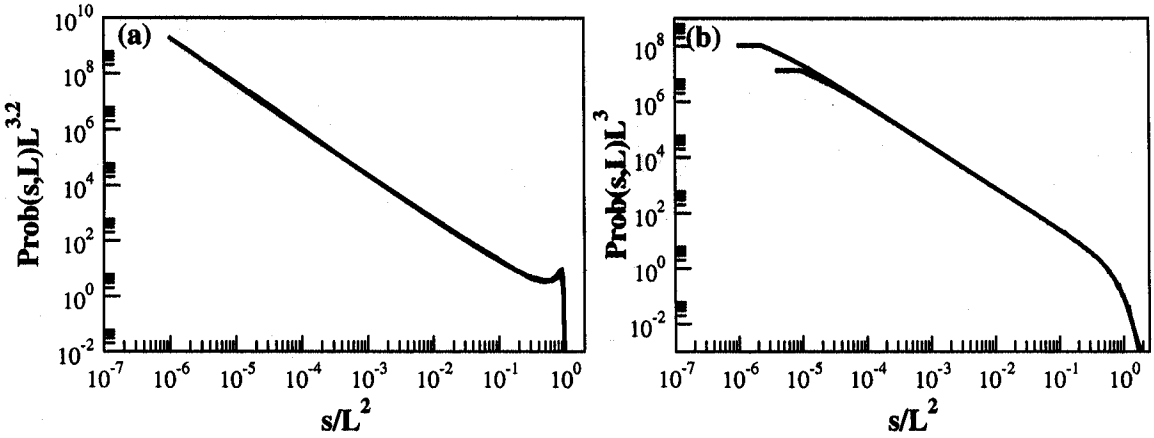

Figure 3.2: Scaling plot of the avalanche size distribution data of the sandpile models on the un-optimized Barabási-Albert scale-free graph on square lattice: (a) BTW model for system sizes: $L = 256$, 512 and 1024 gives the values of the scaling exponents $D \approx 2$, $\beta \approx 3.2$ and the avalanche size exponent $\tau_{un-opt}^{BTW} \approx 1.6$ whereas (b) Manna model for system sizes: $L = 512$ and 1024 gives $D \approx 2$, $\beta \approx 3.0$ and $\tau_{un-opt}^{Manna} \approx 1.5$.

linked to all other m vertices forming a $(m+1)-$clique. After that new vertices are added to the graph one by one and each such new vertex is connected to m randomly selected distinct vertices of the already grown graph with probability $\pi_i(t) \propto k_i(t)$. This process stops when the graph size has grown to L^2 vertices. In our calculation we use $m = 2$, therefore our graph has L^2 vertices, $2L^2 - 3$ edges among the vertices and a large number of loops. The vertices of the graph are then assigned randomly with uniform probability the sites of the square lattice. If two vertices are linked, the corresponding lattice sites are connected by straight lines. Thus we embed the BA SFG on the square lattice (Fig.3.1(left)).

Clearly the degree distribution of such an Euclidean SFG is exactly the same as that of the BA SFG. To study the sandpile model we assume that each site (except for sites on the boundary) has a site dependent critical height H_i of stability which is equal to the degree k_i of the vertex at that site. Therefore when $h_i \geq H_i$, the height of the sand column at site i is reduced to :

$$h_i \rightarrow h_i - H_i \tag{3.2}$$

and in a deterministic toppling dynamics like BTW model, all the k_i neighbors receive one grain each. The outlet of the system is at the boundary. Therefore every boundary site (except the corner sites) has the threshold heights $H_i = k_i + 1$. This implies that in a toppling at the boundary site one grain goes out of the system and never comes back. Similarly at the corner sites the threshold heights are $H_i = k_i + 2$. Such mechanism of outflow of grains through the boundary sites ensures that the sandpile dynamics on the Euclidean SFG must reach a stationary state.

In this Euclidean SFG any site is connected to any other site with equal probability and therefore the average edge length $\langle \ell_{ij} \rangle$ is large and of the order of the system size L (Fig.3.1(left)). In a toppling the grains therefore jump large distances

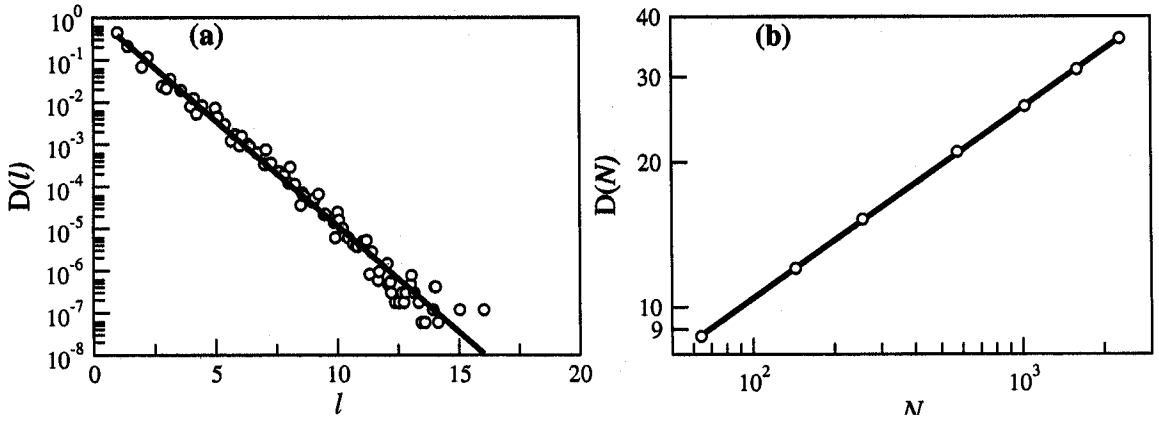

Figure 3.3: (a) The edge length distribution $\mathcal{D}(\ell)$ for a optimized SFG on a square lattice of size $L = 32$. (b) The average diameter $\mathcal{D}(N)$ of the optimized SFG on square lattices of size $L = N^{1/2}$ as a function of the number of vertices N.

on the average. We first study a deterministic sandpile model on such a graph. In this sandpile model a grain jumps a distance around L in a toppling. Consequently, the spatial extent of all avalanches, small or big, are around L.

3.3.2 Avalanche statistics for sandpile model on a SFG on the square lattice

We first attempted a finite size scaling following Eqn. 2.6 of the avalanche size distribution data of the BTW sandpile on un-optimized SFGs embedded on a square lattice by a data collapse of the plot of L^{β}Prob vs. s/L^{D} with trial values of the exponents. In Fig.3.2(a) we show such plots for lattice sizes $L = 256$, 512 and 1024. The best collapse works for $D \approx 2$ and $\beta \approx 3.2$, giving $\tau_{un-opt}^{BTW} = \beta/D \approx 1.6$. Similar slight deviation from 1.5 was also observed in [96] for the deterministic case.

In addition the stochastic Manna sandpile is also studied on the un-optimized BA SFG on the square lattice for system sizes up to L=1024 again. We estimated $D \approx 2$ and $\beta \approx 3.0$ giving $\tau_{un_opt}^{Manna} \approx 1.5$ (Fig.3.2(b)) for the stochastic Manna sandpile on the un-optimized BA SFG on a square lattice. We believe that τ_{un-opt} for both the BTW and Manna sandpiles on the un-optimized BA SFGs are indeed mean-field like and both the exponents should be actually 3/2. It is observed that sites hardly topple multiply and the area a has a similar distribution.

3.4 Optimized SFG on Euclidean space

Recently a cost optimized scale-free graph on Euclidean space has been constructed [92] where the cost function, which is the total sum of the edge lengths is optimized keeping the nodal degree distribution exactly same as that of the original SFG. For such a construction one defines the cost function $\mathcal{C}(N)$ as the total wiring length in terms of the symmetric adjacency matrix $\mathbf{A}$ of size $N \times N$ (which has elements $a_{ij} = 1$ if there is an edge between the pair of vertices i and j and $a_{ij} = 0$ otherwise)

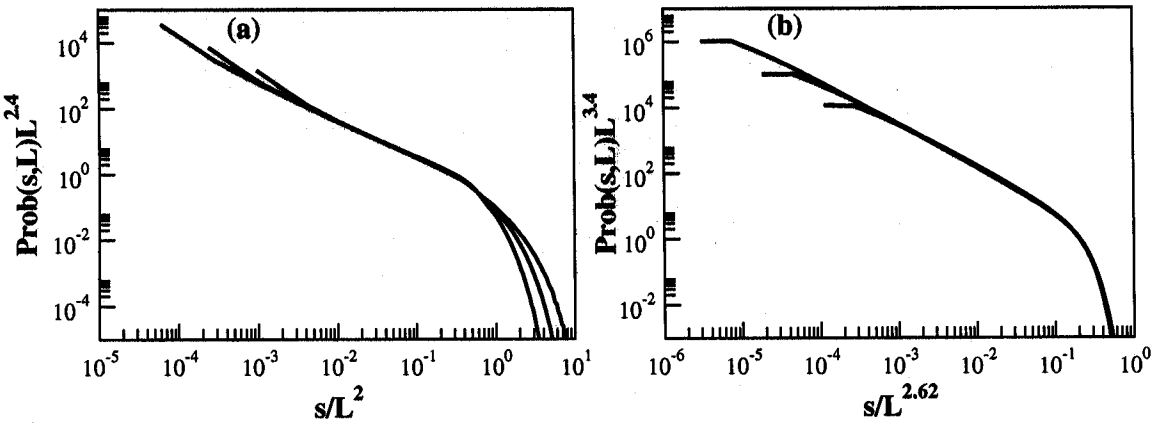

Figure 3.4: Scaling plot of the avalanche size distribution data of the sandpile models on the optimized Barabási-Albert scale-free graph on square lattice for system sizes: $L = 32$, 64 and 128 give: (a) $D \approx 2$, $\beta \approx 2.4$ for the BTW model and (b) $D \approx 2.62$, $\beta \approx 3.4$ and $\tau_{opt}^{Manna} \approx 1.3$ for the Manna model.

and the distance ℓ_{ij} between vertices i and j as $\mathcal{C}(N) = \Sigma_{i>j} a_{ij}\ell_{ij}$. The optimization process is essentially a rewiring process maintaining the degree distribution intact.

The optimization process starts with a BA SFG constructed on a square lattice as mentioned above. A pair of distinct edges of the SFG is chosen whose vertices are not linked otherwise. One end of each edge then opened and rewired suitably to another vertex of the quartet so that total sum of the rewired length is smaller. More precisely, the first vertex n_1 is randomly selected from the set of N vertices and the second vertex n_2 is randomly selected from the k_1 neighbors of n_1. In the same way $n_3(\neq n_1 \neq n_2)$ is selected randomly from N vertices and $n_4(\neq n_1 \neq n_2)$ is chosen from k_3 neighbors of n_3. Clearly this move conserves the edge numbers as well as the degree distribution. Rewiring is done following this decision: If both n_1n_3 and n_2n_4 are not linked and also $\ell_{12} + \ell_{34}$ is greater than $\ell_{13} + \ell_{24}$ we link n_1n_3 and n_2n_4. Another possibility is if n_1n_4 and n_2n_3 are not linked but $\ell_{12} + \ell_{34}$ is greater than $\ell_{14} + \ell_{23}$ then we link n_1n_4 and n_2n_3. If both cases are possible we accept one of them with probability 1/2. If only one is satisfied we accept that. After rewiring we remove the edges n_1n_2 and n_2n_4. If none of the two is satisfied we go for a fresh trial.

On repeated trials of these moves the cost function gradually decreases. Initially it decreases very fast but eventually the success rate becomes very slow. To monitor the optimization process we kept track of the average edge length. Our best possible effort yields the average edge length $\langle \ell_{ij} \rangle \approx 1.75$ lattice constant. A picture of the optimized graph is given in Fig.3.1(right). In this best possible optimized graph the edge lengths ℓ have an exponential distribution as: $\mathcal{D}(\ell) \sim \exp(-g\ell)$ with $g \approx 1.16$ (Fig.3.3(a)). Also the diameter of the graph $\mathcal{D}(N)$ is measured and is observed to grow as N^{μ} where μ is estimated to be 0.40 ± 0.02 (Fig.3.3(b)). Therefore this graph is scale-free but not a small-world graph.

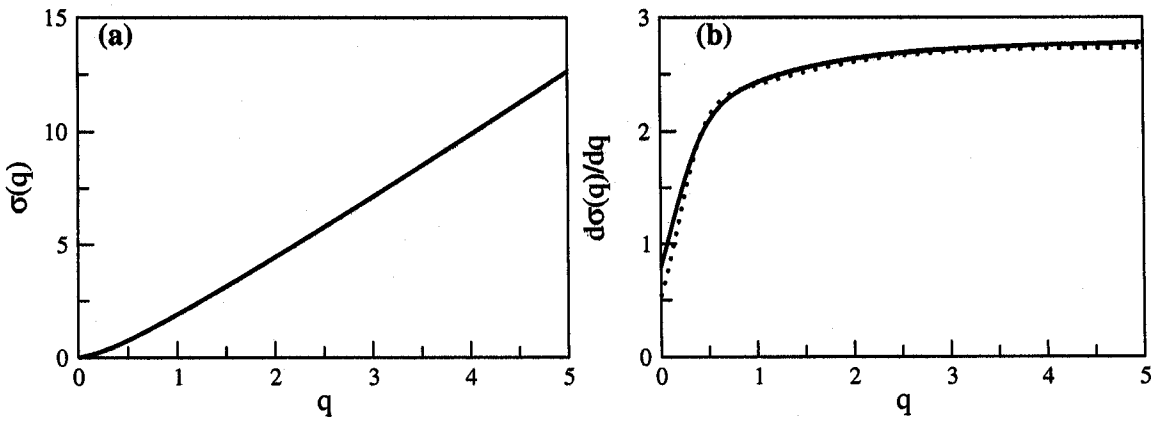

Figure 3.5: Comparison of the (a) the moment exponents $\sigma(q)$ vs. q and (b) $d\sigma(q)/dq$ vs. q for the BTW model on ordinary square lattice (solid line) and the optimized SFG on square lattice (dotted line).

3.5 Sandpile model on an optimized SFG on Euclidean space

The deterministic BTW sandpile model is then studied on such an optimized SFG on a square lattice [91]. The avalanche size distribution is calculated for three different system sizes $L = 32$, 64 and 128. It was difficult to go beyond this size because of the large optimization times required. First we tried to make a scaling plot of the size distribution data. In Fig.3.4(a) we show this plot, which shows reasonably well collapse of the data in the intermediate range of the avalanche sizes. The corresponding β and D values fitted are 2.4 and 2 respectively giving a possible value of $\tau_{opt}^{BTW} \approx 1.2$. However for large avalanche sizes the collapse is much worse and the data for different system sizes separate out. This is a typical behavior of the BTW like models which indicates strongly the presence of the multi-scaling behavior [26, 29].

The multi-scaling behavior is studied in more detail by the evaluation of the various moments of the avalanche size probability distribution. The q-th moment of the distribution is defined as $\langle s^q \rangle = \int s^q \text{Prob}(s, L) ds$. In case the distribution $\text{Prob}(s, L)$ obeys the finite size scaling behavior for the whole range of avalanche sizes, it can be shown that $\langle s^q \rangle \sim L^{\sigma(q)}$ where $\sigma(q) = D(q - \tau + 1)$ for $q > \tau - 1$ and $\sigma(q) = 0$ for $0 < q < \tau - 1$. The q dependent exponent $\sigma(q)$ is determined from the slope of the plot of $\log\langle s^q(L)\rangle$ with $\log L$, which in our case are for $L =$ 32, 64 and 128. The interval between successive q values is 0.02 and moments are calculated at 251 values of q between 0 and 5. In Fig.3.5(a) we show a plot of $\sigma(q)$ vs. q on a linear scale. In Fig.3.5(b) the derivative of $\sigma(q)$ is plotted with q. Had the $\text{Prob}(s, L)$ followed a simple FSS behavior the $d\sigma(q)/dq$ in Fig.3.5(b) would have saturated for large q values. In stead, the curve gradually increases with q, very similar to the multi-scaling behavior of BTW model. To compare we plot both $\sigma(q)$ and $d\sigma(q)/dq$ of the ordinary BTW on square lattice studied for same system sizes with different line styles. We see that in both plots the behavior is very similar and the difference between the two curves is very small, within 2-3 %.

The stochastic Manna sandpile is also studied on the optimized SFGs for the same system sizes. The scaling exponents are estimated as: $D = 2.62$ and $\beta = 3.4$ giving $\tau_{opt}^{Manna} \approx 1.3$ (Fig.3.4(b)). This value of τ is compared with the corresponding $\tau \approx 1.28$ value of the ordinary Manna sandpile.

3.6 Conclusion

In conclusion, we studied the BTW sandpile model on a Barabási-Albert scale-free graph of $N = L^2$ vertices where the vertices are the sites of a square lattice of size L. The number of outflowing grains H_i at each lattice site i except the boundary sites is equal to the degree k_i of the corresponding vertex of the SFG situated at that lattice site. The SFG is then optimized minimizing the total wiring length but keeping the degree distribution intact. On such an optimized SFG on the Euclidean space we observe that the sandpile model has the same scaling behavior as the BTW model where as the deterministic sandpile on the un-optimized SFG has a mean-field like behavior.

Chapter 4

Particle-hole symmetry in a sandpile model

4.1 Introduction

In this chapter we describe our work on a particle-hole symmetry in a sandpile model [99]. Holes are defined as the absence of particles (sand grains) and the toppling of 'hole columns' are defined in terms of a similar but reverse set of rules as described below.

The main question we would like to ask in this paper is, for an arbitrary deterministic sandpile model to attain the BTW critical behavior is it absolutely necessary that the stationary states should only be the recurrent states of the BTW model? Can it happen that the neighboring transient states which are very close to the recurrent states of the BTW model are also acceptable in the stationary states to achieve the BTW critical behavior? In other words we would like to investigate that to what extent the BTW critical behavior is robust.

In a stable state of the sandpile model the number of particles at all sites are less than their threshold heights. Addition of a particle takes the system from one stable state to another stable state through a number of successive unstable states through a series of topplings. Dhar had shown that under this sandpile dynamics, a system spontaneously evolves to a stationary state where it passes through only a subset of all possible stable states. The states of this subset are called 'recurrent states' and they are characterized by the absence of forbidden sub-configurations (FSCs) [22]. All recurrent states occur with uniform probabilities in the stationary state. A stable state which is not a recurrent state is called a 'transient state' and it never appears in the stationary state.

In the following we introduce the concept of holes in the framework of BTW sandpile and show that on addition of holes to the system the stationary states of the resulting sandpile model cannot be anymore strictly restricted to the recurrent states of the BTW model since the FSCs can very well be present in the stationary states of this model. In fact the recurrent and stationary states coincide in this model. However the distribution of weights of these states may be quite non-trivial and this question remains open. Our numerical results show that even in such a case the critical behavior is very similar to that of the BTW model.

In §4.2 we discuss the particle-hole addition model, in §4.3 we discuss our results

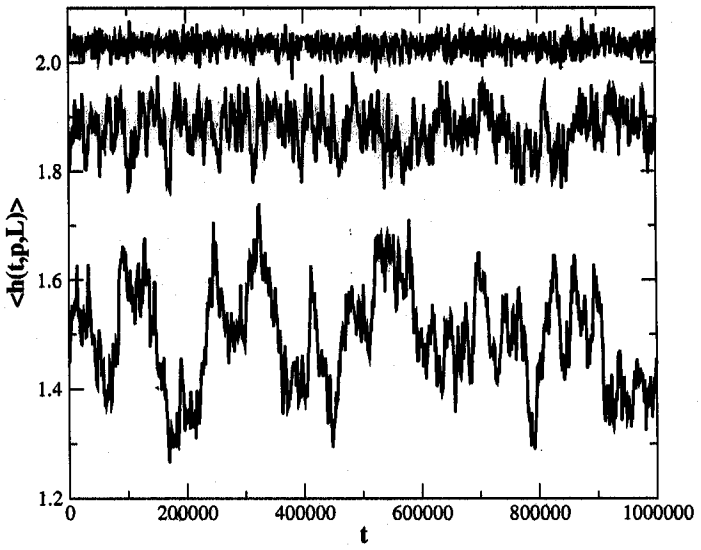

Figure 4.1: The fluctuation of the mean number of particles per site with time in a system of size $L = 64$ for the probabilities $p = 0.60$ (top) 0.52 (middle) and 0.50 (bottom). Both the width of fluctuation and the correlation time increases as p approaches $p_c = 1/2$.

for the above model and finally we conclude in §4.4.

4.2 Particle-hole addition model

Here we start restating the usual BTW sandpile model on a square lattice: Particles are added to the system one by one as $h_i \rightarrow h_i + 1$. If the number h_i of particles at a site is greater than the threshold height H_p then the site i looses four particles and each neighboring site gets one each:

$$h_i \rightarrow h_i - 4 \qquad \text{and} \qquad h_j \rightarrow h_j + 1 \tag{4.1}$$

On the other hand a 'hole' may be defined as the absence of a particle. Therefore adding a hole to a lattice site implies removing one particle from that site: $h_i \rightarrow h_i - 1$. Repeated addition of holes at randomly selected sites may reduce the number of particles at a site less than another pre-assigned threshold H_h. If this model is studied on a square lattice then if h_i is less than H_h, the site losses four holes i.e., four particles are added to this site and each neighboring site gets one hole (looses one particle) each:

$$h_i \rightarrow h_i + 4 \qquad \text{and} \qquad h_j \rightarrow h_j - 1 \tag{4.2}$$

We call this event as a 'reverse toppling'. Consequently at some of the neighboring sites particle numbers may also decrease below the H_h which again reverse topple and thus an avalanche of reverse topplings takes place in the system. Addition of a particle creates a particle avalanche where as the addition of a hole creates a hole

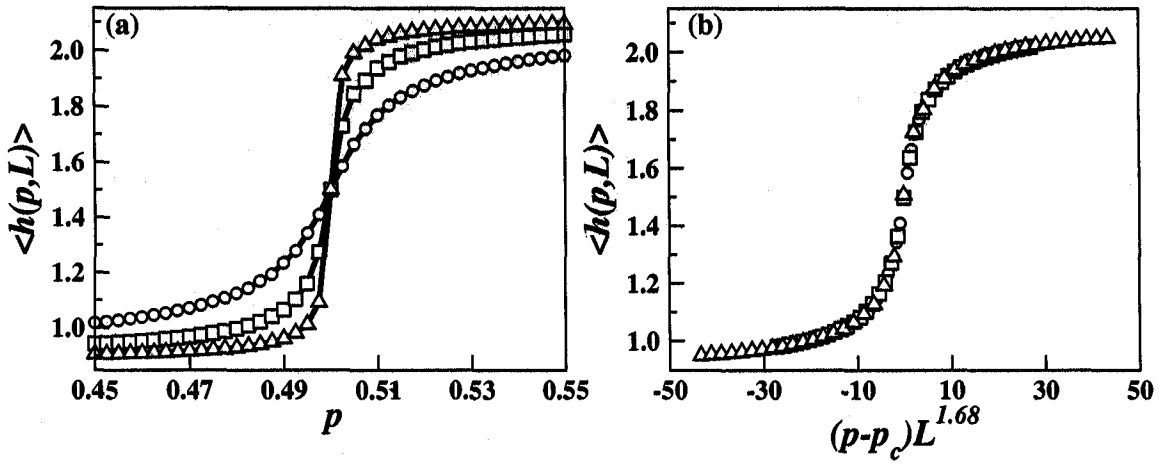

Figure 4.2: The time averaged number of particles per site $\langle h(p,L)\rangle$ in the stable stationary states as a function of the probability of adding a particle p. This variation is symmetric about the mid point $p_c = 1/2$ and $\langle h(p_c,L)\rangle = 3/2$. The data is for $L = 32$ (circle), $L = 64$ (square) and for $L = 128$ (triangle).

avalanche. We assign $H_p = 3$ and $H_h = 0$. Inverse avalanches were introduced previously to get back the recursive configuration corresponding to the particle deletion operator [100].

During the particle avalanches particle current flows into the system by addition of particles in the bulk of the system and then they flow out of the system through the boundary. On the contrary in hole avalanches particle current flows into the system through the boundary and flows out of the system through the bulk of the system.

In [99] we study a combination of particle and hole avalanches. We probabilistically add either a particle with a probability p or add a hole with a probability $1-p$. Therefore when $p = 1$, the situation is identical to the ordinary BTW model of sand avalanches when no hole is added. On the other hand for $p = 0$ only holes are added to the system and no particle. Therefore for $p > 1/2$ more particles are added to the system than the number of holes and therefore the net particle current is $2p - 1$ and it flows from the bulk of the system to the boundary. However for $p < 1/2$ holes are dropped more frequently than particles and the net particle current flows in the opposite direction. At $p = 1/2$ however there is no net current in the system. We consider $p = p_c = 1/2$ is a critical probability and study the behavior of this system around this critical probability. The time t is measured by the number of particles and holes dropped in the system.

4.3 Results

4.3.1 Mean number of particles per site

Let $h_i(t,p,L)$ be the generalized notation for the number of particles at site i, then the total number of particles in the system is: $h(t,p,L) = \Sigma_{i=1}^{L^2} h_i(t,p,L)$. The mean

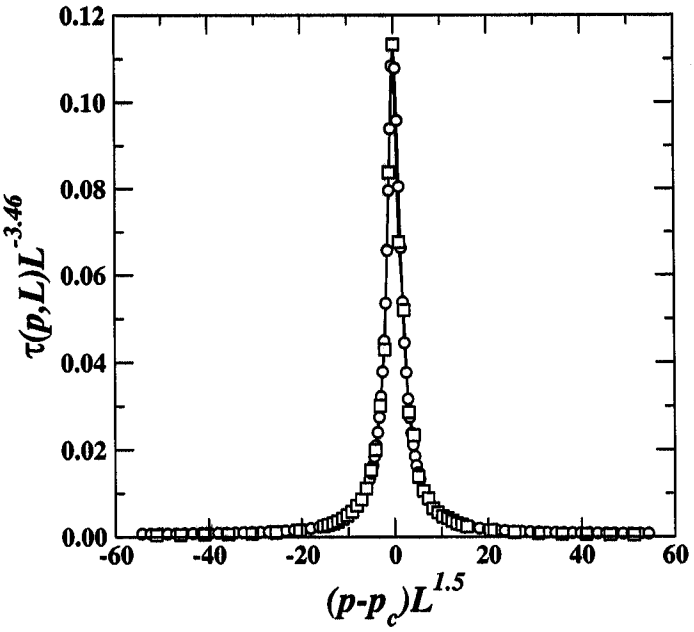

Figure 4.3: Scaling of the correlation time $\tau(p, L)$ of fluctuation of the particle density $\langle h(p, L)\rangle$ with the probability p for system size L. The data collapse is shown for two system sizes: $L = 32$ and 64.

number of particles per site is then $\langle h(t, p, L)\rangle = h(t, p, L)/L^2$. In the stationary state $\langle h(t, p, L)\rangle$ fluctuates rapidly around its time averaged value $\langle h(p, L)\rangle$. These fluctuations are shown in Fig.4.1 for the system size $L = 64$ and for $p = 0.60$, 0.52 and for 0.50. It is observed from this figure that both the width as well as the correlation time of fluctuation increases as p approaches p_c from either side of it.

The time averaged number of particles per site $\langle h(p, L)\rangle$ is a function of p and the system size L. At $p = 1$ it is equal to the average number of particles per site in the ordinary BTW model which is $h_1 = 2.125$ in the asymptotic limit of large system sizes [31, 39]. As p decreases $\langle h(p, L)\rangle$ slowly decreases but near $p_c = 1/2$ it decreases very fast to a value of $\langle h(1/2, L)\rangle$ =3/2. When p decreases from 1/2 even further, $\langle h(p, L)\rangle$ decreases fast but eventually saturates to a value of $h_0 = 3 - h_1 = 0.875$. In Fig.4.2(a) we show this variation. To see if the steep rise of $\langle h(p, L)\rangle$ around p_c is associated with some critical exponent, we make a scaling plot of $\langle h(p, L)\rangle$ with $p - p_c$ for a number of different system sizes L in Fig.4.2(b). The data collapse shows:

$$\langle h(p, L)\rangle \sim \mathcal{G}[(p - p_c)L^{1.68}]. \tag{4.3}$$

where, $\mathcal{G}$ is the scaling function.

The width of fluctuation is calculated as: $w(p, L) = \langle h^2(p, L)\rangle - \langle h(p, L)\rangle^2$. For a given L the width is maximum at $p = p_c$ and then monotonically decreases as $|p-p_c|$ increases. On the other hand for a given p the width also decreases with increasing L. It is observed from numerical estimation that at $p = p_c$, $w(p_c, L)$ decreases with system size as $w(p_c, L) = w_o + w_1 L^{-1/2}$ where $w_o \approx 0.076$ and $w_1 \approx 0.527$ are estimated. Beyond p_c the width decreases as: $w(p, L) = |p - p_c|^{-\nu}$ with $\nu \approx 0.82$ is estimated.

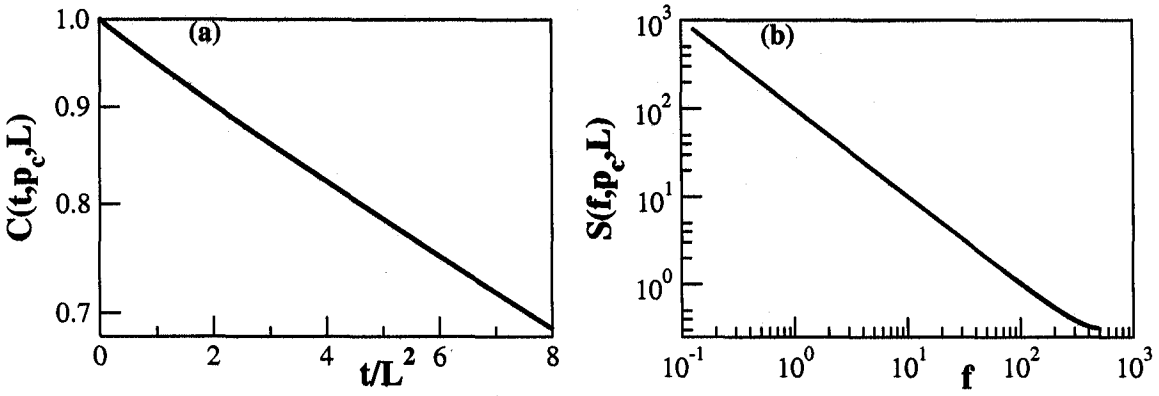

Figure 4.4: (a) The autocorrelation $C(t, p_c, L)$ of the time series of the fluctuating mean number of particles per site $\langle h(t, p_c, L)\rangle$ for the system size $L = 64$ at $p_c = 1/2$. $C(t, p_c, L)$ is plotted with the scaled time axis t/L^2 on a semi-log scale. In (b) the power spectrum $S(f, p_c, L)$ is plotted with the frequency f on a double logarithmic scale showing a power law decay of the spectrum with the spectra exponent being nearly equal to one.

4.3.2 Autocorrelation of the fluctuating mass

The time-displaced autocorrelation of the fluctuating mass per site is defined as:

$$C(t, p, L) = \frac{\langle h(t_o + t, p, L)h(t_o, p, L)\rangle - \langle h(p, L)\rangle^2}{\langle h^2(p, L)\rangle - \langle h(p, L)\rangle^2} \tag{4.4}$$

This autocorrelation is observed to decay exponentially as:

$$C(t, p, L) \sim exp(-t/\tau(p, L)) \tag{4.5}$$

where $\tau(p, L)$ is the correlation time. On a semi-log plot of $C(t, p, L)$ vs. t the slope of the plot gives the value of the correlation time $\tau(p, L)$ which is measured for different probabilities p and for different L values. For a given system size the correlation time is maximum at p_c and then decreases monotonically with increasing $|p-p_c|$. Also $\tau(p, L)$ increases with L at a given p. A scaling plot of the data collapses very nicely as (Fig.4.3):

$$\tau(p, L)L^{-3.46} \sim \mathcal{F}((p - p_c)L^{1.5}) \tag{4.6}$$

At p_c, $\tau(p_c, L)$ increases as L^μ where μ is estimated to be 3.46 ± 0.10.

Fourier transform of the autocorrelation function $C(t, p, L)$ is known as the spectral density or power spectrum $S(f, p, L)$ defined as

$$S(f, p, L) = \int_{-\infty}^{\infty} e^{-ift} C(t, p, L)dt \tag{4.7}$$

In Fig.4.4(a) we show the plot of the autocorrelation function $C(t, p_c, L)$ with scaled time t/L^2 for a system size $L = 64$ and exactly at p_c. A straight line plot on a semi-log scale implies an exponential decay of the correlation function. In

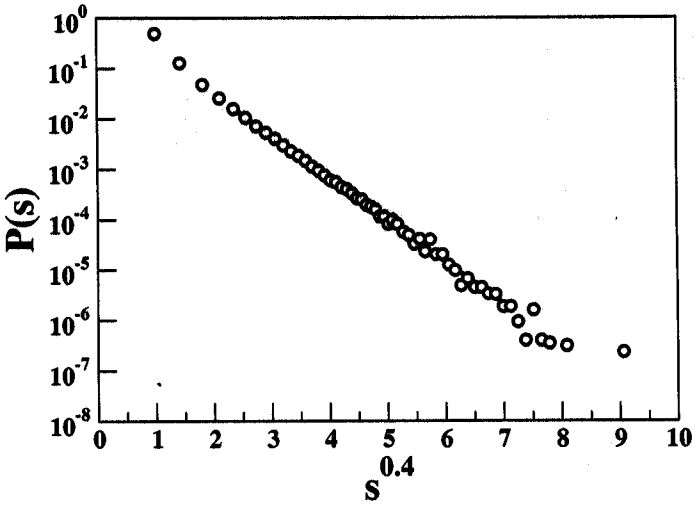

Figure 4.5: The stretched exponential decay of the particle avalanche size distributions $P(s)$ with the avalanche size s at $p_c = 1/2$. The estimated exponent is $\gamma \approx 0.4$

Fig.4.4(b) we show the Fourier transform of the autocorrelation function plotted in Fig.4.4(a) generated by the plotting routine '*xmgrace*'. On a double logarithmic scale the power spectrum $S(f, p_c, L)$ vs. the frequency f plot gives a very good straight line for the intermediate range of frequencies implying a power law decay of the spectral density: $S(f, p_c, L) \sim f^{-\beta}$. We estimate $\beta \approx 1$ showing the existence of $1/f$ type of noise in the power spectrum.

4.3.3 Particle-hole avalanche statistics

The avalanche size distributions for both particle as well as hole avalanches are measured. It is observed that in the range of $p > p_c$ the particle avalanche sizes are of widely varying magnitudes and of all length scales where as the hole avalanche sizes are very small and of the order of unity. Opposite is the situation for the range $p < p_c$. At p_c however both the particle as well as hole avalanche size distributions are similar and they are found to follow a stretched exponential distribution like:

$$P(s) \sim \exp(-as^{\gamma}) \tag{4.8}$$

where γ is estimated to be around 0.4 (Fig.4.5).

Away from this critical point p_c, the particle avalanches have power law distribution for $p > p_c$ and hole avalanches follow power law distributions for $p < p_c$. Particle avalanche size distributions are calculated at $p = 0.51$ and for system sizes $L = 256, 512, 1024$ and 2048. These distributions are very similar to the avalanche distributions in BTW model. For small avalanche sizes they do follow a power law distribution $P(s) \sim s^{-\tau}$ where the exponent τ slowly varies with the system size and gradually increases towards 1.2. The large avalanches have multi-fractal distribution and simple scaling does not work for the full distribution [29, 26]. Also the average avalanche size, area and life times have system size dependences very similar to those in the BTW sandpile: $\langle s(L) \rangle \sim L^2$, $\langle a(L) \rangle \sim L^{1.72}$ and $\langle t(L) \rangle \sim L$.

4.4 Conclusion

In a sandpile model addition of a hole is defined as the removal of a grain from the sandpile. We show that hole avalanches can be defined very similar to particle avalanches. A combined particle-hole sandpile model is then defined where particle avalanches are created with probability p and hole avalanches are created with the probability $1 - p$. It is observed that the system is critical with respect to either particle or hole avalanches for all values of p except at the symmetric point of $p_c = 1/2$. Specifically at $p = 1$ the system is identical to the ordinary BTW model for only particle avalanches. Similarly at $p = 0$ there is only hole avalanches and their distribution are very similar to the avalanche size distribution for the BTW model. In the range $1/2 < p < 1$ there are particle as well as hole avalanches, but the net current is due to the particles which flows into the bulk of the system. Critical behavior of the particle avalanches are observed to have multi-scaling behavior and is very similar to those of the BTW model. Reverse situation happens in the range $0 < p < 1/2$ where net current is due to holes which flows into the bulk of the system. The hole avalanche sizes have multi-scaling distributions very similar to the BTW model. However at p_c the fluctuating mass density is having non-trivial correlations characterized by $1/f$ type of power spectrum.

Chapter 5

Directed fixed energy sandpile model

5.1 Introduction

Application of a global directional bias onto a system has been proved to have strong effect on the critical behaviors of various models in Statistical Physics. In these directed systems, degrees of freedom of the individual elements is reduced, which shrinks the configuration space of the system compared to undirected system. As a result a directed system is simpler and easily tractable analytically. Examples include Directed percolation [64], Directed Sandpile Model [33, 35, 36], Directed River networks [101] and Directed Self-avoiding walks [102] etc.

In this chapter we study fixed energy sandpile (FES) model with a directional bias. Our motivation is to find a simpler yet non-trivial fixed energy sandpile which may have non-trivial critical behavior.

The fixed energy sandpile model [66, 67, 68] is defined within a closed system with no external driving. Thus the total mass of the system is conserved fixed by the initial condition. The control parameter is the density ζ of grains. The dynamics of the system starts with a random distribution of $N = \zeta L^2$ grains. Initially some sites may be unstable, which topple. Consequently some of the neighboring sites may topple again and the activity continues. The activity or the order parameter at a certain time is measured by the fraction ρ of lattice sites which are unstable at that time. For an infinitely large system there exists a critical threshold ζ_c such that if $\zeta < \zeta_c$ the activity terminates and the system gets absorbed in an inactive state where as for $\zeta > \zeta_c$ the activity of the system fluctuates but maintains a steady mean value [66]. In between these two regimes there exists a critical point ($\zeta = \zeta_c$) separating an absorbing phase from an active phase. The order parameter equals zero for $\zeta < \zeta_c$, and follows a power law $\rho_a \sim (\zeta - \zeta_c)^\beta$ for $\zeta > \zeta_c$. The correlation length ξ and relaxation time τ both diverges as $\zeta \to \zeta_c$, their critical behavior is characterized by the exponents $\nu_\perp$ and $\nu_\parallel$, defined via $\xi \sim |\zeta - \zeta_c|^{-\nu_\perp}$ and $\tau \sim |\zeta - \zeta_c|^{-\nu_\parallel}$ respectively. The dynamical critical exponent is defined via $\tau \sim \zeta^z$ which implies $z = \nu_\parallel / \nu_\perp$.

After the dynamics starts, the system takes some time to relax to the steady state. In general the mean activity $\langle \rho \rangle$ is a function of the density ζ i.e., the deviation from the critical point $\Delta = \zeta - \zeta_c$ and also the system size L. The simultaneous

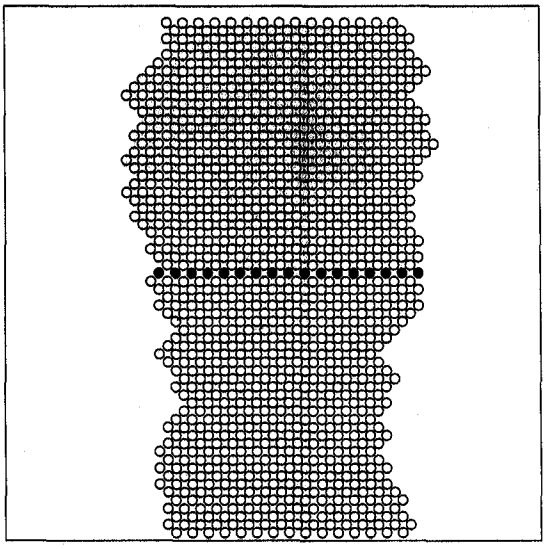

Figure 5.1: Filled circles denote the sites on the toppling front in an infinite avalanche of DDFES on an oriented square lattice of size $L = 32$. This avalanche is periodic and has a period 64. Horizontal empty circles denote positions of the TF in another 63 time units. The two end sites of the TF fluctuates but maintains a mean distance of $L/2$.

dependence of activity on Δ and L is expressed by the following scaling form:

$$\langle \rho(\Delta, L) \rangle \propto L^{-\beta/\nu_\perp} \mathcal{G}(L^{1/\nu_\perp} \Delta) \tag{5.1}$$

where $\mathcal{G}(x)$ is an universal scaling function such that $\mathcal{G}(x) \rightarrow x^\beta$ when $x >> 1$. This implies that for a certain range of Δ if L is so large that $L^{1/\nu_\perp}\Delta >> 1$ then $\langle \rho(\Delta, L) \rangle$ is independent of L and depends solely on Δ as $\langle \rho(\Delta, L) \rangle \sim \Delta^\beta$. On the other hand when $x << 1$, $\mathcal{G}(x) \rightarrow$ constant, independent of both Δ and L implies that right at the critical point $\zeta = \zeta_c$ the order parameter varies with the system size as: $\langle \rho(L) \rangle \sim L^{-\beta/\nu_\perp}$, independent of Δ.

To which universality class the FES model exponents should correspond to? Intensive research has been done to study the universality class of the phase transitions in FES models. It has been suggested that FES belongs to the universality class of the linear interface models (LIM) but not of that of the Directed percolation (DP) universality class [66, 67, 68, 103]. DP is generic for continuous absorbing state transitions in the absence of a conservation law where as in FES there exists a conserved field which is the density and it couples the order parameter, i.e., the mean activity. We, in the present study like to examine if an explicit application of the directional bias to the FES system makes the system behave as DP or it results to another new universality class.

In §5.2 we discuss the directed fixed energy sandpile model - both deterministic and stochastic case, in §5.3 we compare deterministic and stochastic directed FES and finally we conclude in §5.4.

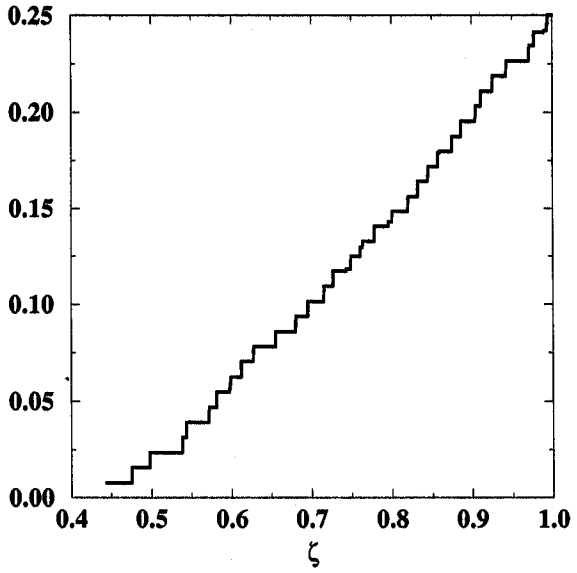

Figure 5.2: For DDFES the mean activity $\langle\rho\rangle$ in a system of size $L = 64$ which grows with the density in a step like manner where the step heights are $\Delta\rho = 1/(2L)$.

5.2 Directed fixed energy sandpile (DFES)

We studied directed fixed energy sandpile(DFES) models on an oriented square lattice of size L placed on the xy plane, with closed boundary [104]. A preferred direction is imposed on the system along the -y direction. The critical height of the sand column at all sites is $H_c = 2$. Initially ζL^2 grains are randomly distributed among the lattice sites. Due to toppling two grains of sand are distributed to the two neighbouring sites along the preferred direction i.e. at the lower-left (LL) and lower-right (LR) positions. We studied two different cases depending on the grain distribution process during toppling. In one case both the LL and LR sites get one grain each which is called the 'deterministic directed fixed energy sandpile' model (DDFES). In another case each of the two grains is distributed randomly to any of the LL or LR positions which we call the 'stochastic directed fixed energy sandpile' (SDFES) model.

5.2.1 Deterministic directed FES (DDFES)

The critical point of DDFES can be arrived at from an inactive state by adding grains one by one on an initial empty lattice followed by the relaxation of the avalanche. On the average both the size and the life times of the avalanches increase as the density grows. For the DDFES model the toppling front (TF) of an avalanche is a set of horizontal contiguous sites which travels downward with unit speed. The length of the TF however fluctuates as shown in Fig.5.1. If at an intermediate time the TF has n sites, then at the next time step its length can be only $n-1, n$ or $n+1$. For a finite avalanche the TF first grows from a single site to a certain length and then shrinks to zero. The set of sites covered by the left and right end sites of TF are the paths of two annihilating random walkers [33]. For a finite avalanche they meet

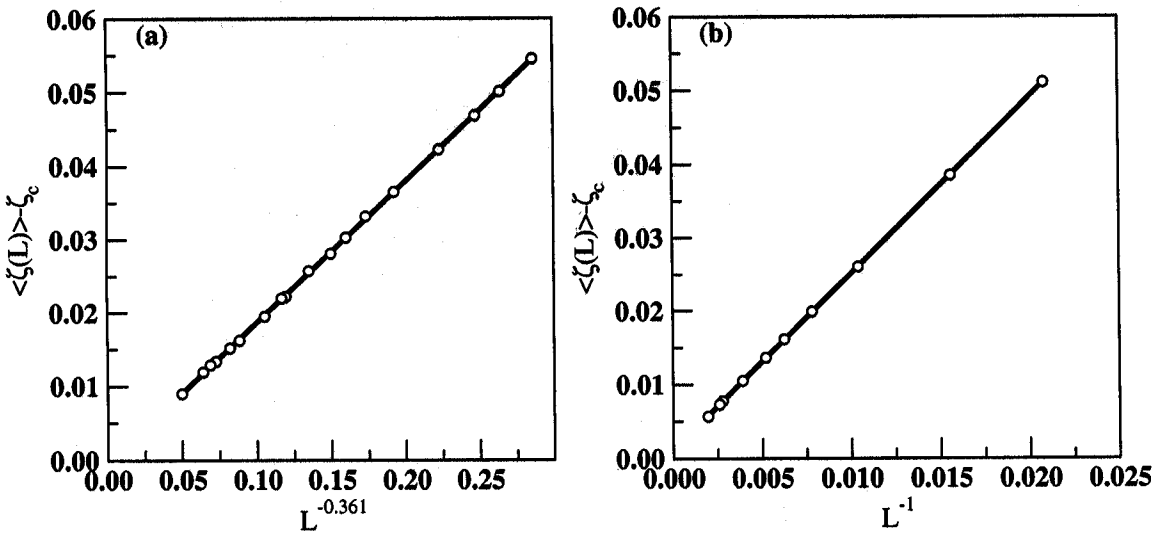

Figure 5.3: The variation of the deviation of the critical density $\zeta_c(L)$ of a system of size L from its critical value ζ_c is plotted with $L^{-1/\nu_\parallel}$. We obtained (a) for DDFES $\zeta_c \approx 0.4115, \nu_\parallel = 1/0.361 \approx 2.77$ and (b) for SDFES $\zeta_c \approx 0.5, \nu_\parallel \approx 1$.

and annihilate, however for an infinite avalanche these two random walkers cannot meet and the best possible way it can be ensured if they can maintain a distance of $L/2$ on the average from each other.

Therefore the minimum possible sustained activity for DDFES in a system of size L is $\rho = 1/(2L)$. For the DDFES it is found that if the density is slightly increased the avalanches created by the additional grains die away and the system maintains the activity of the infinite avalanche. In a sense the system gets locked with this activity for a certain range of grain density. However on increasing the density even further, a second infinite avalanche is created and both the TFs run simultaneously resulting a sudden jump in the activity by doubling its magnitude to $1/L$. This continues for some range of grain density which ends at another jump in activity to $3/(2L)$. Thus in general the variation of activity is discrete and has a step like variation with step heights $1/(2L)$ (Fig.5.2). As the system size increases the step height decreases to zero and the variation of ρ with ζ becomes more and more smooth. Similar step-like behavior of the order parameter was also observed in [69].

The configurations at the steady state are periodic and the same detailed distribution of grain numbers at all sites repeat at regular intervals of time. The periodic time is always multiples of L in a $L \times L$ system. For small systems this period has different values for different initial configurations but in most (about 95%) cases the period is $2L$ and rarely L, $3L$, $4L$ etc. However, for bigger system sizes e.g., for $L = 512$, 1024 or more the period is always $2L$. This helps to calculate the order parameter. Given an initial distribution of grains, it therefore needs to find out the mean activity over only a period and then average over many initial configurations.

The critical density ζ_c actually has a system size dependence. To study this variation we start with a closed empty lattice of size $L \times L$ and go on adding sand grains one by one at randomly selected lattice sites similar to what is done in an

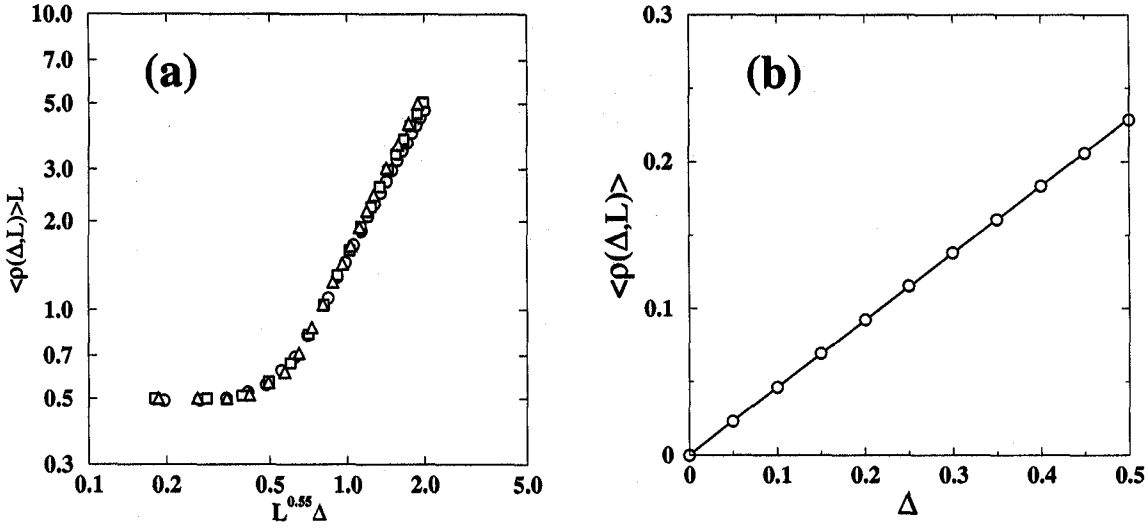

Figure 5.4: (a) Scaling of the order parameter $\langle\rho(\Delta, L)\rangle$ with the deviation $\Delta = \zeta - \zeta_c$ from the critical point for DDFES. From this data collapse and Eqn. (5.1) we find, $\beta/\nu_\perp = 1$ and $1/\nu_\perp = 0.55$. (b) Variation of the order parameter $\langle\rho(\Delta, L)\rangle$ with the deviation $\Delta = \zeta - \zeta_c$ from the critical point for SDFES of a system of lattice size $L = 64$. The plot of data for different system sizes fall on top of one another. Thus using Eqn. (5.1) we conclude, $\beta \approx 1$ and $1/\nu_\perp \approx \infty$.

open sandpile. The dynamics of the avalanche is followed for each sand grain added. The mean avalanche size increases with the density of grains in the system and at a certain $\zeta = \zeta_c(L)$ depending on the sequence of randomly selected sites at which the grains were dropped, the activity does not stop any more and an "infinite" avalanche continues for ever. In practice, in our simulation we followed an avalanche up to a certain relaxation time $T = 10^6$ for $L < 128$ and $T = 5 \times 10^6$ for $L \geq 128$ to declare the avalanche as infinite. Repeating this simulation a large number of times, every time starting from an empty system, we calculate the average critical density $\langle\zeta_c(L)\rangle$. These values are then extrapolated as: $\langle\zeta_c(L)\rangle = \zeta_c + AL^{-1/\nu_\parallel}$ for DDFES as shown in Fig.5.3(a) to obtain $\zeta_c = 0.4115 \pm 0.002$ and $1/\nu_\parallel = 0.361$ giving $\nu_\parallel \approx 2.77$. We also estimated ζ_c by the scaling plot of mean avalanche size $\langle s(L)\rangle L^{-0.05}$ vs. $\Delta L^{0.03}$ which is also consistent with our estimate of $\zeta_c = 0.4115$.

Initially after randomly distributing ζL^2 grains the system is allowed to evolve up to a relaxation time T after which the activity is measured at every time step. To measure the mean activity $\langle\rho(\Delta, L)\rangle$ for a slightly higher density $\zeta + \delta\zeta$ we take the advantage of the fact that the system dynamics is deterministic. On the same initial distribution of grains corresponding to the density ζ another $(\delta\zeta)L^2$ grains are randomly added. This ensures that if certain density gives sustained activity, its higher density necessarily gives a non-stop activity. These measurements are then repeated for different system sizes. In Fig.5.4(a) we show the scaling of the order parameter on double logarithmic scale for DDFES. Plotting $\langle\rho(\Delta, L)\rangle L$ with $L^{0.55}\Delta$ we observe a nice data collapse for system sizes L =128, 256 and 512. Comparing with the Eqn. 5.1 we conclude $\beta/\nu_\perp = 1$ and $1/\nu_\perp$=0.55. This implies that $\beta = \nu_\perp \approx 1.82$.

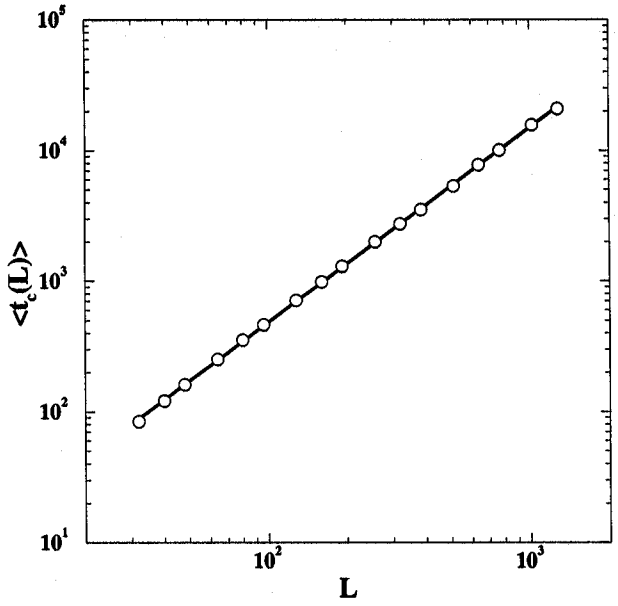

Figure 5.5: The average of maximal life-time $\langle t_c(L)\rangle$ of the avalanche prior to the infinite avalanche is plotted with L for DDFES. The slope gives a measure of the dynamical exponent $z = 1.49$.

From the analysis made so far we can estimate the dynamical exponent $z = \nu_{\|}/\nu_{\perp} \approx 1.52$. This value of the dynamical exponent is directly verified by measuring the survival probability. The survival probability $P(t)$ that the initial activity in a random distribution of grains survives a time t has an exponential distribution as: $P(t) \sim exp(-t/\tau)$. At the critical point ζ_c the characteristic time is a function of only the system size as: $\tau(L) \sim L^z$ where, z is the dynamical exponent $z = \nu_{\|}/\nu_{\perp}$ of the system. Therefore we calculate the average survival time $\langle t_c(L)\rangle$ which is also proportional to L^z at ζ_c for different system sizes. This is done again by dropping grains of sand one by one into a closed system and calculating the life time of the largest avalanche before the system gets locked into an infinite avalanche. Averaging over many initial configurations the largest life-time $\langle t_c(L)\rangle$ is plotted in Fig.5.5 for DDFES on a double logarithmic scale. The slope of the straight line gives the value for the dynamical exponent $z = 1.49 \pm 0.05$ for DDFES compared to 1.52 obtained previously.

5.2.2 Stochastic directed FES (SDFES)

In the stochastic directed fixed energy sandpile model the critical density ζ_c is found to be very close to 0.5. A similar to DDFES calculation of the system size dependent critical density after extrapolation $\langle \zeta_c(L)\rangle = \zeta_c + A' L^{-1/\nu_{\|}}$ gives $\nu_{\|} \approx 1$ and $A' \approx 2.4$ (Fig. 5.3(b)). The order parameter for SDFES has a highly linear variation with Δ as: $\rho(\Delta) = A\Delta$ where $A \approx 0.46$ (Fig.5.4(b)). The plot of $\langle \rho(\Delta, L)\rangle$ vs. Δ is a very nice straight line and the plot of data for different system sizes fall on top of one another. We conclude that $\beta \approx 1$ and $\nu_{\perp} \approx \infty$.

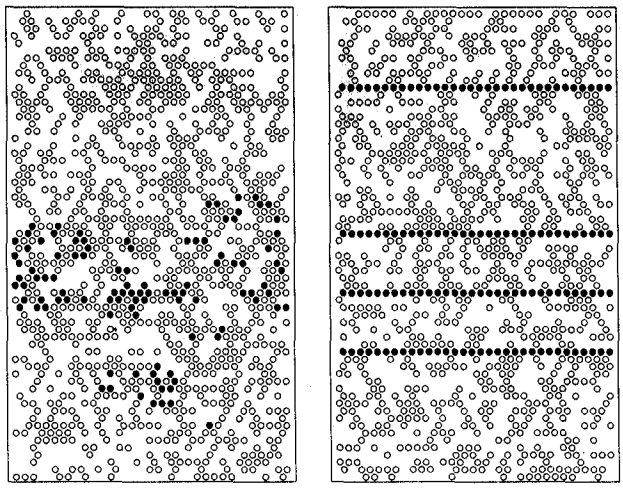

Figure 5.6: Two snapshots of height configurations in the directed fixed energy sandpile model on a 32×64 oriented square lattice, downward direction being the preferred direction. Stochastic DFES is shown on the left where as the deterministic DFES is shown on the right. Active sites are shown by filled circles, open circles denote sites with height 1 and vacant sites are not indicated.

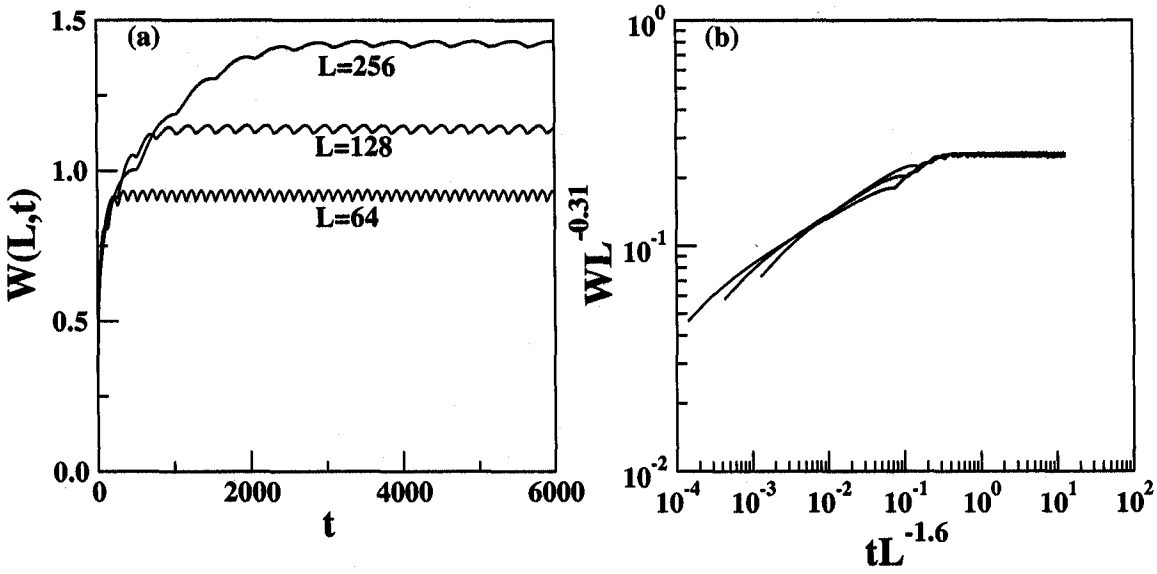

Figure 5.7: (a) Variation of the interface width of $H_i(L,t)$ denoting the number of topplings up to the time t with time t for each site i for lattice sizes $L = 64$, 128 and 256 for DDFES model studied at $\zeta_c(L)$. (b) Data collapse analysis for DDFES at $\zeta_c(L)$ for the interface width of $H_i(L,t)$ in (a) for lattice sizes $L = 64$, 128 and 256.

Model	ζ_c	β	$\nu_\perp$	$\nu_\parallel$
DDFES	0.4115	1.82	1.82	2.77
SDFES	0.5	1.00	∞	1.00
BTW FES	2.125	0.7	0.90	1.49
Manna FES	0.71695	0.64	0.82	1.29
DP		0.583	0.733	1.295

Table 5.1: Comparison of critical points and exponents for different models of fixed energy sandpiles. Exponent values for BTW and Manna sandpiles are taken from [67], DP exponents from [105].

5.3 Comparison: DDFES and SDFES

We also studied the DFES models on oriented square lattices of rectangular shapes, the longer sides being parallel to the preferred direction. For DDFES model the TFs are contiguous sites covering the transverse direction in the form of rings. These toppling rings are perfectly stable, once formed they never change in shape. As density increases, the number of such rings increases. On the other hand for SDFES, the toppling sites are randomly scattered throughout the system (Fig.5.6).

The roughening of the associated interface [65] in our FES models is studied. If $H_i(L,t)$ denotes the number of topplings up to the time t for each lattice site i then the set of $H_i(L,t)$s for all i represent an interface [67]. For DDFES the width of this interface fluctuates periodically (Fig.5.7(a)) but its average grows as: $W(L,t) \sim L^\alpha \mathcal{G}(t/L_i^z)$ where we find $\alpha = 0.31$ and $z = 1.6$ (Fig.5.7(b)) in comparison to the Linear Interface Model results $\alpha = 0.75$ and $z = 1.56$ [106].

5.4 Conclusion

In this chapter we have discussed the directed version of the fixed energy sandpile on the oriented square lattices. Like isotropic FES, our directed FES also shows a continuous phase transition from an absorbed phase to an active phase. Two versions of the model are studied. In the deterministic FES, the grain number configurations are periodic and repeats at regular time interval of $2L$. For this model the critical points as well as the critical exponents are found to be non-trivial and belong to a new universality class. The other version has the stochastic toppling dynamical rules and exponents of mean-field nature are found for this model. In Table 5.1 we compare the critical points and the exponents for different models of fixed energy sandpiles.

Chapter 6

A Percolation model of Diagenesis

6.1 Introduction

It is well known that sedimentary rocks have highly porous structures, typically the pore space is highly branched and connected networks of pores exists in the macroscopic length scales, even when the porosity is very negligible. This connected pore space plays a very important role in transport properties like conductivity and permeability in rocks, where the brine solution filling up the pore-space is responsible for transport properties. Study and understanding of the properties of the pore structures of these rocks are very important in oil-exploration, ground water flow, spread of pollutants etc.

An interesting property of these rocks is that they appear not to have a finite percolation threshold [72]. It has been observed that samples of sedimentary rocks show finite conductivity even when the porosity is less than 1%. This implies that a connected network of pores exists in the macroscopic length scales, even when the porosity which is the volume fraction of the void space is very little.

Several empirical laws reflect this property. Archie's law [73] describes the electrical conductivity of brine filled rocks $\sigma(\phi)$ and the porosity ϕ in the following way:

$$\sigma(\phi)/\sigma_w = a\phi^z \tag{6.1}$$

Here, σ_w is the conductivity of water, $a \sim 1$ is an empirical parameter and $z \sim 2$ is a non-universal exponent that depends on characteristics of the rock structure. This law suggests that a finite conductivity persists even in the limit of $\phi \to 0$ and therefore the percolation threshold is zero.

Another empirical law known as the Kozeny equation [74] relates the permeability $K(\phi)$ of the rock structure to the porosity ϕ through a similar power law,

$$K(\phi) = c\phi^{z'}/S_o^2 \tag{6.2}$$

where, $z' \sim 3$, S_o is the specific surface area and c is an empirical constant. This equation also suggests that the pore space is connected in the $\phi \to 0$ limit.

The permeability of rock structure is defined as the velocity of the fluid per unit pressure gradient times the viscosity of the fluid. This is known as Darcy's law [75, 76].

$$J = (AK/\mu)\nabla P \tag{6.3}$$

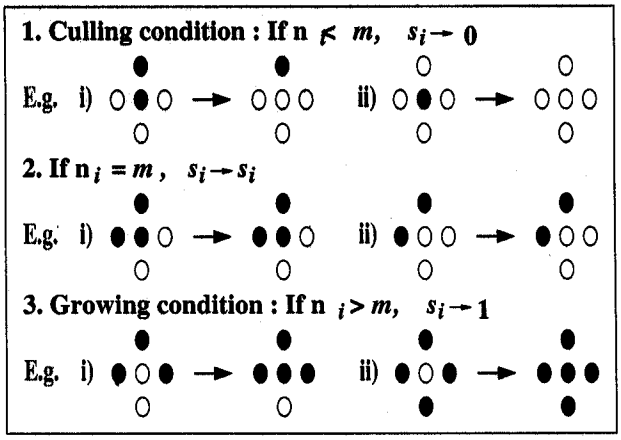

Figure 6.1: Diagenetic conditions for $m = 2$ on a square lattice.

where J is the volumetric flow rate, A is the cross-sectional area of the sample, K the permeability, μ the viscosity of the fluid flowing through the porous medium and ∇P the pressure gradient.

A physical process which is responsible for achieving a connected pore structure at very low porosity is known as "diagenesis". Diagenesis is a complex restructuring process by which granular systems evolve in geological time scales from unconsolidated, high-porosity packings toward more consolidated, less porous structures. Formation of sedimentary rocks starts with deposition of sand grains under water or in air [77, 78, 79]. Initially this gives an unconsolidated and highly porous $\sim 40-50\%$ sediment. Sedimentation is followed by compaction under pressure and diagenesis, before the consolidated sandstone is formed from the loosely packed sediment [80]. Diagenesis may reduce porosity by an order of magnitude and permeability by as much as four orders of magnitude [77].

The final characteristic of the pore network depends strongly on the diagenetic process. Sandstones are usually formed under water, which contains dissolved salts. Depending on the nature of the pore-filling fluids, salts may be deposited as crystallites in the crevices or along walls of the rock structure, a process called "cementation". Otherwise, portions of the existing solid structure may get eroded or dissolved out in a "dissolution" process. The former decreases the porosity of the rock while the latter increases porosity. The two processes may take place simultaneously. The details of the chemical nature of the solid and pore filling fluid determines whether diagenesis leads finally to a stable structure, or to a continuously developing structure eventually giving rise to caverns of macroscopic size.

Sahimi had classified the theoretical studies of modeling diagenesis in two ways [79]. The approach of "chemical modeling" relies on solving continuum equations of transport and reactions ignoring the morphology of the pore space. The second approach is "geometrical modeling" in which the reaction kinetics and mass transfer are ignored. These models start with geometrical descriptions of initial unconsolidated pore space which evolves under simple rules leading to reduction of porosity but maintaining the connectivity.

For example the model of Wong et. al. [81] starts with a regular lattice in

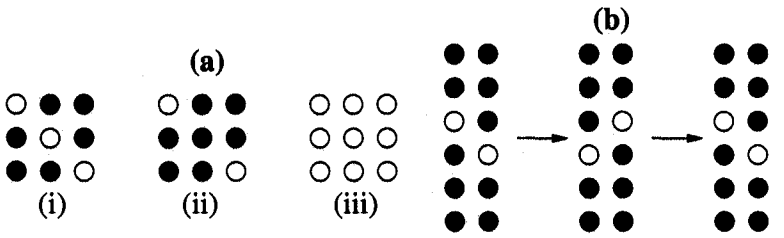

Figure 6.2: (a) On an initial configuration as in (i) if the central site is first updated one gets the SC in (ii). However if the sequential updating rule (I) (see text) is used one gets the SC as in (iii). (b) In parallel updating this configuration is locked in a period of cycle 2.

which each bond is a fluid filled cylindrical tube of uniform radius and conductivity. This system evolves to a random resistor network through a random bond-shrinkage mechanism where randomly selected bonds of the network shrinks its radius by a constant factor. This model maintains global connectivity even in the limit of $\phi \to 0$ and reproduces power law behavior as in Archie's law.

A second model of Roberts and Schwartz [82] starts with a Bernal distribution of dense random spheres of equal radii modeling grains. These spheres grow in unison and the pore space, i.e. the space not covered by the spheres shrinks its volume. This model gives a low but non-zero percolation threshold $\phi_c \approx 3.5\%$. The bimodal ballistic deposition model (BBDM) [83] tries to represent the deposition realistically, but does not address the problem of diagenesis.

In our model, we do not take into account the effect of chemical reactions explicitly, so this is also a geometrical modeling of diagenesis. We try to simulate the restructuring as it may actually occur in porous rocks due to fluid flow. Isolated projected grains on a wall are smoothed out modeling dissolution, and a gap or cul-de-sac in a solid is filled by deposition modeling cementation. The restructuring involves two processes. Growth of the solid phase at sites with a relatively larger number of occupied nearest neighbors, to represent cementation, and removal or culling of occupied sites which are isolated, or have too few nearest neighbors, to represent dissolution. This algorithm is a stabilizing process leading to a stable structure after several time steps. It may be regarded as a self-organizing process as discussed recently by several authors [107, 108].

Before proposing our model of diagenesis we briefly describe the Bootstrap percolation model which is very related to our model in section §6.1.1. In §6.2 we describe our model for diagenesis in sedimentary rocks, in §6.3 we discuss the results for our model of diagenesis and finally we conclude in §6.4.

6.1.1 Bootstrap percolation

In Bootstrap percolation model (BPM) sites of a regular lattice are occupied with a certain probability p and if these occupied sites have less than certain number of occupied neighbors, m, they are successively removed by a process called 'culling' [109, 110, 111, 112, 113, 114]. On repeated application of the culling process a stable configuration (SC) is reached where no further sites can be culled. There exist a

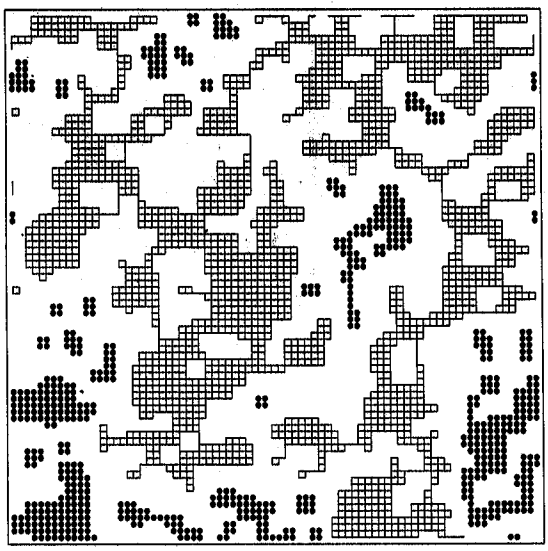

Figure 6.3: A stable configuration of the diagenetic percolation on a square lattice of system size $L = 80$ and with m=2. Sites on the "infinite" incipient cluster are joined by lines and sites on the isolated clusters are shown by filled circles.

threshold value $p_c^m(BPM)$ of the probability p, depending on the value of m, beyond which the stable configuration (SC) is percolating.

The study of BPM was motivated by the behavior of some magnetic materials like $Tb_cY_{1-c}Sb$ where the magnetic moment is determined by a competition of the exchange and the crystal field interactions. In such materials, a spin if surrounded by too many non-magnetic neighbors may become non-magnetic. So if the impurity concentration is gradually increased the magnetic order may get destroyed [109].

It is evident that for $m \leq 2$, the connectivity of the lattice, is not affected by the culling condition since nothing is culled for $m = 0$, isolated sites are culled for $m = 1$ and the dangling chain of sites are culled for $m = 2$. Therefore for all values of m, $p_c^m(BPM)$ is greater or equal to the ordinary percolation threshold, p_c(ord). It is seen in [115] that for $m \geq d + 1$ the SC is a single infinite m-cluster.

The percolation probability $Q_m^{BPM}(p)$ is the fraction of particles that survive on the infinite percolating cluster, which varies as

$$Q_m(p) - Q_m(p_c^m(BPM)) \sim (p - p_c^m(BPM))^\beta \tag{6.4}$$

where,

$$Q_m(p_c^m(BPM)) = \lim_{p \to p_c^m(BPM)} Q_m(p) \tag{6.5}$$

Due to finite size the scaling variable scales as L/ξ where $\xi = (p - p_c^m(BPM))^{-\nu}$ is the correlation length. The scaling relation is,

$$Q_m(p) - Q_m(p_c^m(BPM)) = L^{-\beta/\nu} F[(p - p_c^m(BPM))L^{1/\nu}] \tag{6.6}$$

where, the scaling function $F(x) \to x^\beta$ for large L. In [113] from scaling plot the values obtained are $\nu \approx 4/3$ and $\beta \approx 0.1$ which are comparable to the corresponding values of 4/3 and 5/36 in the ordinary percolation in 2-d.

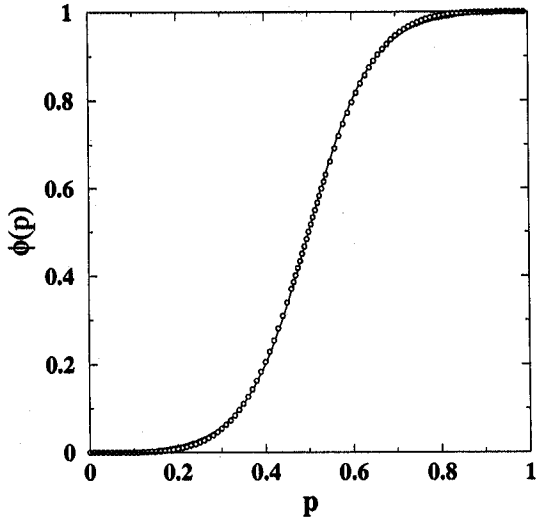

Figure 6.4: The porosity $\phi(p)$ as a function of the initial occupation probability p for a square lattice of system size $L = 64$. The continuous curve is a fit to the data having the form given in Eqn. 6.7.

For the nearest neighbor Ising model at the zero temperature with Glauber spin-flip dynamics in the absence of an external magnetic field the direction of a spin follows the direction of the majority of the neighboring spins. In the case when there are equal number of up and down spins in the neighborhood, a spin decides its direction with equal probability. It has been observed in [116] that starting from an arbitrary random initial configuration of spins this system does not reach the global ground states where all spins are either up or down but arrive at a frozen two-stripe state in a finite fraction of cases [116].

6.2 Our model of Diagenesis

In our model [117, 118], the sites of a regular lattice are randomly occupied ($s_i = 1$) with a probability p representing pores and are kept vacant ($s_i = 0$) with a probability $1 - p$ representing solid grains. This configuration therefore models the initial unconsolidated porous structure with porosity $\phi(p) = p$. The occupation status of a site i depends on its neighbor number i.e., the number of occupied neighbors $n_i = \Sigma_j s_j^i$ where, s_j^i is the occupation of the j-th neighbor of the site i. All sites of the lattice are sequentially updated according to the following diagenetic conditions (Fig.6.1) :
(i) *Culling condition*: Occupied sites having fewer than m occupied nearest neighbors are vacated i.e., $s_i \rightarrow 0$ if $n_i < m$. This condition models the cementation process
(ii) the sites with exactly m occupied neighbors remain unaltered i.e., $s_i \rightarrow s_i$ if $n_i = m$ and
(iii) *Growing condition*: Vacant sites having more than m occupied nearest neighbors are occupied i.e., $s_i \rightarrow 1$ if $n_i > m$. This condition models the dissolution process.

Starting from a random initial configuration the system evolves in different time

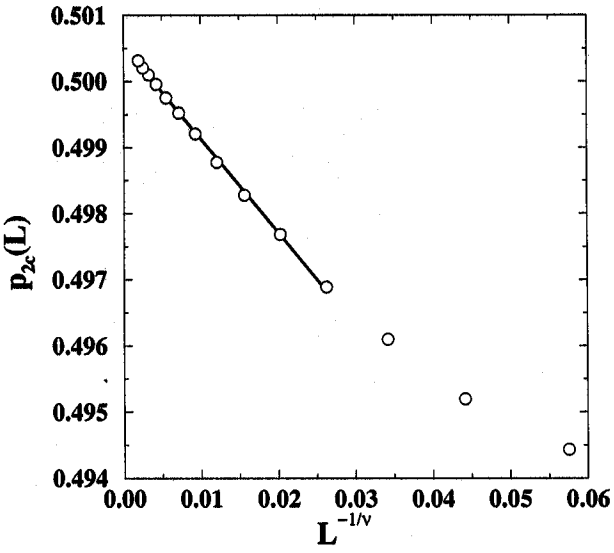

Figure 6.5: The plot of the percolation thresholds $p_{2c}(L)$ for $m = 2$ for a square lattice of system sizes L as a function of $L^{-1/\nu}$. Using $\nu = 4/3$, the correlation length exponent for ordinary percolation, we get the linear fit for large L values. The extrapolated value for p_{2c} is 0.5005.

steps following these rules. One time step consists of update attempts of all the lattice sites. One sweep of the lattice results in another occupied configuration which is again updated by the same rules. This process is continued till the system reaches a stable configuration (SC) where no further site changes its occupied or vacant status. In general the SC may have many clusters of occupied sites. However, there exists a percolation threshold p_{mc} of p depending on the value of m so that the SC must have a spanning ("infinite") cluster of occupied sites for $p > p_{mc}$ in an infinitely large system.

6.2.1 Stable configuration (SC)

Like the cellular automata models, the sequence of updating different sites is important in our problem. Three possible sequential updating procedures are as follows:
(I) Sites are labeled from 1 to L^2 from left to right along a row and from the first row to the last row.
(II) Only sites with $n_i \neq m$ are randomly selected and updated.
(III) The lattice is divided into odd and even sub-lattices and are updated alternately but sequentially as in (I).

For BPM, it has been shown in [113] that the SC is independent of the updating sequence. In contrast here [117, 118]the SC does depend on the updating sequence because culling at one site may inhibit growth at a neigboring site and vice versa. This is seen by considering the neighbor numbers at all sites of the lattice. When $n_i < m$ the culling of the site i reduces the neighbor numbers at all neighboring sites by one i.e., $n_j \rightarrow n_j - 1$ where as the growth at i enhances the neighbor numbers at all neighboring sites i.e., $n_j \rightarrow n_j + 1$. Therefore the culling at one site may suppress

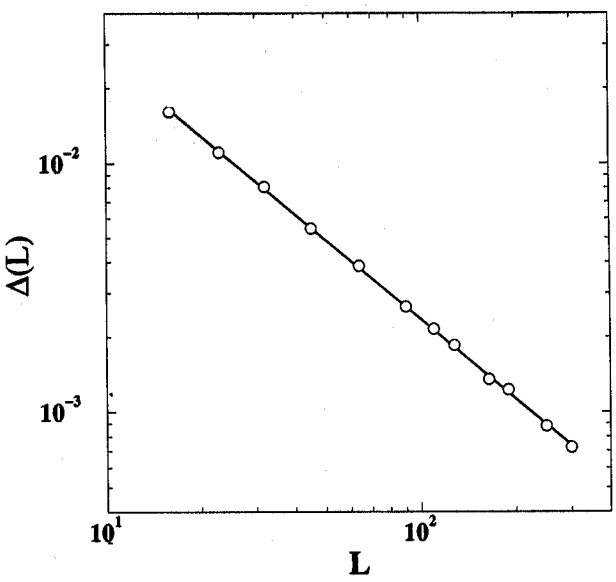

Figure 6.6: The plot of the standard deviation in $p(seq)$ for $m = 3$ on a cubic lattice for finite system sizes L as a function of L. From the plot we get the value of ν to be 0.90(3).

the growth at a neighboring site and vice versa. In Fig.6.2(a) we show an example where two different updating sequences lead to different SCs. On the other hand, in a fully parallel update all sites of the lattice are updated simultaneously at a certain time depending on the configuration at the previous time. There may arise some situations as shown in Fig.6.2(b) where a particular cluster of sites never goes to a stable configuration but takes two different configurations alternately in a two cycle periodic state.

6.2.2 Clusters in the stable configurations

A cluster of occupied sites, in which every site has at least m occupied neighbors, is called an m-cluster [110]. Imposition of our diagenetic rules imply that the surviving clusters in SC must be m clusters. An isolated cluster of occupied sites in a d-dimensional hypercubic lattice always has some convex corners on the surface with d neighbors. Therefore in the case when $m \geq d + 1$ these sites are always unstable and therefore, the SC cannot have any finite cluster and has only one infinite m-cluster. A SC at the percolation threshold for $m = 2$ on a square lattice is shown in Fig.6.3, the smallest isolated clusters being of size 4.

6.3 Results

The average fraction $\phi(p)$ of the occupied sites in the SC is defined as the porosity of this model. We measure this porosity as a function of the probability p and this variation is plotted in Fig.6.4. We find no trace of any system size dependence on

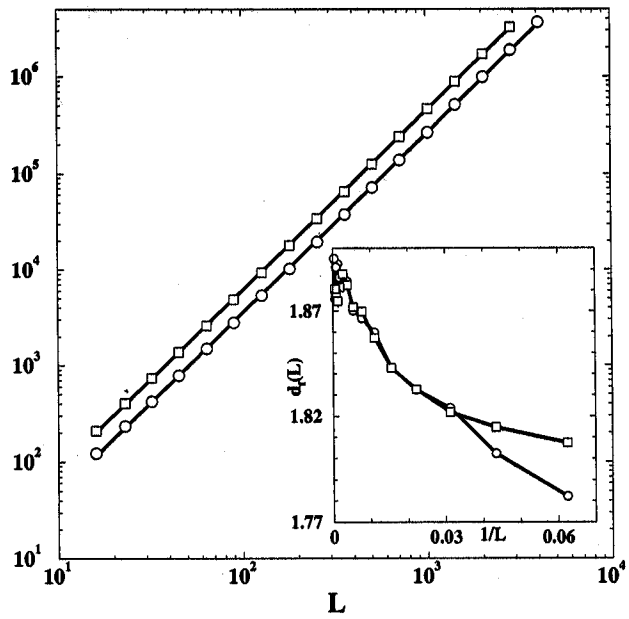

Figure 6.7: The average mass of the infinite cluster S^1_∞ (circle) and the largest cluster $2S^2_\infty$ (square) at the diagenetic percolation threshold $p_{2c}(L)$ are plotted with the system size L on a square lattice. Average fractal dimension is obtained from the linear fits shown by continuous lines. The inset shows the variations of the local slopes $d_f(L)$ and we conclude a value of the fractal dimension $d_f = 1.89 \pm 0.02$.

this variation. A functional form like

$$\phi(p) = 1/[1 + \exp((1/2 - p)/\Delta p)] \tag{6.7}$$

fits very well to this data both in two and in three dimensions with a value of $\Delta p = 0.072$ in two dimension [117] whereas Δp=0.031 in three dimensions [118]. The data as well as the fit are very well consistent to $\phi(1/2) = 1/2$ as expected from the symmetry of occupied and vacant sites. Compared to the porosity $\phi(p) = p$ in the initial random distribution of occupied and vacant sites, the porosity in SC is reduced by an order of magnitude when $p < 0.35$. We consider this as the reflection of the diagenesis process in nature observed in our model.

6.3.1 The Diagenetic percolation threshold

Like BPM, the culling condition in our model does not contribute to change the percolation threshold for $m \leq 2$. For example, nothing is culled for m=0, isolated sites are culled for $m = 1$ and the dangling chain of sites are culled for $m = 2$. Since the connectivity of the system is not affected by these culling processes, the difference between p_{mc} and $p_c(ord)$ is due to the growing condition for $m \leq 2$, where $p_c(ord)$ is the ordinary percolation threshold. For p values very close to $p_c(ord)$ but smaller than it, there may be some initial configurations which are not connected because of the presence of only few vacant sites. If these sites have more than m occupied neighbors they will now be occupied ensuring the global connectivity of the

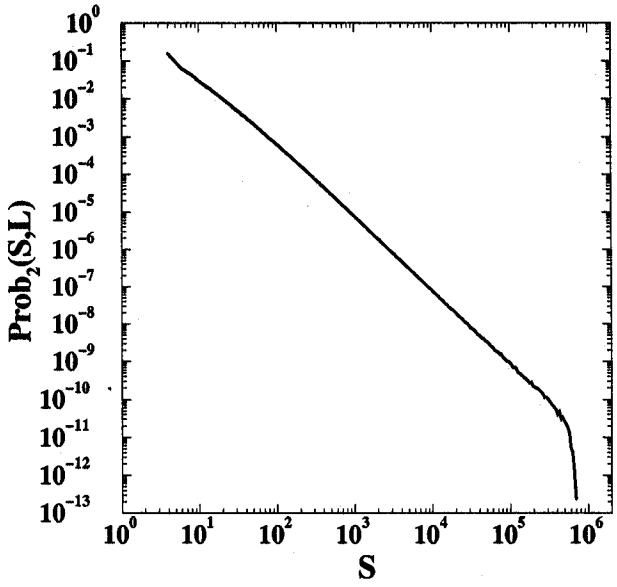

Figure 6.8: The distribution of the cluster sizes of the stable configuration at the percolation threshold of a square lattice of size $L = 2048$ and with $m = 2$.

system. Therefore it is expected that the $p_{mc} \leq p_c(ord)$ for $m \leq 2$ on an arbitrary lattice. Therefore as the growth rule helps in attaining a connectivity in the system we expect $p_{mc} \leq p_c(BPM)$ for any arbitrary lattice and for any arbitrary value of m.

The percolation threshold p_{mc} is the minimum value of the probability p beyond which an infinite cluster of occupied sites exists with probability one in the SC on an infinitely large system. However, for systems of finite size this threshold $p_{mc}(L)$ depends on the system size. The correlation function $g(r)$ for the percolation problem is defined as the probability that a site at a distance r apart from an occupied site belongs to the same cluster. For $p < p_{mc}$ the correlation function is expected to decay exponentially as $g(r) \sim \exp(-r/\xi)$ where the correlation length ξ, a measure of the typical cluster diameter, diverges as $\xi \sim (p_{mc} - p)^{-\nu}$ where, ν is the correlation length exponent for the diagenetic percolation.

We use the standard method of estimating the value of the percolation threshold. Using a specific sequence of random numbers, the lattice is filled at some high value of $p = p_{hi}$ such that its SC has an infinite cluster. Similarly using the same sequence of random numbers, the lattice is filled at some low value of $p = p_{lo}$ so that its corresponding SC does not have an infinite cluster. It is then similarly tried at a $p = (p_{hi} + p_{lo})/2$. If its SC is connecting then p_{hi} is equated to p, otherwise p_{lo} is equated to p. This process is continued till the difference $(p_{hi} - p_{lo})$ is less than a certain pre-assigned small number $\epsilon = 10^{-5}$ when $p(seq) = (p_{hi} + p_{lo})/2$ is taken for the percolation threshold for this particular sequence of random numbers. Averaging over the $p(seq)$ values for a large number of independent random number sequences one obtains the estimate for $p_{mc}(L)$.

In this process, we tune the probability p to the percolation threshold $p_{mc}(L)$ on a system of size L so that the correlation length is of the same order as the system

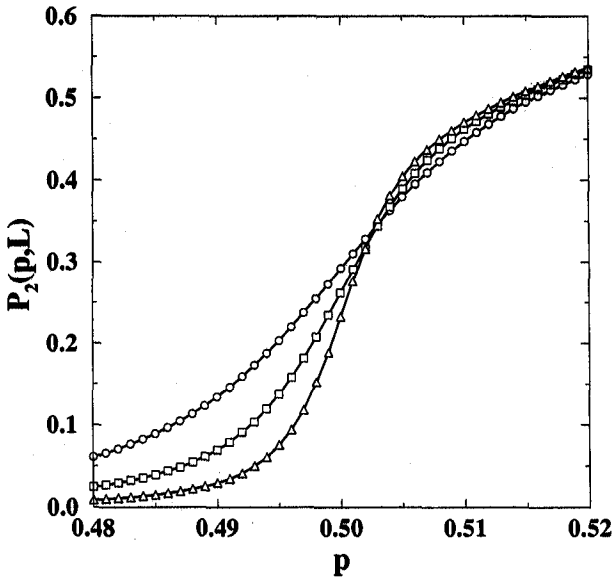

Figure 6.9: The plot of the percolation probability $P_2(p, L)$ for $m = 2$ of the diagenetic percolation on the square lattice for three different system sizes $L = 256$ (circle), 512 (square) and 1024 (triangle).

size. Therefore, $L \sim (p_{mc} - p_{mc}(L))^{-\nu}$ which implies

$$p_{mc}(L) = p_{mc} + A.L^{-1/\nu} \tag{6.8}$$

We plot $p_{2c}(L)$ on a square lattice in Fig.6.5. with $L^{-1/\nu}$ and we try $\nu = 4/3$, the value for the correlation length exponent in the ordinary percolation in 2-d. We observe a linear variation for large L values. On extrapolation, we find a slightly larger value of $p_{2c} = 0.5005(2)$ for sequential updating of type (I) as stated above. The $p_{2c}(L)$ values for L=2048, 2896 and 4096 are found larger than 1/2. For the random and sub-lattice sequential updatings the p_{2c} values are 0.5013 and 0.5009 respectively. These values should compared to the ordinary percolation threshold of 0.592746 on square lattice [119].

Since $m = 2$ is the middle point of the five possible values of the neighbor numbers on a square lattice (i.e. from 0 to 4) and due to the equivalence of vacant and occupied sites, it may be expected that p_{2c} should be exactly equal to 1/2. However, we argue that the value of p_{2c} very close to 1/2 is actually accidental and there is no reason why it should be 1/2. We believe that first appearance of the global connectivity through occupied sites determining the percolation threshold is a very special situation and since we want this connectivity through the occupied sites we break the symmetry between the occupied and vacant sites. Similar to Fig.6.5, in 3-dimension from the plot of $p_{3c}(L)$ with $L^{-1/\nu}$ we tried $\nu = 0.878$ [119], the value of the correlation length exponent for ordinary percolation in 3-dimension. We observe a linear variation for large L values. On extrapolation, we find the value of $p_{3c} = 0.444(5)$ for sequential updating where sites are labeled from 1 to L^3 sequentially increasing the x, y and z coordinates. However, for $m = 3$ on the triangular lattice the value of the percolation threshold is obtained as 0.50 ± 0.01.

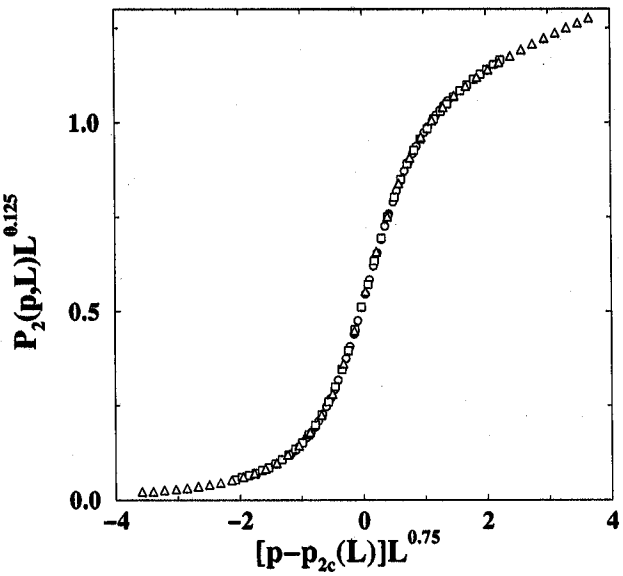

Figure 6.10: The diagenetic percolation probability $P_2(p, L)$ as shown in the previous figure for the square lattice of different system sizes are scaled as $P_2(p, L)L^{\beta/\nu}$ with $[p - p_{2c}(L)]L^{1/\nu}$. The collapse is obtained using ν=4/3 and β/ν =0.125.

The $p(seq)$ values corresponding to different sequences of random numbers are spread around their mean value $p_{mc}(L)$. The root mean square deviation from the average value

$$\Delta(L) = (< p(seq)^2 > -[p_{mc}(L)]^2)^{1/2} \tag{6.9}$$

is supposed to have a dependence on the system size L as: $\Delta(L) \sim L^{-1/\nu}$. Plotting $\Delta(L)$ vs. L for $m = 2$ on a square lattice on a double logarithmic scale which fits nicely to a straight line gives a value for the correlation length exponent $\nu = 1.35(2)$. In Fig.6.6 we plot $\Delta(L)$ vs. L for $m = 3$ on a cubic lattice on a double logarithmic scale which fits nicely to a straight line giving a value for the correlation length exponent $\nu = 0.90(3)$.

A spin model on a square lattice where each spin ± 1 was flipped only when more than half of its four neighbors point into the opposite direction was studied in [120]. Using a much bigger system size ($L \approx 7 \times 10^5$) compared to what we used, a percolation threshold of 0.5007 ± 0.0001 was estimated which is consistent with our results.

6.3.2 Cluster statistics

The fractal dimension d_f of the "infinite" incipient cluster (IIC) of the SC exactly at the percolation threshold is also calculated. A large number of SCs are generated at $p = p_{2c}$. The average size S_∞ of the IIC is calculated in two ways: (i) Average size $S^1_\infty(L)$ of the infinite clusters is measured over the spanning SCs only (ii) Average size $S^2_\infty(L)$ of the largest cluster is calculated over all SCs. Defining the percolation probability on a square lattice as, $S^2_\infty(L) = L^2 P_2(p_{2c}(L), L)$. Both measures of the IIC are expected to give the fractal dimension: $S^{1/2}_\infty(L) \sim L^{d_f}$. In Fig.6.7 we plot

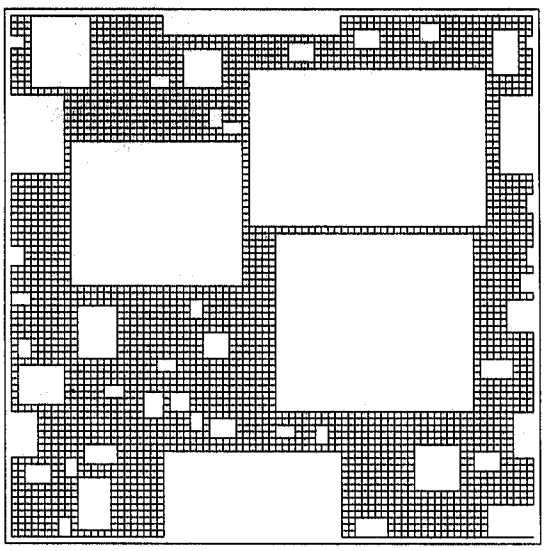

Figure 6.11: A stable configuration (SC) at the percolation threshold for a square lattice of system size of $L = 80$ and with m=3. Sites on the "infinite" incipient cluster are joined by lines.

both $S^1_\infty(L)$ and $2S^2_\infty(L)$ with L for a square lattice on a double logarithmic scale for the system sizes varying from 16 to 4096. The average slopes are 1.863 and 1.860 for $S^1_\infty(L)$ and $S^2_\infty(L)$ respectively. Further, we plot the local slopes $d_f(L)$ with $1/L$ in the inset of Fig.6.7. After considerable variation over the small systems the fractal dimension seems to converge at 1.89 ± 0.02 for the large system sizes compared to 91/48 of the ordinary percolation [72] in 2-d. Using the same procedure for 3-dimension we obtained the value for the fractal dimension to be 2.32(10).

The cluster size distribution of occupied sites on the SCs are also measured at the percolation threshold. We define $\text{Prob}_2(S, L)$ as the probability of a cluster of S occupied sites on a SC of a square lattice of system size L with $m = 2$. We start from many independent configurations at $p_{2c}(L) \approx 0.5001$ for $L = 2048$. These are sub-critical configurations for the ordinary percolation. We measure the $\text{Prob}_2(S, L)$ at each time step and keep track of how this distribution changes from the initial exponential distribution to the power law distribution as shown in Fig.6.8. We notice that at very short times of the order of 1, the distribution takes the form of the steady state distribution. In this distribution we do not include the "infinite" cluster spanning the system. As expected the distribution appears to be a power law: $\text{Prob}_2(S, L) \sim S^{-\tau}$ where $\tau = 2.02 \pm 0.06$ is obtained compared to 187/91 for the ordinary percolation [72] in 2-d. For $m = 3$ on a cubic lattice we start from many independent configurations at $p_{3c}(L) \approx 0.4428$ for $L = 150$. We measure the $\text{Prob}_3(S, L)$ at each time step. We find that this distribution changes from the initial exponential distribution to the power law distribution $\text{Prob}_3(S, L) \sim S^{-\tau}$ where $\tau = 2.19(5)$ is obtained compared to 2.18 for the ordinary percolation [72] in 3-d.

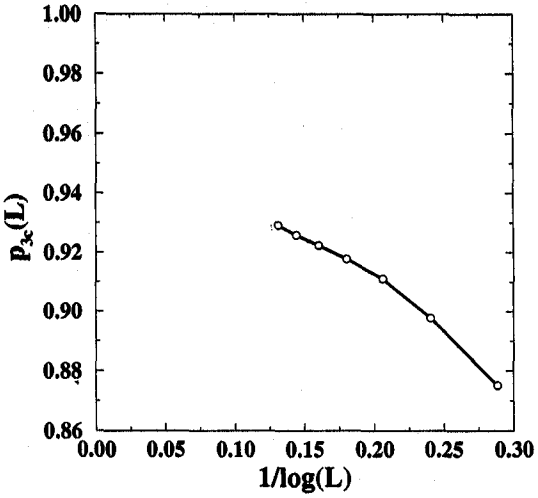

Figure 6.12: On a square lattice plot of $p_{3c}(L)$ with $1/\log(L)$ which on extrapolation to $L \to \infty$ gives $p_{3c} = 0.96 \pm 0.01$.

6.3.3 Order parameter

The order parameter is the percolation probability $P_m(p)$ that is the average fraction of sites on the largest occupied cluster in the SC. For finite systems it is denoted by $P_m(p, L)$. Variation of the percolation probability is shown in Fig.6.9 and it varies as:

$$P_m(p, L) \sim [p - p_{mc}(L)]^{\beta} \tag{6.10}$$

This variation is true in the limit of $L \to \infty$. For finite systems however, according to the scaling theory [72], the scaling variable should be L/ξ, where the correlation length is defined as $\xi = [p - p_{mc}(L)]^{-\nu}$. Therefore for a finite system of size L the variation of percolation probability should be:

$$P_m(p, L) = L^{-\beta/\nu} F[(p - p_{mc}(L))L^{1/\nu}] \tag{6.11}$$

where, the scaling function $F(x) \to x^{\beta}$ for large L. We show the collapse of the data for $m = 2$ on a square lattice in Fig.6.10 using this scaling formulation. We again try $\nu = 4/3$ and then obtain a value of $\beta/\nu = 0.125$ for the data collapse, giving $\beta = 0.166$ for $m = 2$ on a square lattice compared to 5/36 for the ordinary percolation in 2-d [72]. For $m = 3$ on a cubic lattice we obtain $\nu = 1/1.1 = 0.909$ and β/ν=0.54 giving β=0.49 compared to 0.41 in ordinary percolation in the three dimensions [72].

6.3.4 Percolation threshold for different m-values

Next we studied the case of m=3 on the square lattice. In this case the SC can only be completely vacant or it can have only one infinite cluster but cannot have isolated clusters. Since in general there will always be some sites which have less than 3 occupied neighbors on the surface of an isolated cluster, these sites will be unstable under the diagenetic rules and the cluster will therefore cannot survive in

m	d=2	d=3
1	0.04(2)	≈ 0
2	0.5005(2)	0.20(2)
3	0.96(2)	0.444(5)
4		0.80(2)
5		≈ 1

Table 6.1: The diagenetic percolation thresholds p_{mc} for different values of m for two and three dimensions.

SC. In Fig.6.11 we show the picture of a SC for m=3 on a square lattice. It is a simple spanning cluster having many rectangular holes as in BPM [112]. The percolation threshold $p_{3c}(L)$ also has L dependence and on extrapolation with $1/\log(L)$ (as was done in BPM) we get $p_{3c} = 0.96 \pm 0.01$ (Fig.6.12).

Finally we studied the diagenetic percolation thresholds for m=1,2,4,5 as well again on the cubic lattice. These values are given in Table 6.1.

6.4 Conclusion

We studied a geometrical model using the percolation theory of critical phenomena of disordered systems for the process of diagenesis active in natural sedimentary rock formations. The restructuring process of diagenesis involve two basic processes namely the cementation and dissolution which have been studied using a percolation type of model by the culling of occupied sites in rarefied and growth of vacant sites in dense environments sites depending on some preassigned integer parameter value m. We numerically study the percolation thresholds of this model for different values of m both in two and in three dimensions and observe that they are always lower than the ordinary percolation thresholds in similar lattices. This implies that though our model indeed reduces the percolation threshold (compare it with porosity in sedimenary rocks) it is not successful enough to reduce it near zero.

We also studied the critical behavior of such diagenetic percolations. The most interesing situation is when growth and culling are equally competitive i.e., the case when $m = 2$ on a square lattice and the case when $m = 3$ on a simple cubic lattice. Our numerical study indicates a percolation like continuous transition for these situations. Simulations shows that the porosity is highly reduced due to restructuring as is observed in rocks. We also observe that starting from the sub-critical configurations of ordinary percolation at a certain threshold value p_{mc} of the pore probability the system evolves to a globally connected porous space at the stable state. This configuration is critical since it shows long range correlations. Our numerical results give strong indications that the stable states in this model have the same critical behavior as that of ordinary percolation. We view the dynamics under diagenetic rules as a self-organizing dynamics in a limited sense since one has to tune p to arrive at a specific sub-critical configuration at p_{mc} so that it organizes to show criticality in the stable state.

Bibliography

[1] B. B. Mandelbrot, *Fractals: Form, Chance, and Dimension.* (W. H. Freeman, San Fransisco).

[2] B. B. Mandelbrot, *The Fractal Geometry of Nature*(Freeman, New York, 1983).

[3] J. Feder, *Fractals*(Plenum, New York, 1988).

[4] R. Voss, and J. Clarke, Phys. Rev. B. **13**, 556 (1976).

[5] W. H. Press, Comments Astrophys. **7**, 103 (1978).

[6] P. Bak and K. Chen, Physica D **38**, 5 (1989).

[7] P. Bak, C. Tang, and K. Wiesenfeld, in *Random Fluctuations and Pattern Growth: Experiments and Models*, edited by H. E. Stanley and N. Ostrowsky (Kluwer Academic, Dordrecht, 1988).

[8] P. Bak, C. Tang, and K. Wiesenfeld, Phys. Rev. Lett. **59**, 381 (1987).

[9] P. Bak, C. Tang, and K. Wiesenfeld, Phys. Rev. A **38**, 364 (1988).

[10] P. Bak, *How Nature Works: The Science of Self-Organized Criticality*, (Copernicus, New York, 1996).

[11] B. Drossel, and F. Schwabl, Phys. Rev. Lett. **69**, 1629 (1992).

[12] P. Bak, K. Chen, and C. Tang, Phys. Lett. A **147**, 297 (1990).

[13] H. Takayasu, and H. Inaoka, Phys. Rev. Lett. **68**, 966 (1992).

[14] A. Rinaldo, I. Rodriguez-Iturbe, R. Rigin, E. Ijjasz-Vasquez, and R. L. Bras, Phys. Rev. Lett. **70**, 822 (1993).

[15] S. S. Manna, and B. Subramanian, Phys. Rev. Lett. **76**, 3460 (1996).

[16] A. Sornette, and D. Sornette, Europhys. Lett. **9**, 197 (1989).

[17] K. Chen, P. Bak, and S. P. Obukhov, Phys. Rev. A **43**, 625 (1991).

[18] P. Bak, and K. Sneppen, Phys. Rev. Lett. **71**, 4083 (1993).

[19] H. M. Jaeger, C-H Liu, and S. R. Nagel, Phys. Rev. Lett. **62**, 40 (1989).

[20] G. A. Held, D H Solina II, D. T. Keane, W. J. Haag, P. M. Horn, and G. Grinstein, Phys. Rev. Lett. **65**, 1120 (1990).

[21] V. Frette, K. Christensen, A. Malte-Sorensen, J. Feder, T. Josang, and P. Meakin, Nature (London) **379**, 49 (1996).

[22] D. Dhar, Phys. Rev. Lett. **64**, 1613 (1990).

[23] D. Dhar, arXiv:cond-mat/9909009.

[24] S. N. Majumdar, and D. Dhar, Physica A **185**, 129 (1992).

[25] S. S. Manna, J. Phys. A **24**, L363 (1992).

[26] C. Tebaldi, M. De Menech, and A. L. Stella, Phys. Rev. Lett. **83**, 3952 (1999).

[27] S. Lübeck, Phys. Rev. E. **61**, 204 (2000).

[28] O. Biham, E. Milshtein, and O. Malcai, Phys. Rev. E **63**, 61309 (2001).

[29] M. De Menech, A. L. Stella, and C. Tebaldi, Phys. Rev. E. **58**, 2677 (1998).

[30] E. V. Ivashkevich, D. V. Ktitarev, and V. B. Priezzev, Physica A **209**, 347 (1994).

[31] D. V. Ktitarev, S. Lübeck, P. Grassberger, and V. B. Priezzhev, Phys. Rev. E **61**, 81 (2000).

[32] M. De Menech, and A. L. Stella, Phys. Rev. E **62**, R4528 (2000).

[33] D. Dhar, and R. Ramaswamy, Phys. Rev. Lett. **63**, 1659 (1989).

[34] B. Tadic, and D. Dhar, Phys. Rev. Lett. **79**, 1519 (1997).

[35] R. Pastor-Satorras, and A. Vespignani, Phys. Rev. E. **62**, 6195 (2000).

[36] R. Pastor-Satorras, and A. Vespignani, J. Phys. A. **33**, L33 (2000).

[37] P. K. Mohanty, and D. Dhar, Phys. Rev. Lett. **89**, 104303 (2002).

[38] Y.-C. Zhang, Phys. Rev. Lett. **63**, 470 (1989).

[39] S. S. Manna, J. Stat. Phys. **59**, 509 (1990).

[40] P. Grassberger, and S. S. Manna, J. Phys. (France) **51**, 1077 (1990).

[41] S. S. Manna, Physica A **179**, 249 (1991).

[42] A. Chessa, H. E. Stanley, A.Vespignani, and S. Zapperi, Phys. Rev. E **59**, R12 (1999).

[43] S. Lübeck, and K. D. Usadel, Phys. Rev. E. **55**, 4095 (1997).

[44] S. Lübeck, and K. D. Usadel, Phys. Rev. E. **56**, 5138 (1997).

[45] L. Pietronero, A. Vespignani, and S. Zapperi, Phys. Rev. Lett. **72**, 1690 (1994).

[46] A. Vespignani, S. Zapperi, and L. Pietronero, Phys. Rev. E **51**, 1711 (1995).

[47] A. Ben-Hur, and O. Biham, Phys. Rev. E **53**, R1317 (1996).

[48] E. Milshtein, O. Biham, and S. Solomon, Phys. Rev. E **58**, 303 (1998).

[49] A. Díaz-Guilera, Europhys. Lett. **26**, 177 (1994).

[50] A. Corral, and A. Díaz-Guilera, Phys. Rev. E. **55**, 2434 (1997).

[51] K. Christensen, H. C. Fogedby, and H. J. Jensen, J. Stat. Phys. **63**, 653 (1991).

[52] D. Dhar, Physica A **270**, 69 (1999).

[53] H. Jeong, S.P. Mason,A. L.Barabási, and Z.N. Oltvai, Nature, **411**, 41 (2001).

[54] J. Scott, *Social Network Analysis: A Handbook*, (Sage Publications, London, 2000).

[55] S. Wasserman and K. Faust, *Social Network Analysis*, (Cambridge University Press, 1994).

[56] M. Faloutsos, P. Faloutsos and C. Faloutsos, Proc. ACM SIGCOMM, Comput. Commun. Rev., **29**, 251 (1999).

[57] D. J. Watts and S. H. Strogatz, Nature (London) **393**, 440 (1998).

[58] M. E. J. Newman, Proc. Natl. Acad. Sci. USA **98**, 404 (2001).

[59] S. Redner, Europhys. Lett. **4**, 131 (1988).

[60] P. Erdös and A. Rényi, Publ. Math. **6**, 290 (1959).

[61] D. J. Watts,*Small Worlds: The Dynamics of Networks Between Order and Randomness* (Princeton University Press, Princeton, 1999).

[62] S. Lawrence and C. L. Giles, Science, **280**, 98 (1998); Nature, **400**, 107 (1999).

[63] R. Albert and A.-L. Barabási, Rev. Mod. Phys. **74**, 47 (2002).

[64] W. Kinzel, in *Percolation Structures and Processes*, edited by G. Deutscher, R. Zallan, and J. Adler (Adam Hilger, New York, 1983), Vol. 5, p. 425.

[65] A. L. Barabasi and H. E. Stanley, *Fractal Concepts in Surface Growth*, (Cambridge University Press, Cambridge, 1995).

[66] M. Rossi, R. Pastor-Satorras, and A. Vespignani, Phys. Rev. Lett. **85**, 1803 (2000).

[67] A. Vespignani, R. Dickman, M. A. Muñoz, and S. Zapperi, Phys. Rev. E **62**, 4564 (2000).

[68] R. Dickman, M. Alava, M. A. Muñoz, J. Peltola, A. Vespignani, and S. Zapperi, Phys. Rev. E **64**, 56104 (2001).

[69] F. Bagnoli,F. Cecconi, A. Flammini, and A. Vespignani, Europhys. Lett. **63**, 512 (2003);

[70] H. K. Janssen, Z. Phys. B: Condens. Matter **42**, 141 (1981).

[71] P. Grassberger, Z. Phys. B: Condens. Matter **47**, 465 (1982).

[72] D. Stauffer and A. Aharony, *Introduction to Percolation Theory* (Taylor and Francis, London, 1994).

[73] G. E. Archie, AIME Trans. **146**, 54 (1942).

[74] J. Kozeny, Sitzungsber. Akad. Wiss. Wien. **136**, 271 (1927).

[75] M. Sahimi, Rev. Mod. Phys. **65**, 1393 (1993).

[76] A. Scheidegger, *The Physics of Flow through Porous Media* (University of Toronto Press, Toronto, 1974).

[77] O. M. Phillips, *Flow and Reactions in Permeable Rocks*, (Cambridge University Press, 1991).

[78] F. J. Pettijohn *Sedimentary Rocks*, (CBS Publishers & Distributors, 1984).

[79] M. Sahimi, *Applications of Percolation Theory*, (Taylor and Francis, 1994).

[80] G. V. Chilingarian in *Sediment Diagenesis* ed. by A. Parkar and B. W. Selwood, NATO ASI Series, vol 115, D. Reidel, Dordrecht, 1981.

[81] P-z. Wong, J. Koplik and J. P. Tomanic, Phys. Rev. B. **30**, 6606 (1984).

[82] J. N. Roberts and L. M. Schwartz, Phys. Rev. B. **31**, 5990 (1985).

[83] R. Dasgupta, S. Roy and S. Tarafdar, Physica A, **275**, 22 (2000).

[84] R. Karmakar, S. S. Manna and A. L. Stella, Phys. Rev. Lett. **94**, 88002 (2005).

[85] R. Karmakar and S. S. Manna, Phys. Rev. E. **71**, 15101 (2005).

[86] A. Malakis, J. Phys. A **8**, 1885 (1975).

[87] A. Malakis, J. Phys. A **9**, 1283 (1976).

[88] S. Hemmer, and P. C. Hemmer, J. Chem. Phys. **81**, 584 (1984).

[89] J. Majid, N. Jan, A. Coniglio, and H. E. Stanley, Phys. Rev. Lett. **52**, 1257 (1984).

[90] J. W. Lyklema, and K. Kremer, J. Phys. A, **17**, L691 (1984).

[91] R. Karmakar and S. S. Manna, J. Phys. A, **38**, L87 (2005).

[92] S. S. Manna and A Kabakcioglu, J. Phys. A, **36**, L279 (2003).

[93] B. Waxman, IEEE J. Sel. Areas Commun. **6**, 1617 (1988).

[94] S. Yook and H. Jeong and A.-L. Barabási, PNAS, **99**, 13382 (2002).

[95] S. S. Manna and Parongama Sen, Phys. Rev. E **66**, 66114 (2002).

[96] K.-I. Goh, D.-S. Lee, B. Kahng and D. Kim, Phys. Rev. Lett. **91**, 148701 (2003).

[97] A.-L. Barabási and R. Albert, Science, **286**, 509 (1999);

[98] A.-L. Barabási, *Linked: The New Science of Networks*, Perseus Publishing, 2002.

[99] R. Karmakar and S. S. Manna, J. Stat. Mech, L01002 (2005).

[100] D. Dhar and S. S. Manna, Phys. Rev. E. **49**, 2684 (1994).

[101] A. E. Scheidegger, Bull. I.A.S.H. **12**, 15 (1967).

[102] B. K. Chakrabarti, and S. S. Manna, J. Phys. A. **16**, L113 (1983).

[103] M. A. Muñoz, R. Dickman, R. Pastor-satorras, A. Vespignani and S. Zapperi, arXiv:cond-mat/0011447.

[104] R. Karmakar and S. S. Manna, Phys. Rev. E. **69**, 67107 (2004).

[105] P. Fröjdh, M. Howard and K. B. Lauritsen, Int. J. Phys. C, **15**, 1761 (2001).

[106] H. Leschhorn, T. Nattermann, S. Stepanow and L.-H. Tang, Ann, Phys. (N.Y.) **6**, 1 (1997).

[107] E. Salmon, M. Ausloos and N. Vandwalle, Phys. Rev. E. **55**, R6348 (1997).

[108] Y. Bernabe, Geophys. Res. Lett. **23**, 3039 (1996).

[109] M. Pollak and I. Riess, Phys. Status Solidi B. **69**, K15 (1975).

[110] P. M. Kogut and P. L. Leath, **12**, 3187 (1981).

[111] J. Chalupa, P. L. Leath and G. R. Reich, J. Phys. C., **12**, L31 (1979).

[112] J. Adler, Physica A, **171**, 453 (1991).

[113] S. S. Manna, Physica A **261**, 351 (1998).

[114] S. Sabhapandit, D. Dhar and P. Shukla *Hysteresis in the Random Field Ising Model and Bootstrap Percolation*, TIFR preprint, 2001.

[115] R. H. Schonmann, J. Stat. Phys. **58**, 1239 (1990).

[116] V. Spirin, P. L. Krapivsky and S. Redner, Phys. Rev. E. **63**, 036118 (2001).

[117] S. S. Manna, T. Datta, R. Karmakar and S. Tarafdar , Int. J. Mod. Phys. C, **13**, 319 (2002).

[118] R. Karmakar, S. S. Manna and T.Datta, Physica A, **318**, 113 (2003).

[119] R. M. Ziff, Phys. Rev. Lett. **69**, 2670 (1992).

[120] D. Stauffer, Int. J. Mod. Phys. C **8**, 1141 (1997).